DESIGN AND FABRICATION OF WHEELS FOR A LUNAR SURFACE VEHICLE

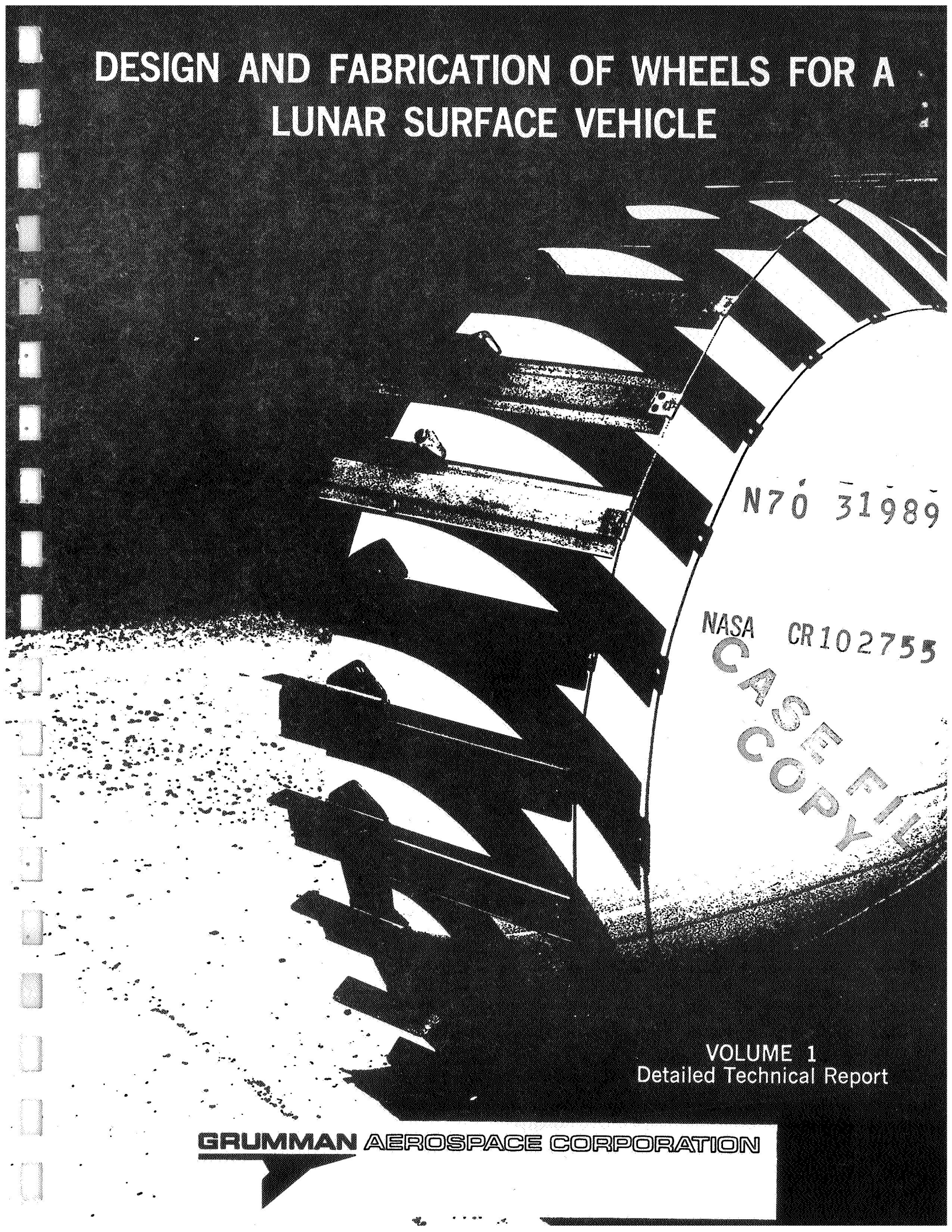

VOLUME 1
Detailed Technical Report

GRUMMAN AEROSPACE CORPORATION

FINAL REPORT
June 1970

DESIGN AND FABRICATION OF WHEELS FOR A LUNAR SURFACE VEHICLE

VOLUME 1
Detailed Technical Report

Prepared for

GEORGE C. MARSHALL SPACE FLIGHT CENTER
HUNTSVILLE, ALABAMA 35812
CONTRACT NO. NAS 8-25193

GRUMMAN AEROSPACE CORPORATION
BETHPAGE, NEW YORK 11714

TABLE OF CONTENTS

VOLUME I

1 INTRODUCTION

2 DESIGN CRITERIA

2.0 General
2.1 Dynamics Criteria
2.1.1 Response to Random Terrain
2.1.2 Loads Due to Obstacle Encounter
2.1.3 Selection of Wheel and Suspension Characteristics
2.1.4 References for Section 2.1
2.2 Loads and Structural Design Criteria
2.2.1 Stowed Condition Loads
2.2.2 Deployment Loads
2.2.3 Lunar Operation Loads
2.3 Environmental Criteria
2.3.1 Ground Environments
2.3.2 Lunar Environment
2.4 Mobility Considerations
2.4.1 Material Selection
2.4.2 Wheel Preliminary Design
2.4.3 Mobility Performance
2.4.4 Rolling Resistance
2.4.5 Slope Climbing
2.4.6 References for Section 2.4
2.5 Summary of Dynamic Design Criteria

3 DESIGN DEVELOPMENT AND SELECTION

3.0 General
3.1 Structural Analysis
3.2 Prior Grumman Testing
3.2.1 Strain Gage Instrumented Test Wheel
3.2.2 Test Set Up
3.2.3 Test Results
3.2.4 Evaluation of Results
3.2.5 Conclusions
3.3 Wheel Design "A"
3.3.1 Fabrication Process
3.3.2 Test Plan
3.3.3 Test Results
3.4 Design Iteration

TABLE OF CONTENTS (Continued)

3.4.1 Test Results
3.5 Final Design Selection
3.5.1 Final Design Characteristics
3.5.1.1 Spring Rate
3.5.1.2 Stress Distribution

4 FABRICATION PROCESS

4.0 Fabrication Requirements
4.1 Test Wheels
4.2 Deliverable Wheels
4.3 Cleat Fabrication
4.4 Wheel Weight

VOLUME II

PROPOSED TEST PLAN

1.0 Purpose
2.0 Description of Test Article
3.0 Test Conditions
3.1 Static Tests
3.2 Dynamic Tests
3.2.1 Traffic Mobility
3.2.2 Ambient Endurance Tests
3.2.3 Thermal/Vacuum Tests
4.0 Test Fixtures
4.1 Wheel Suspension
4.2 Road Bed
4.3 Instrumentation
4.3.1 Static Testing (Wheel)
4.3.2 Mobility Testing (Wheel)
4.3.3 Dynamic Endurance Testing
4.3.4 Static Testing (Drive Unit)
4.3.5 Dynamic Testing (Drive Unit)
5.0 Test Procedures
5.1 Establishment of Initial Test Conditions
5.1.1 Static Measurements
5.1.2 Load Increments
5.1.3 Obstacles
5.1.4 Side Loads
5.1.5 Inspection

TABLE OF CONTENTS (Continued)

5.2 Mobility Testing
5.2.1 Suspension
5.2.2 Soil
5.2.3 Measurements
5.2.4 Inspection
5.3 Endurance Testing (Partial Vacuum)
5.3.1 Setup
5.3.2 Test Segments
5.3.3 Inspection
5.4 Endurance Testing (Full Thermal Vacuum)

1 INTRODUCTION

Long before man had set foot on the lunar surface the requirements for a powered surface transportation vehicle had been established. Prior to the success of Apollo 11, however, little quantitative data were available to accurately define the mobility effecting characteristics of the lunar surface. Ten years ago when the first lunar vehicles began to evolve, they were based on the assumption that only the most lightly loaded vehicles could operate on the soft homogenous surface. Later, data from the Ranger, Orbiter, Surveyor and now the Apollo program have incrementally increased our understanding of the properties of the lunar surface. As the data bank of information grew, proposed vehicle concepts were altered to meet the revised missions and mobility criteria. Grummans Molab design (shown in prototype form in Figure 1-1) with large metalastic wheels typically satisfied the early mobility criteria.

As our knowledge of the lunar surface grew in detail, the concept of a homogenous surface gave way to a debris strewn surface with large quantities of widely dispersed rocks in the 2-4 inch size. Initial vehicle mobility system concepts were reevaluated and discarded because of the possibility of debris entrapment within the wheel geometry, leading to ultimate wheel failure.

At Grumman a single element elastic conical wheel (Figure I-2) was evolved through an extensive company funded design and test program addressed to resolving the lunar mobility problem. The results of full scale wheel and model tests in addition to Grummans full scale LRV simulator attest to the success of this concept.

The objective of this study was to refine the existing conical wheel design in order to provide an optimum configuration compatible with the NASA defined Dual Mode Lunar Roving Vehicle (DLRV) mission requirements. The unique wheel form does not allow the normal analytic analyses techniques therefore

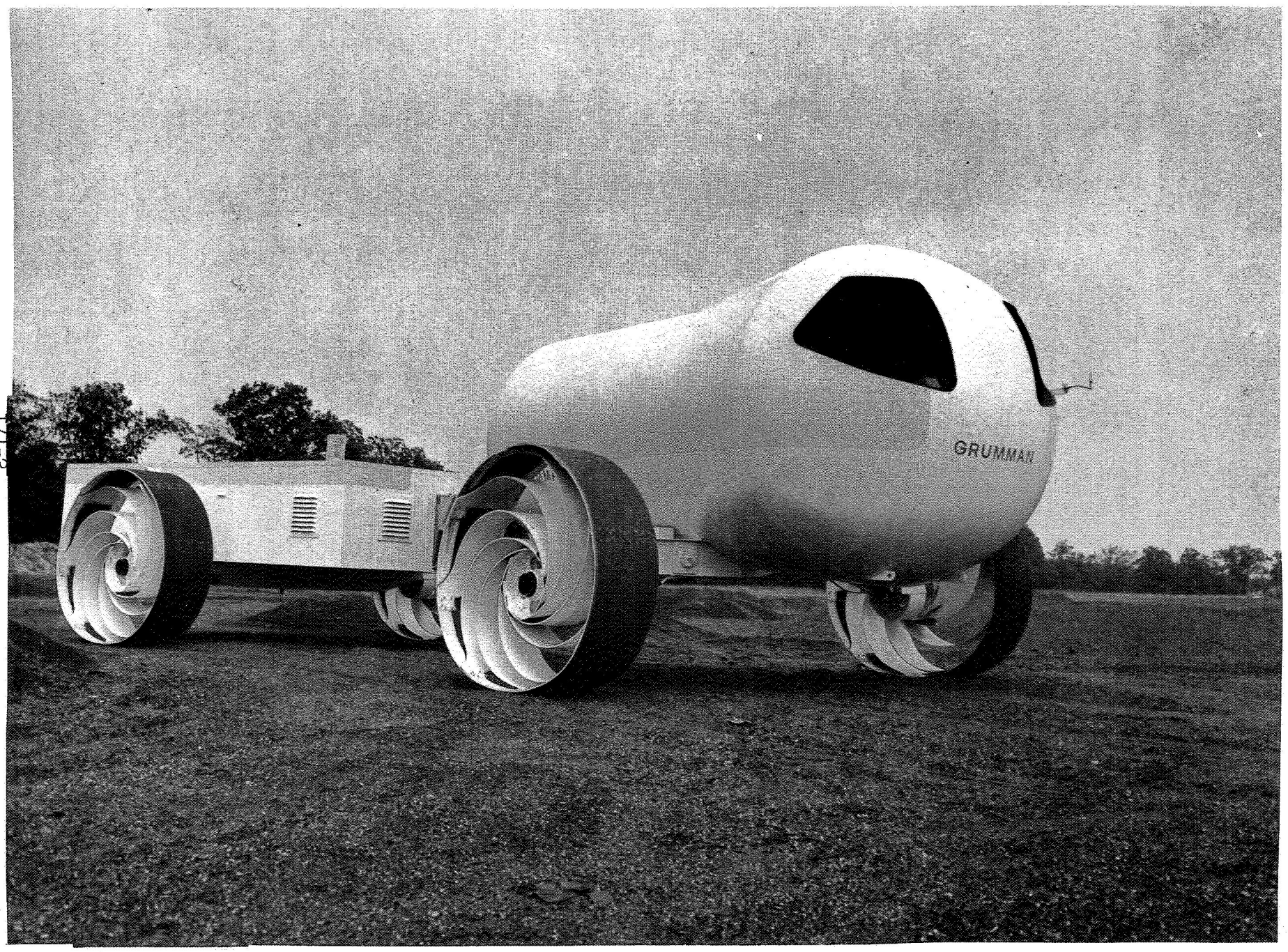

Molab Concept

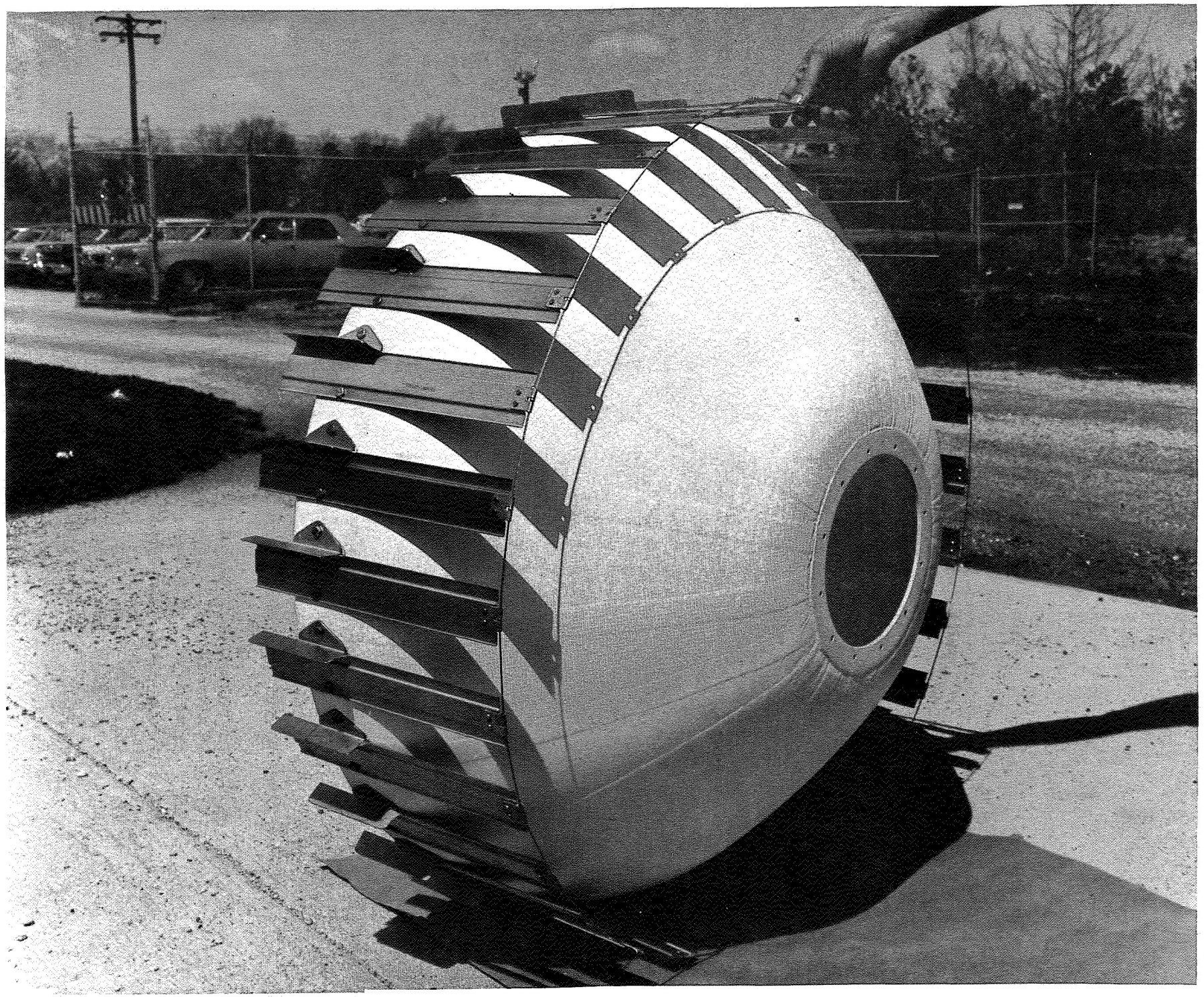

Grumman's Elastic Cone Wheel

Figure 1-2

an empirical test program was used to evolve an optimum design. Because of the interrelated nature of the previous testing and the DLRV concepts, prior data which was felt to be pertinent to the final design selection shown herein has been included in this report. Three wheels of the final design have been provided to NASA for testing. A proposed lunar qualification test plan is provided for the entire wheel drive assembly.

2 DESIGN CRITERIA

2.0 GENERAL

The design criteria used to develop the final wheel configuration was based on the DLRV mobility requirements which defined static and dynamic loadings, and the non mobility requirements of earth launch and lunar operations. These criteria were documented in detail in Grumman's DLRV final report, excerpts of which are incorporated below.

2.1 DYNAMICS CRITERIA

Wheel design criteria are developed by assessing the interaction of the wheel suspension system, the vehicle itself and a lunar soil model. The following discussion shows how the surface model, loads and vehicle motions are related, and the rational for selection of the wheel-suspension configuration.

Vehicle/wheel dynamics studies were performed to optimize ride qualities, maximize vehicle controllability (related to the amount of time the wheels are off the ground), and determine damping power dissipation, turning stability boundaries, and dynamic loads during lunar operation.

The dynamics effort consisted of three main areas: analog computer studies of the response to random terrain, and digital studies of turning stability and the response to obstacle encounters.

2.1.1 Response to Random Terrain

The design of the vehicle suspension is determined largely by ride quality and vehicle controllability objectives for constant-speed traverse of random terrain. An analog computer is ideal for studying these characteristics, since it can readily accommodate random excitation, and the outputs of the computer can be connected to a mechanical simulator.

The initial analog modeling consisted of a four-degree-of-freedom roll-plane module with a trilinear suspension and non-linear point-follower wheels with "scuff" damping. Subsequent analog models consisted of two coupled roll-plane modules capable of pitch motion also as shown in Fig. 2-1. A modular approach

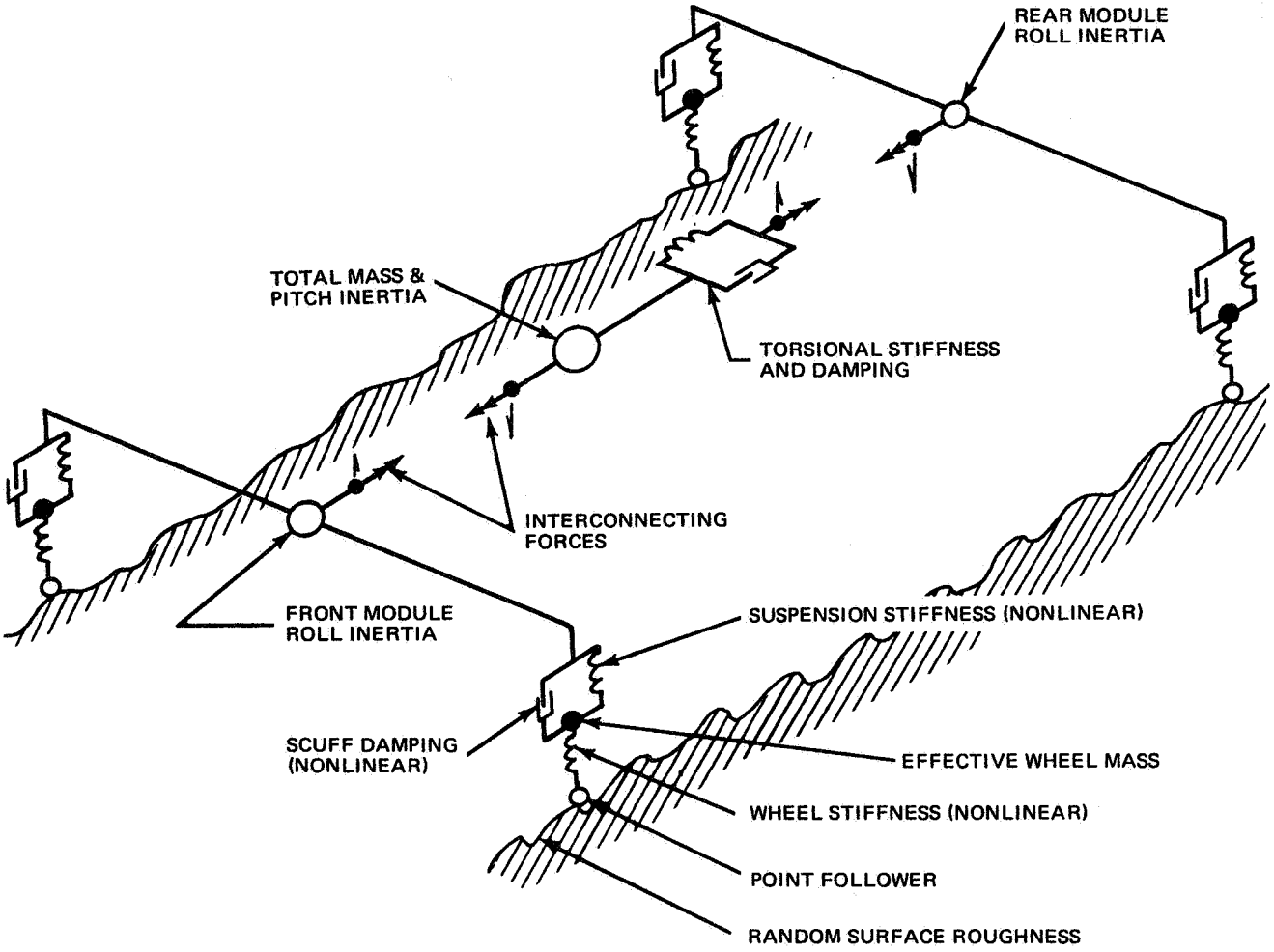

Fig. 2-1 **MATH MODEL FOR ANALOG STUDY**

to math modelling was selected for the ease with which it allowed coupling of two or more roll-plane modules for complete vehicle analysis. The major parameters recorded were chassis accelerations, suspension deflection, wheel load, power dissipated, and wheel lift-offs. Wheel and suspension characteristics and inter-modular torsional flexibility were varied.

The trilinear suspension spring used in the analysis combined a linear spring with a motion-limiting snubber at each end. The three suspensions shown in Fig. 2-2 were investigated; these were designated as the 5, 10 and 20 lb/in suspensions after their linear normal-operating-range spring rates. Static deflection positions and deflection before snubber contact are also shown.

The nominal stiffness characteristc used for the wheel is shown in Fig. 2-3. Wheel stiffness ranging from half to twice that shown were considered. The point follower assumption which was used was reasonable for the analog studies because the detailed wheel/terrain geometry characteristics have small effect on ride qualities. The modelling allowed the wheels to leave the ground when they were unloaded. The "scuff" damping mechanism dissipates energy by means of a lateral scuffing action between the wheel and the lunar surface. This action was modelled as non-linear viscous damping, whose coefficient varied with wheel normal force and vehicle forward velocity. Auxiliary mechanical damping across the suspension was also considered.

Four random terrain roughnesses have been defined for the lunar surface in terms of power spectral densities: smooth mare, rough mare, hummocky upland and rough upland. Upper and lower bounds for these surfaces are given in Ref. 1. Comparison of the spectra showed that using rough and smooth mare covered the range, and these were actually quite close to the remaining two. Therefore, only these two spectra were used. For each spectrum a straight-line approximation of the average of the upper and lower bounds in the frequency range of interest was used. The analytical spectra increased at 6 db/oct with decreasing frequency down to 0.1 Hz, below which they were made flat to prevent displacement overload of the analog computer, which was scaled for smaller amplitudes

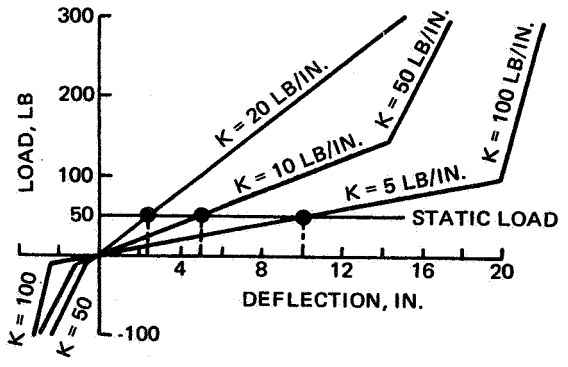

Fig. 2-2 **IDEALIZED SUSPENSION STIFFNESSES**

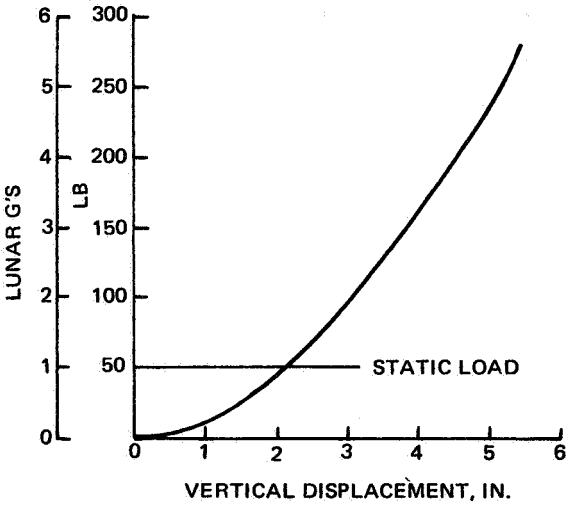

Fig. 2-3 **IDEALIZED WHEEL STIFFNESS**

on the order of wheel and suspension deflections. This low-frequency deviation would have no significant effect on the dynamic responses since it was well below vehicle resonances. Uncorrelated random excitations were used for the left and right sides; left and right rear wheel excitations were the same as those of the respective front wheels except that a time delay dependent on vehicle velocity was used.

The initial analog computer work was done using a 2 x 2 roll-plane model. Results of the suspension variation study using this model are shown in Fig. 2-4. Astronuat roll and heave acceleration responses are lowest for the softest suspension, as would be expected. Both the 5-and 10-lb/in. suspensions provide ride qualities within the human tolerance range for both smooth and rough mare surfaces (Ref. 2). RMS suspension deflections increased with speed. The time histories of the runs revelaed that snubber contact occurred infrequently; on a rough mare at 12 km/hr, only one contact in a two-minute run occurred with the 5-lb/in. suspension, and no contacts were observed with the 10-lb/in. suspension. (The unexpected order of the deflection curves for smooth mare operation is attributable to the abrupt non-linearities of snubber contact.) Also shown are the peak wheel loads that occurred in a two-minute run. Damping power dissipation increased with speed and suspension stiffness; however, a more marked increase occurred for travel on rough surfaces. Thus, the penalty for rough mare operation is a bigger drain on the batteries. It can also be seen that no simultaneous two-wheel lift-offs occurred on smooth mare for the 5 and 10 lb/in. suspension systems. This implies good steering control at all speeds. Analysis was also made of the peak probability distributions associated with the suspension deflections and wheel loads for both rough and smooth mare. The distributions for both parameters were found to be approximately Rayleigh, as shown in Fig. 2-5 a result which greatly facilitates determination of fatigue damage due to vehicle traverse on random terrain. (Determination of fatigue damage for the wheel is complicated by the fact that the loading cycles are distributed around the rim rather than applied at a fixed location. This

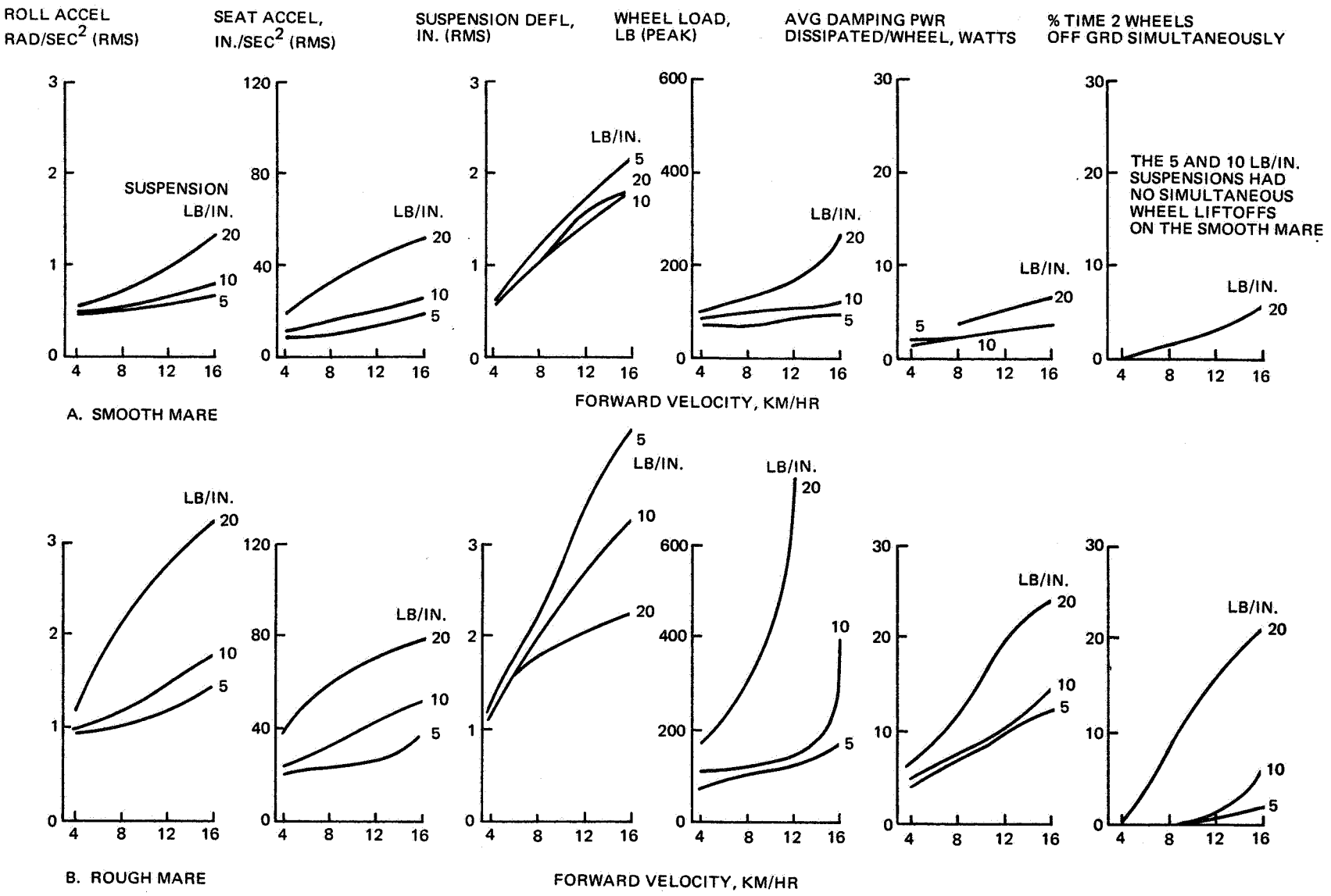

Fig. 2-4 RESPONSE TO RANDOM TERRAIN, 2 WHEEL MODEL

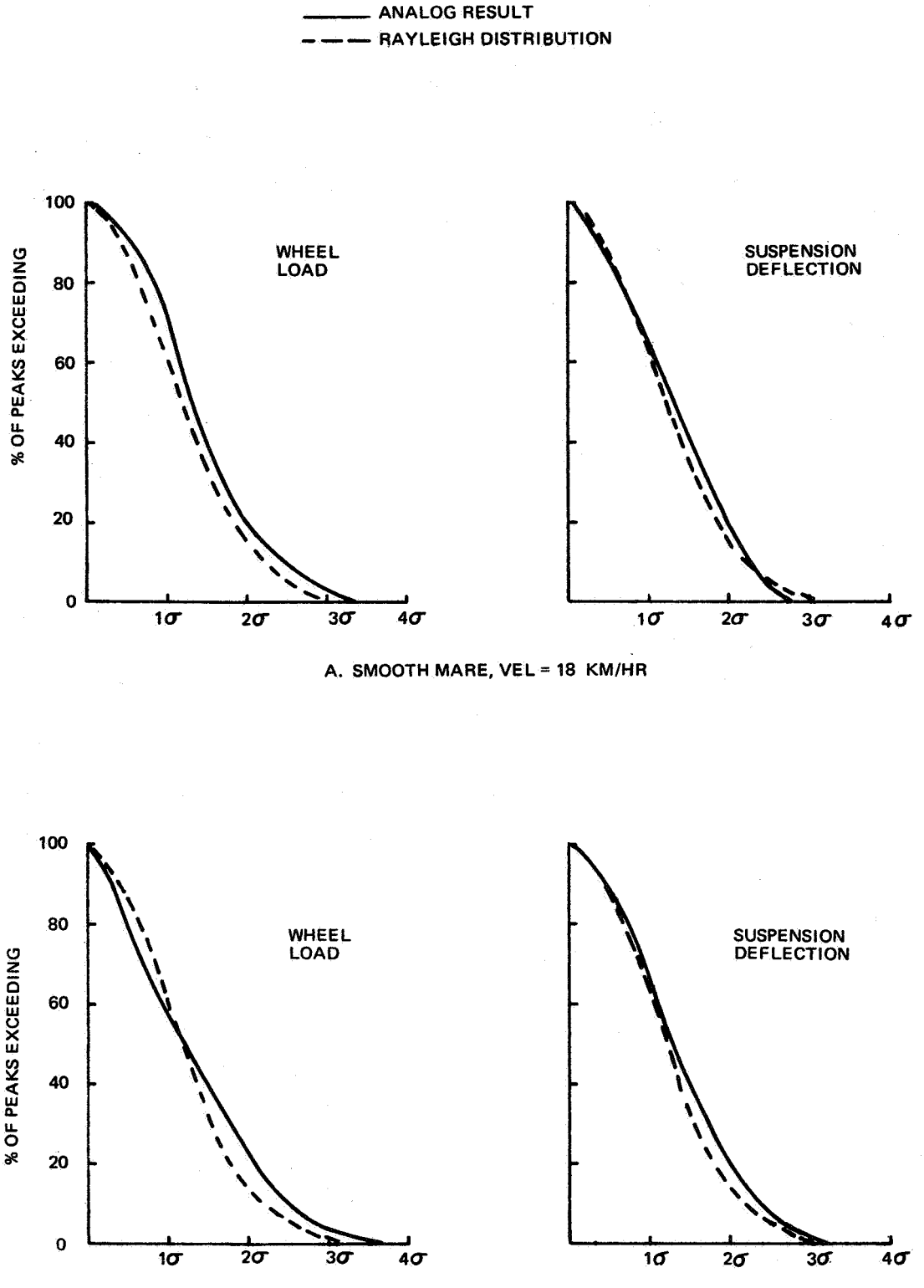

Fig. 2-5 PEAK PROBABILITY DISTRIBUTIONS

difficulty can be surmounted if damage to the wheel for each complete revolution at a particular load level is estimated and summed for the total number of wheel revolutions at that particular load level.) The rougher the terrain or the greater the vehicle velocity, the more the wheel and suspension peak distributions deviate from a Rayleigh distribution because of the non-linearity of wheel and suspension stiffnesses and wheel lift-off from the ground. The distributions shown in Fig. 2-5 represent relatively severe operating conditions; thus, deviations from the Rayleigh distribution significantly larger than those shown would not be expected during normal operation of the DLRV.

Following the initial 2 x 2 work, the program was expanded to accommodate the 4 x 4 vehicle. Results for the 4 x 4 analysis are shown along with comparable 2 x 2 results in Figure 2-6. The intermodular torsional stiffness for these runs was 200 in-lb/rad, a value approximating that of the actual structure. A practical range of torsional stiffness was run, but no significant difference in the results was observed.

The response obtained with the 4 x 4 analysis are seen to be similar to, but generally less than, those of the 2 x 2. The slight conservatism of the simpler analysis is in the right direction. Agreement between the results is close enough to validate the conclusions drawn from the simpler analysis.

2.1.2 Loads Due to Obstacle Encounter

It is evident that loads due to encounter of large-size obstacles would be greater than loads produced by response to rough mare traverse. To accurately evaluate obstacle encounter loads, a more detailed representation of bump/wheel geometry than that provided by the point-follower assumption was required. Because such a representation could not be incorporated into the analog analysis without undue complication, a digital computer analysis was performed. The digital modelling, which is shown in Fig. 2-7, consisted of a two-mass, two-degree-of-freedom heave module, with a nonlinear bump-contouring wheel and a trilinear suspension with viscous damping. Wheel radial loads and suspension vertical and drag loads were determined for spike bumps of 4, 8, and 12 inches at

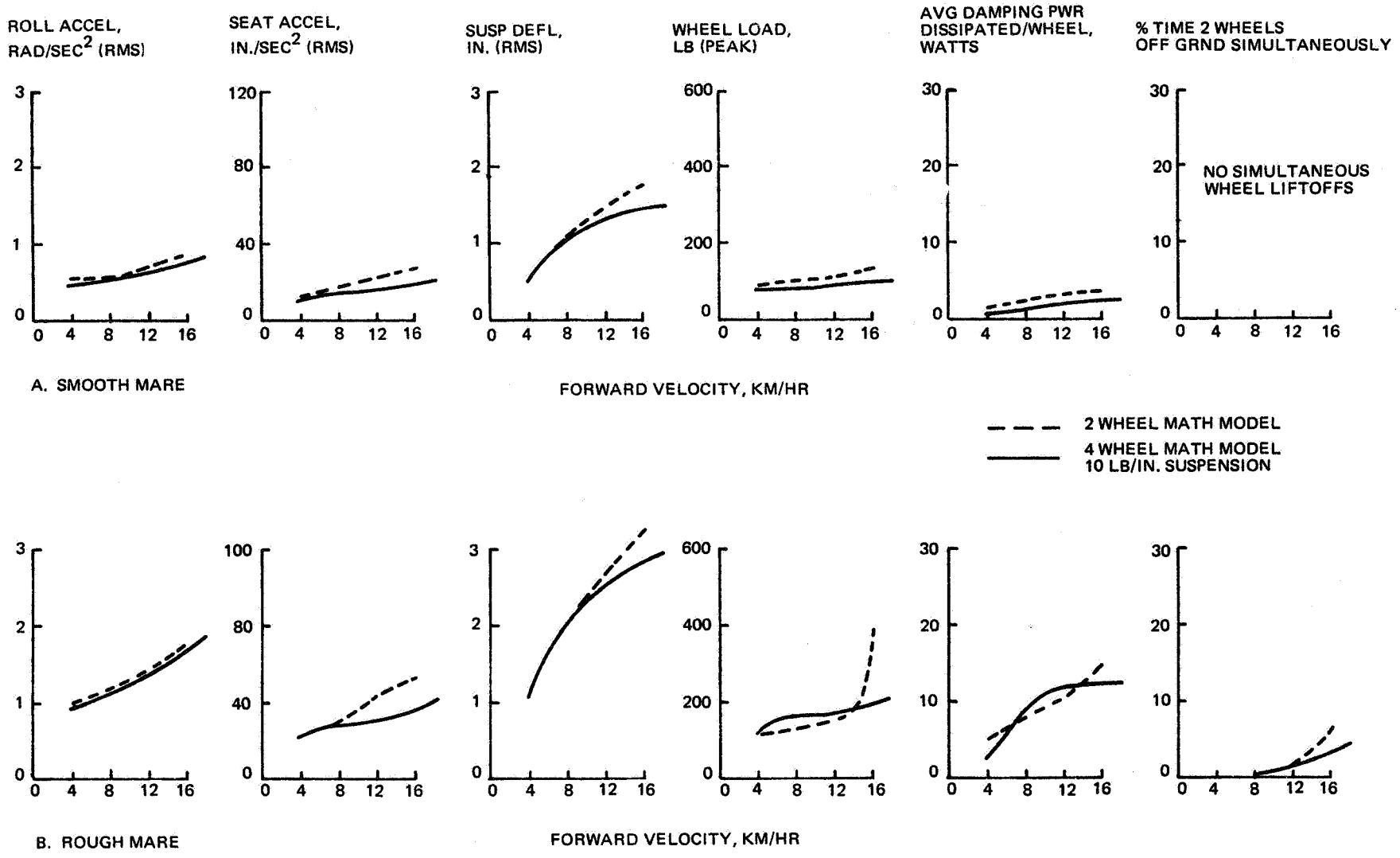

Fig. 2-6 COMPARISON OF RANDOM TERRAIN RESPONSE FOR 2 AND 4 WHEEL MATH MODELS

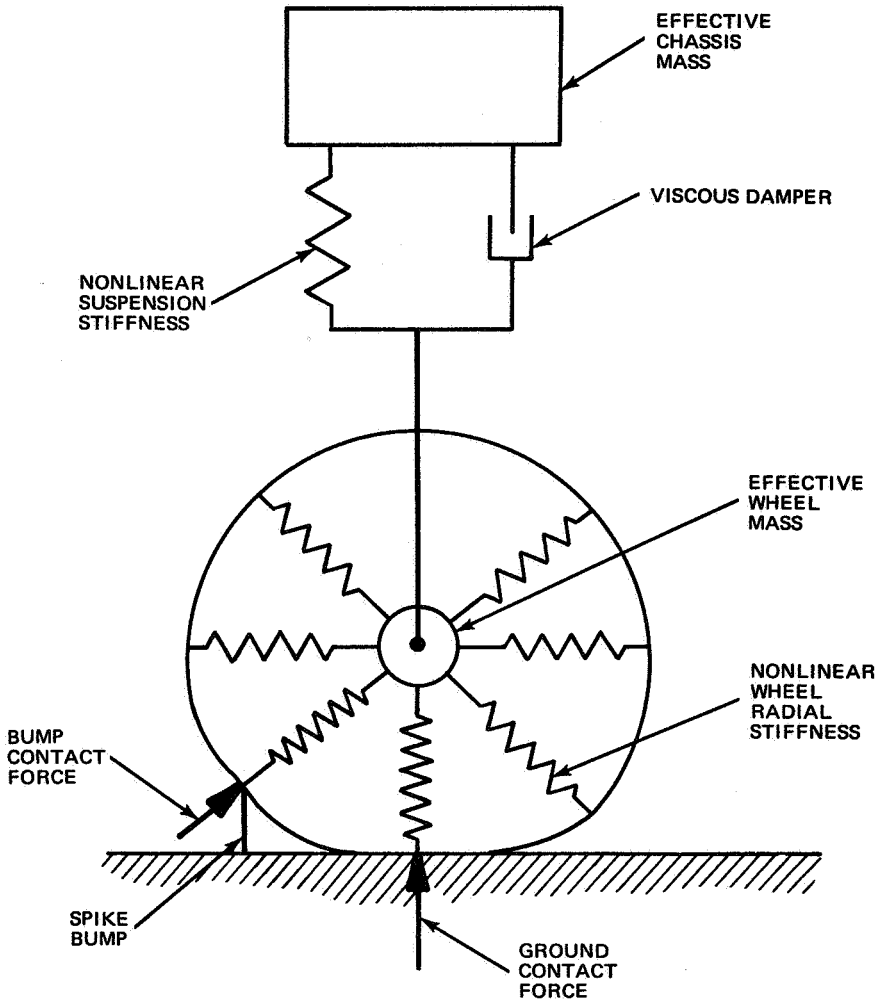

Fig. 2-7 MATH MODEL FOR BUMP ENCOUNTER ANALYSIS

velocities ranging from 4 km/hr to 16 km/hr. Results are shown in Figs. 2-8 and -9 for the 10 lb/in suspension and the nominal stiffness wheel. The effects of other suspension stiffnesses on the loads were small. The limit load of the nominal stiffness wheel is 300 lbs which corresponds to a 5.5 lunar g loading. It is seen in Fig. 2-9 that 4-inch bumps, which probably are so numerous as to be unavoidable, can be negotiated at all speeds. Eight-inch bumps, which would be less numerous and much more visible can be taken at speeds up to 9 km/hr.

The effects of varying wheel stiffness on wheel radial and suspension drag loads are shown in Fig. 2-10 for a 10 lb/in. suspension and an 8-in. spike bump. Three wheel stiffnesses were considered. As expected, the loads decreased with decreasing wheel stiffness, but decreasing wheel stiffness implies decreasing load capability.

It might appear, intuitively, that bump-encounter capability could be materially increased by the addition of a deflection-limiting snubber to the wheel. To investigate this possibility, a snubber with a spring rate of approximately 1000 lb/in in parallel with the cone wheel was considered. The fourth curve in Fig. 2-10 shows the result. Although this snubber increased the wheel load capability from 5.5 to 19 g's, it only increased the allowable velocity over an 8-in. bump from 9 to 12.4 km/hr. Suspension drag loads increased correspondingly from 140 to 690 lb., which would necessitate redesign of the suspension arms and chassis support area. It was concluded that the addition of a wheel snubber could not substantially increase bump encounter velocities without prohibitive weight penalties. It should be noted that there are no specific obstacle encounter requirements for DLRV; however, it is believed that the vehicle should at least be capable of withstanding bumps on the order of 4 in. at maximum speed.

2.1.3 Selection of Wheel and Suspension Characteristics

The information derived from the analog and digital studies was analyzed to determine the "optimum" wheel and suspension system combination. The analog

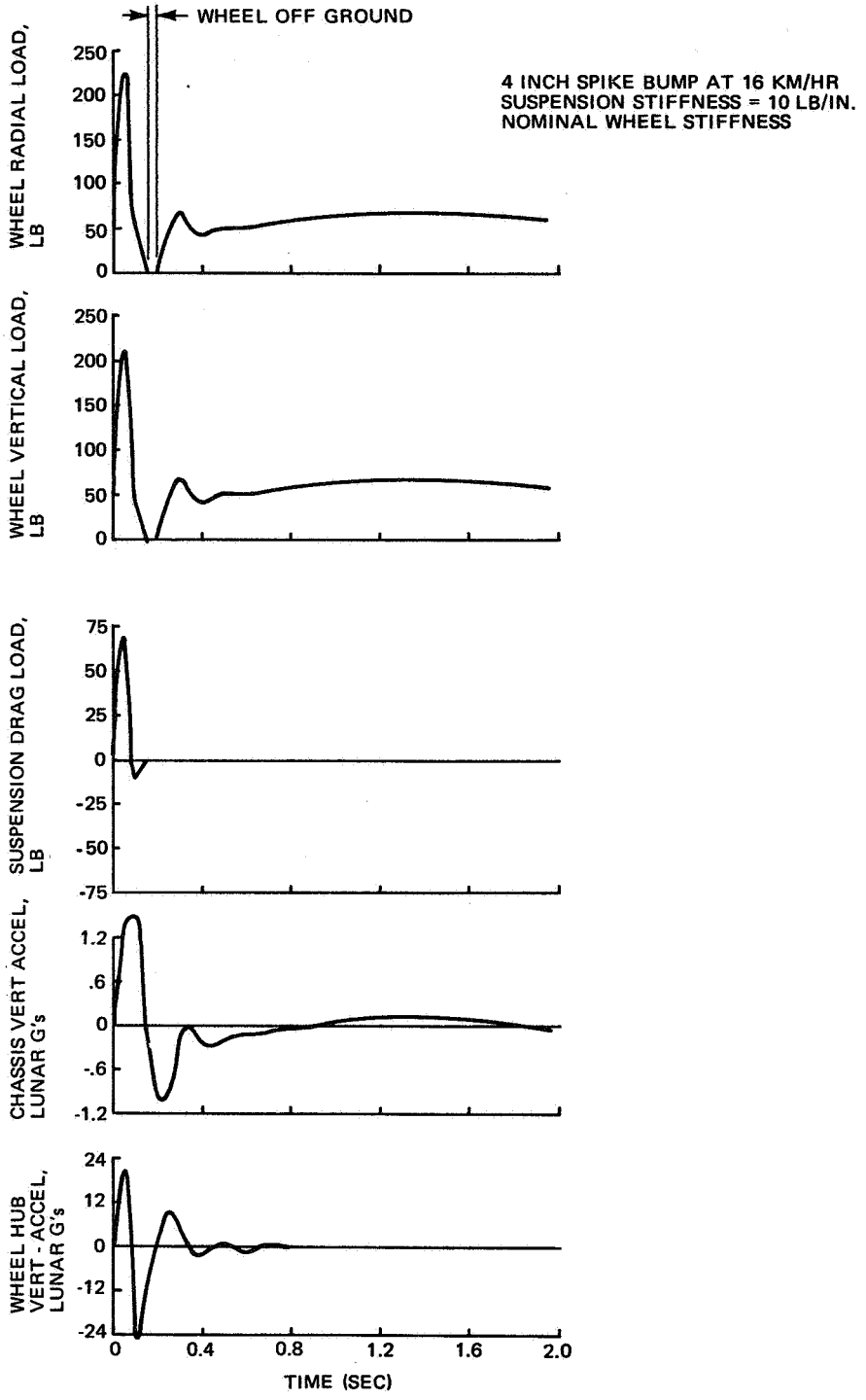

Fig. 2-8 TIME HISTORIES OF BUMP RESPONSE

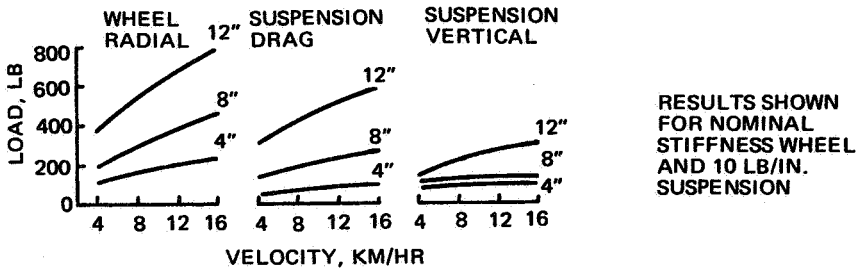

Fig. 2-9 **LOADS DUE TO 4, 8, AND 12 IN. SPIKE BUMP ENCOUNTERS**

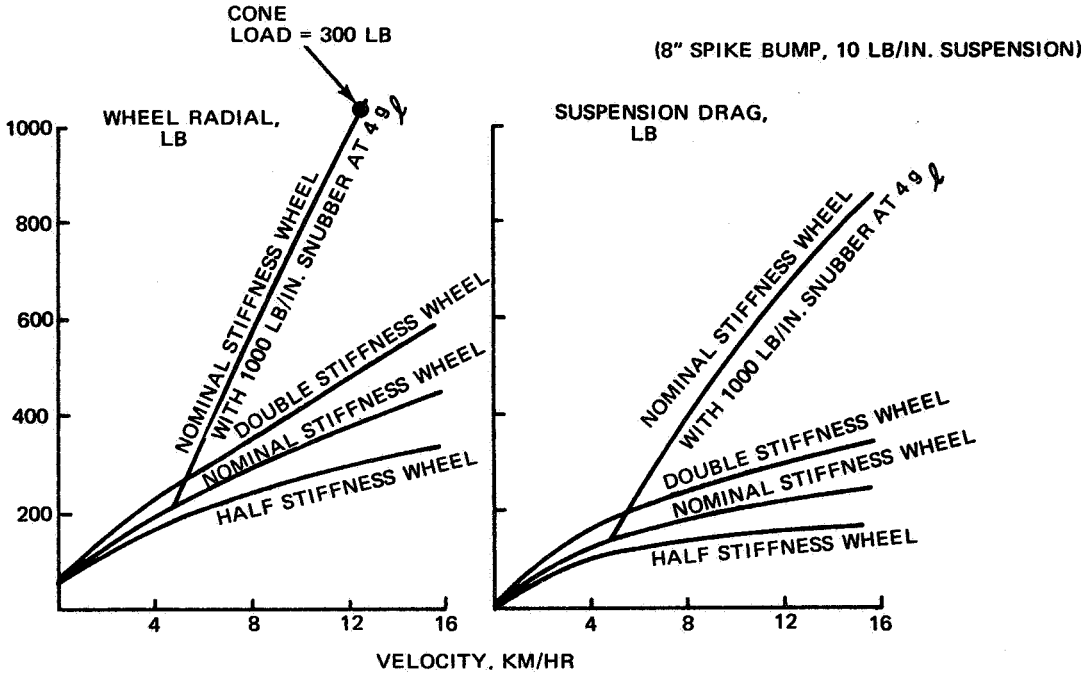

Fig. 2-10 **EFFECT OF WHEEL STIFFNESS ON BUMP ENCOUNTER LOADS**

and digital computer results made readily apparent the effect of varying the wheel and suspension system stiffness parameters. The stiffest wheels and suspension springs produced the smallest deflections, but contributed the largest wheel loads and vehicle roll and heave accelerations; the softest wheels and springs produced the smallest loads and accelerations, but the largest static and dynamic deflections.

Allowable deflections are limited by vehicle size and obstacle-clearance considerations. On the basis of dynamic response considerations, optimum suspension system deflection would be the maximum deflection possible without snubber contact. It should, however, be noted that occasional contact, which could be expected with a soft spring, would not have a large effect on rms acceleration levels and, presumably, on crew comfort.

After examination of the computer data, and evaluation of the tradeoffs, the combination considered best for both ride qualities on rough terrain and wheel loads due to bump encounter was the nominal stiffness wheel in combination with a suspension stiffness of between 7.5 and 10 lb/in.

2.1.4 References for Section 2.1

1. "Lunar Terrain and Traverse Data for Lunar Roving Vehicle Design Study", H. Moore, R. Pike, G. Ulrich. NASA Report to be published.
2. "Preliminary Design Study of a Lunar Local Scientific Survey Module (LSSM), Final Technical Report: LSSM Mobility Systems", GM Report D2-83012-1, July 1966, p. 5-82.

2.2 LOADS AND STRUCTURAL DESIGN CRITERIA

The DLRV system and subsystem components should be designed to the loads and structural design criteria specified herein. These are based on study and analysis of the mission objectives and requirements, and previous aerospace and lunar roving vehicle engineering and development background. Two primary load environments can be identified:

Stowed lunar transport environment including launch and boost through landing and deployment

Lunar operation, manned and unmanned

2.2.1 Stowed Condition Loads

The DLRV will be exposed to a variety of static and dynamic loads during its delivery from earth to the lunar surface. The dynamic environment for Quad I payload has been specified in a LM interface document. The Quad IV environment will be similar. LM/Apollo experience has shown that overall design loads for units the size of DLRV are determined more by dynamic considerations than static accelerations.

2.2.2 Deployment Loads

The static loads due to deployment will not be significant for the basic structure of the DLRV, since the small lunar gravity force will be much less severe than the forces experienced during delivery to the lunar surface. Dynamic deployment loads depend primarily on the controlled translational and rotational velocities of the DLRV at wheel touchdown.

2.2.3 Lunar Operation Loads

During operation on the lunar surface the DLRV will experience a variety of ground loads deriving from many sources, such as random surface roughness, impact with discrete obstacles and braking accelerating, turning, and obstacle negotiating maneuvers. Loads due to the first two of these conditions came out of the dynamics studies reported in Section 2.1. Mission design loads for the DLRV mobility system were established based on rational consideration of likely loading conditions, in conjunction with the results of the dynamic analysis. A summary of the principal wheel loading conditions, in terms of lunar g units, is given in Table 2-1 while the conditions are discussed in more detail in the following paragraphs:

- Nominal static load: This load, which is due to the lunar weight ($1g_l$), is used as the basis or reference for all the ground load conditions. The static load on the wheels varies with the mission (e.g., manned or unmanned, with or without samples) and with the module (power, control, or science), but for practical considerations only two nominal loadings were defined: 55 lb for the control module and 40 lb for the power and science modules. These values cover all normal conditions on level ground; however, they are less than the manned rescue mode, where degraded operation is assumed.

TABLE 2-1

WHEEL GROUND LOADS CRITERIA

LOAD CONDITIONS	WHEEL DEFLECTION (IN.)	MISSION DESIGN WHEEL LOADS			
		RADIAL FORCE (G_L) *	SIDE FORCE (G_L) *	TRACTIVE TORQUE (FT-LB)	RADIAL TORQUE (FT-LB)
NOMINAL STATIC	1.8	1.0			
DYNAMIC OPERATING	3.1	3.0	0 TO 2.4		
MAX. BRAKING TORQUE	3.1	3.0	0 TO 2.4	$\pm$ 100	
UNSYMMETIC BRAKING	3.1	3.0	$\pm$ 1.44	$\pm$ 100	
PIVOTING	3.1	3.0		$\pm$ 100	$\pm$50
TURNING	2.5	2.0	3.17		
MAXIMUM RADIAL	4.3	5.5	0 TO 2.2		

* EXPRESSED AS LUNAR GRAVITY UNITS (5.4 FT/SEC/SEC). THE NOMINAL STATIC 1-G_L DESIGN LOAD FOR THE CONTROL MODULE IS 55 LB. FOR THE POWER AND SCIENCE MODULES THE LOAD IS 40 LB.

- o Dynamic operating load: The dynamic studies on the analog computer utilizing the specified lunar terrain models showed peak loads of approximately 2 and 4 g_1 on smooth and rough mares, respectively, at 16 km/hr, during a two-minute run. Allowing for higher peaks during the longer-term smooth-mare operation, and selecting a more realistic rough-mare speed of about 8 km/hr, suggests 3 g_1 as a reasonable mission load. This radial load has to be combined with loads caused by maneuvering and braking. An inboard-acting side load due to the scuffing action of the swing arm suspension is associated with vertical loading of the wheel. A frictional coefficient of 0.8 was used to establish the side load shown in the table.
- o Maximum braking torque: The braking design torque corresponds to a maximum braking effort of 100 ft-lbs.
- o Unsymmetrical braking: This condition assumes maximum braking on two wheels on the same side of the vehicle; side loads provide the static balance.
- o Pivoting: This condition involves pivoting the vehicle about a single locked wheel. Uniform soil pressure is assumed over the entire footprint length.
- o Turning: This condition corresponds to a sharp turn which puts the vehicle at the point of insipient instability (all load on the outside wheels).
- o Maximum radial load: This high-load requirement provides for a number of radial overload conditions, such as obstacle encounter, longitudional impact, or a vertical drop.

The dynamic operating loads obtained from the lunar surface spectral densities do not include impacts with discrete short wavelength obstacles. Separate digital computer studies reported in the Dynamics Section (2.1) show that a 5.5-g_1 capability is required to negotiate 4-in. spike bumps at 16 km/hr., and it is believed that no less capability than this should be provided. The provision of this high load capability for the science module allows it to also be used in the manned mode, if called for by future plans.

During unmanned operation, the probability of encountering a large obstacle is increased, but the driving speeds are much lower. A 5.5 g_1 capability allows for longitudinal impact of a vertical wall with a single wheel at a speed of slightly over 2 km/hr.

A large free-fall height capability is desirable, since it provides for added margin during DLRV deployment, and allows for inadvertently driving into a deep depression. The 5.5 g_1 load capability provides for a free-fall height of about 34 inches.

2.3 ENVIRONMENTAL CRITERIA

The induced and natural environmental criteria that must be accommodated by all the DLRV components include prelaunch, launch, translunar, and lunar surface conditions. Summarized below are the relevant vehicle environmental criteria as defined in Grummans DLRV final report specifications.

2.3.1 (a) Pre-Launch - Packaged

NOTE: Simultaneous environment and load conditions shall not be considered unless otherwise noted, at the levels contained herein.

Unless otherwise noted ambient environments are considered to exist outside of the package.

Packaged and Unpackaged - the word "packaged" in this specification refers to containers used for transportation, handling and storage.

(1) Acceleration: 2.67 g vertical with 0.4 g lateral, applied simulteneously to the package. 2.0 g in direction of hoisting (when rings are used, consider applied to any one or any combination of rings). This condition applies to all equipments capable of being hoisted in any direction other than DLRV axis.

(2) Shock: Shock as in Standard MIL-STD-810B, Method 516, Procedure II.

(3) Vibration: The following vibration levels are specified during transportation, handling and storage. Vibration to be applied, along three mutually perpendicular axes, X, Y, Z to the package. Earth Gravity Compensation is not required.

(Time: 1/2 Octave per minute, three times per axis from 5 Hz to maximum Hz and back to 5 Hz).

Hz	g or D.A.
5-7.2	.5 in. D.A.
7.2-26	± 1.3 g
26-52	.036 in. D.A.
52-500	± 5.0 g

(4) Pressure: Ground transportation and storage: minimum of 11.78 psia. Air Transportation: minimum of 3.45 psia for 8 hours (35,000 ft alt).

(5) Temperature:

Ground Transportation: -60°F to +160°F for 2 weeks
Air Transportation: -45°F to +140°F for 8 hours
Storage Temperature: -20°F to +110°F ambient air temperature; plus 360 BTU/ft^2/hr. up to 6 hrs/day for 3 years.

(6) Humidity: In accordance with Standard MIL-STD-810B, Method 507 except that the maximum test temperature shall be 110°F instead of 160°F and the minimum test temperature shall be 40°F instead of 82°F.

(7) Rain: As defined in Standard MIL-STD-810B, Method 506.

(8) Salt Spray: As specified in Standard MIL-STD-810B, Method 509 (No direct impingement on flight hardware).

(9) Sand and Dust: As defined in Standard MIL-STD-810B, Method 510, Procedure 1 except that the total exposure shall be limited to 4 hours at a temperature of 73°F and a relative humidity of 22% with the air velocity maintained at 300 ± 200 fpm. (No direct impingement on flight hardware).

(10) Fungus: In accordance with Standard MIL-STD-810B, Method 508.

(11) Ozone: Three years exposure as follows: 72 hours, at 0.5 PPM, 3 months at 0.25 PPM and remainder at 0.05 PPM concentration.

(12) Hazardous Gases: As defined in Standard MIL-STD-810B, Method 511.

(b) Pre-Launch - Unpackaged

Ground handling shall not produce critical design loads on the DLRV or DLRV equipment and shall not increase the weight of the DLRV.

NOTE: Simultaneous environment and load conditions shall not be considered, unless otherwise noted, at the levels contained herein.

(1) Acceleration: 2.67 g Vertical with 0.4 g lateral applied simultaneously, 2.0 g in direction of hoisting in any direction other than the DLRV X axis direction.

(2) Shock: Shock as in Standard MIL-STD-810B, Method 516, Procedure 1, Basic Design Test of Figure 516-1.

(3) Humidity: Same as pre-launch packaged.

(4) Salt Fog: Same as pre-launch packaged.

(5) Sea-Air Humidity: In lieu of exposure to the individual Humidity and Salt Fog environments noted above, the following Sea-Air Humidity combined environment may be substituted. Salt solution per Method 509, of Standard MIL-STD-810B, except concentration to be 1% instead of 5% by weight of chemically pure sodium chloride. The chamber to be maintained at 90°F ± 5°F and 85% + 15%/-10% relative humidity for the duration of the exposure. The 1% salt spray is applied for two-minute periods on an hourly basis. The duration of the exposure is three days for unsheltered equipment and one day for sheltered equipment where sheltered is defined as protection such as by the DLRV skin.

(6) Rain: Same as pre-launch packaged but no direct impingement.

(7) Fungus: Same as pre-launch packaged.

(8) Ozone: Same as pre-launch packaged.

(9) Pressure: Ambient ground level pressure.

(10) Temperature: -20°F to 110°F ambient air temperature plus 360 BTU/ft^2/hr up to 6 hrs/day.

From the time of hypergolic loading of ELM to lift off (T-0):

40° to 110°F SLA cavity external to DLRV

40° to 110°F equipment mounting tray and environment

(11) Hazardous Gases: Gaseous exposure as defined in Standard MIL-STD-810B, Method 511 and MSFC Drawing 10M01071.

(12) Electromagnetic Interference: In accordance with Specifications LSP-530-001 and MIL-E-6051C.

(13) Sand and Dust: External to the DLRV the particle count shall not exceed level 1,000,000 of Specification LSP-14-006.

2.3.2 Lunar Environment

(a) Lunar Deployment

Temperature:	± 300°F
Pressure:	1×10^{-10} mm Hg
Simulated Lunar Dust	Basalt particles with density of 15. g/cm^3 and grain size of 2mm or less.

(b) Lunar Operation

Pressure	1×10^{-10} mm Hg
Temperature	± 300°F
Radiation	As defined in NASA's DLRV RFP/RFQ No. DCN 1-9-21-00003 ANNEX "C"
Electromagnetic Interference	In accordance with Specifications LSP-530-001 and MIL-E-6051C
Simulated Lunar Dust	Basalt particles with density of 1.5 g/cm^3 and grain size of 2 mm or less.

2.4 MOBILITY CONSIDERATIONS

The mobility capabilities of the DLRV depend greatly on its wheel configuration. As a component, the wheel must satisfy the rigorous DLRV requirements of weak soil mobility, steep slope and obstacle negotiability, and applied vehicle loadings. Generally, the larger the footprint area, and the aspect ratio of this area, the better the mobility performance. Footprint area and its aspect ratio are functions of both the diameter and the flexibility of the

basic shell of the wheel, hence, of the weight of the shell. Ideally, the search for the optimum wheel size and flexibility should be based on a trade-off analysis between wheel weight on the one hand, and a number of tangible and intangible factors such as power requirements, weight and dynamic characteristics of the wheel, and overall probability of mission success on the other hand. Considerations of these factors have been made; however, the trade-off analyses have been constrained by stowage volume. The vertical and lateral space allowed by stowage considerations has restricted the diameter and shape factor of the wheel. Coupled in with these functional requirements are the constraints of low component weight, high operational efficiency, and maximum mechanical reliability.

Weight and reliability received special emphasis; the former because of the tight weight budget on the DLRV and the fact that six wheels are involved, and the latter because of its importance in the successful completion of the prolonged mission.

The cone wheels' strongest points are its light weight, high reliability, and favorable structural characteristics. Its weight for the large diameter wheel was the lightest of those compared. Its reliability is enhanced by self-cleaning tendency and its post-failure behavior. (Cracks at the rim propagate into lower stress areas where degradation proceeds slowly.) Gradual stiffening rather than hard bottoming, high torsional and side load capability, and low one-"g" stress loading (implying long fatigue life) are all desirable structural characteristics. On the negative side, the cone wheel requires more stowage volume. With the selected stowage arrangement, much of the volume taken by the wheel comes from the crew station, where it would not be usable for permanently mounted equipment in any event; however, there is a loss of about 15% in usable stowage volume with cone wheels. This disadvantage is reflected mainly in growth capability, since there is adequate volume to stow all required equipment and science with any of the wheel candidates.

The conical convoluted wheel offers many of the advantages of the cone wheel but it takes less stowage volume. The folded geometry produces a moderate bottoming effect at about 2 g, and it allows for some debris entrapment.

2.4.1 Material Selection

An outstanding feature of the conical wheel is that it permits fabrication from a wide selection of candidate materials. Table 2-2 lists these candidates and compares the resulting wheel designs on the basis of their weight and structural and mission capabilities. The table presents properties at the maximum wheel temperature of 300°F; lower or negative temperatures yeild higher material allowables and are therefore less critical. The various wheel designs all have identical spring rates and the same general size and shape. In the critical weight comparison, the lightest wheel is found to be the aluminum one, with the fiberglass reinforced plastic (FRP) being a close second. The other materials are substantially heavier. Overload capability and fatigue life are also very important. The FRP and titanium wheels, with their low rations of static stress to endurance limit, should have good fatigue characteristics. The greater the overload capability of a wheel, the more forgiving it will be to operational hazards, such as obstacle encounters. The FRP, titanium, and hybrid wheels (titanium/aluminum) are equally good in load capability; the aluminum wheel has the least capability. Based on these results, FRP was selected as the wheel material for DLRV.

Extensive studies of the permanence properties of fiberglass/epoxy show that in air or under vacuum this material degrades primarily as a result of UV radiation. If the surface is protected from UV, there is no degradation, as shown by aging tests equivalent to one year exposure. The protective surface selected for this application is a .002-inch pigmented tedlar film integrally molded onto the wheel. Trevarno F-161 impregnating resin has been thoroughly tested at Grumman under in-house programs and under a contract to PLASTEC Corp. to provide data for the new edition of MIL-HDBK-17. This is

TABLE 2-2 CONE WHEEL MATERIAL EVALUATION

CANDIDATE MATERIALS	NORMALIZED WHEEL WEIGHT	PROPERTIES AT +300°F			
		1G Stress (KSI)	Endur. Limit (KSI)	Ultimate Strength (KSI)	Mission Load Capability (G's)
FRP F-161/7581 181 Fabric Epoxy	1.0	10	21	59	5.5
AL Alloy 2024-T81	.98	22	22	64	3.5
T1 6AL 6V 2SN (ANN)	1.36	29	67	125	5.5
Steel 17-7 PH (TH1050)	1.72	51	78	171	4.5
Dual Material T1 Rim - AL Hub	1.23	29	67	125	5.5

an excellent high-temperature resin and it retains much of its strength at temperatures as high as 400°F. Under low temperature, fiberglass becomes considerably stronger with little change in its modulus. "E" glass fabric may be used; however, "S" glass is a better choice since it provides at least 20% higher mechanical properties, and, in addition, appears to have superior fatigue properties.

Since the wheel component is critical to the design and performance of the DLRV, it might be advisable to carry a backup design of titanium or the hybrid titanium/aluminum into the hardware program. In this way, should any unforeseen problem arise with the FRP design, a completely compatible alternative would be available. (Grumman is pursuing in-house fabrication technology for both hot spinning and cold forming titanium.) The hybrid wheel design, which uses an aluminum hub section and a titanium rim offers good thermal and structural performance at a relatively low weight.

2.4.2 Wheel Preliminary Design

The design criteria for the wheel evolved from the configuration studies, and the mobility, dynamics and loads results discussed previously. These criteria are summarized in Table 2-3. Because of the large differences in static loads on the wheels during the mission, it was found advisable to design two wheel configurations, one for the heavily loaded control module, the other for the more lightly loaded power and science modules.

The preliminary design of the cone wheel is shown in Figure 2-11. It consists of three basic elements, a nominal .060-inch thick conical shell of revolution measuring 36 inches in diameter and 15 inches in depth, twenty-four grouser cleats fastened in a space-link arrangement to the wheel rim section, and a .090-inch diameter cable assembly which interconnects the cleats aiding their support. The wheel assembly with cleats attached has a 38-inch diameter and a 17-inch depth.

The conical shell element provides the wheel assembly with its necessary spring and structural characteristics. A combination of shape, thickness

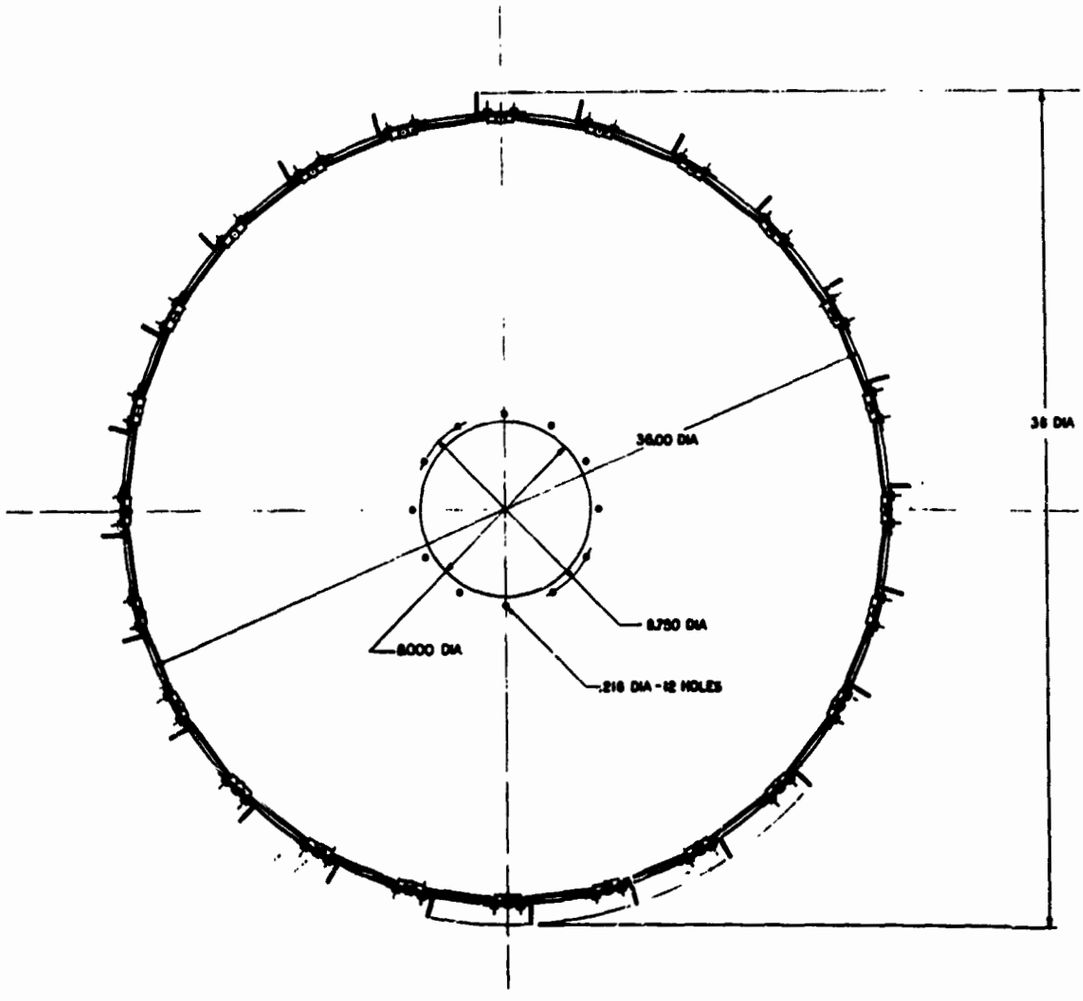

FOLDOUT FRAME 1

NOTES:

1. TEXARMID F-161 PREP FROM COAST MFG., DIVISION OF HEXCEL USE 7781-950 GLASS FABRIC.
2. FABRICATE PER GRUMMAN STD. SPEC. 11102A AND MATERIAL PER GRUMMAN MATERIALS PROCUREMENT SPEC 4001
3. LAY UP TO BE ISOTROPIC WITH 3 PLIES MINIMUM.
4. CURE AND POSTCURE PER G.S.S.11102A.
5. STRUCTURAL FILLER MATERIAL TO BE EPOCAST 1310 OR EQUIVALENT.
6. OUTSIDE COATING TO BE EITHER TEDLAR FILM, .002" THICK, ONE SURFACE TREATED FOR ADHESION (DUPONT) OR A PIGMENTED EPOXY ENAMEL PER G.S.S.4505.
7. ALL FAYING SURFACES TO HAVE A PEEL PLY.
8. .002" ALL OVER AND TFE FILLED POLYURETHANE COATING ON SURFACE INDICATED

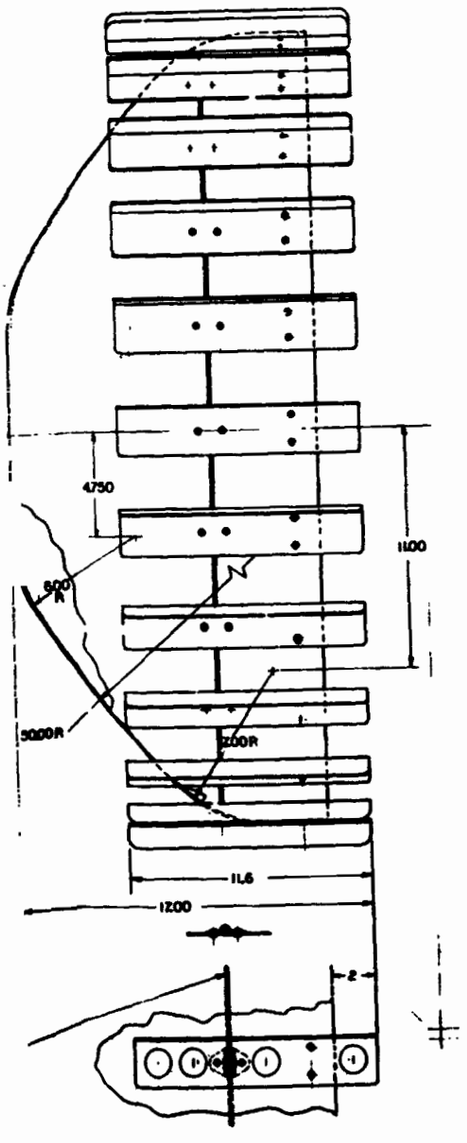

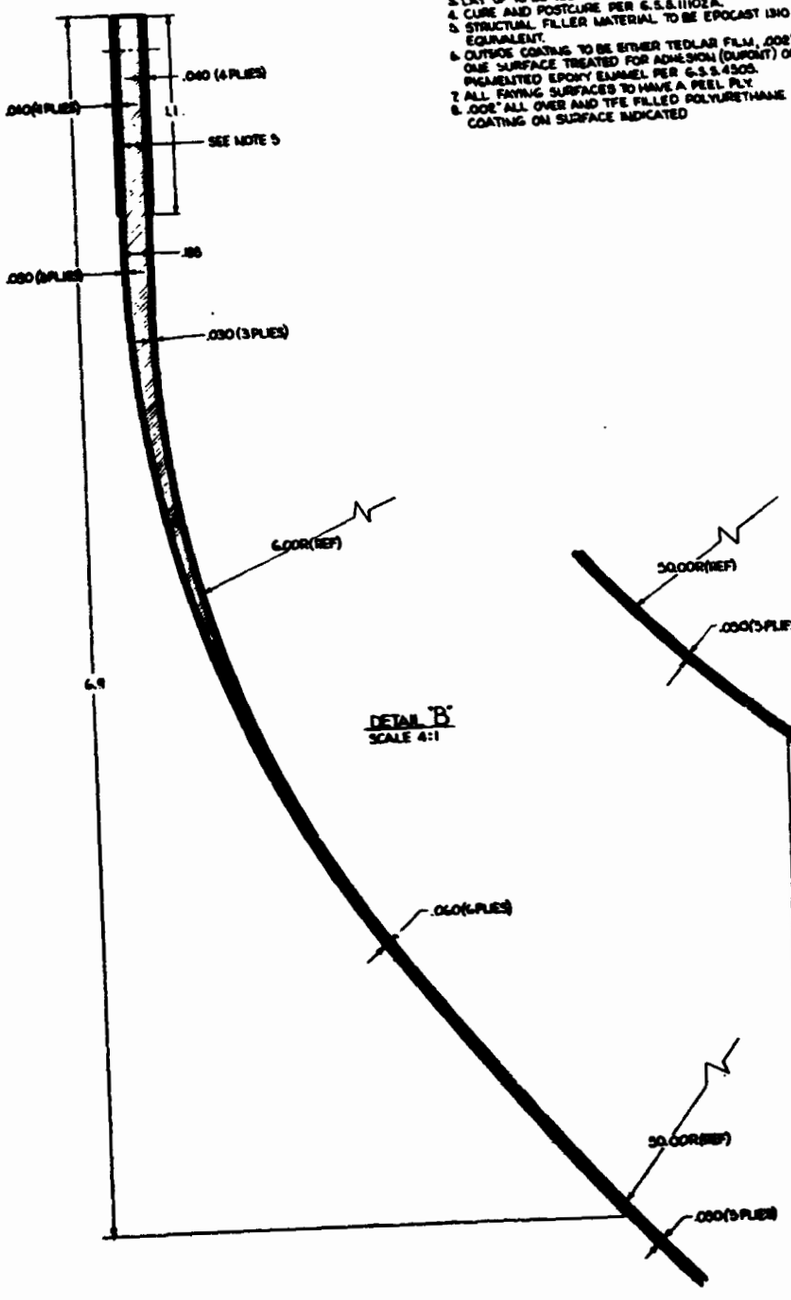

DETAIL "B"
SCALE 4:1

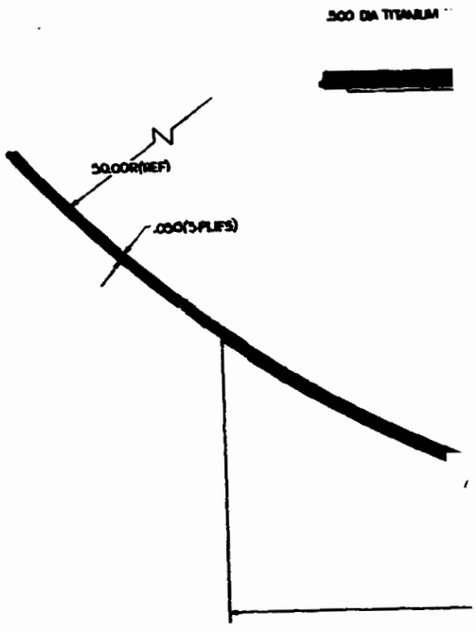

FOLDOUT FRAME 2

NOTES:

1. TERNARIO F-161 FREP FROM COAST MFG. DIVISION OF HEXCEL USE 7781-550 GLASS "ASBRIC.
2. FABRICATE PER GRUMMAN STD. SPEC. 11102A AND MATERIAL PER GRUMMAN MATERIALS PROCUREMENT SPEC 4001
3. LAY UP TO BE ISOTROPIC WITH 5 PLIES MINIMUM.
4. CURE AND POSTCURE PER G.S.S.11102A.
5. STRUCTURAL FILLER MATERIAL TO BE EPOCAST 1310 OR EQUIVALENT.
6. OUTSIDE COATING TO BE EITHER TEDLAR FILM, .002" THICK, ONE SURFACE TREATED FOR ADHESION (DUPONT) OR A PIGMENTED EPOXY ENAMEL PER G.S.S.4505.
7. ALL FAYING SURFACES TO HAVE A PEEL PLY.
8. .002" ALL OVER AND TFE FILLED POLYURETHANE COATING ON SURFACE INDICATED

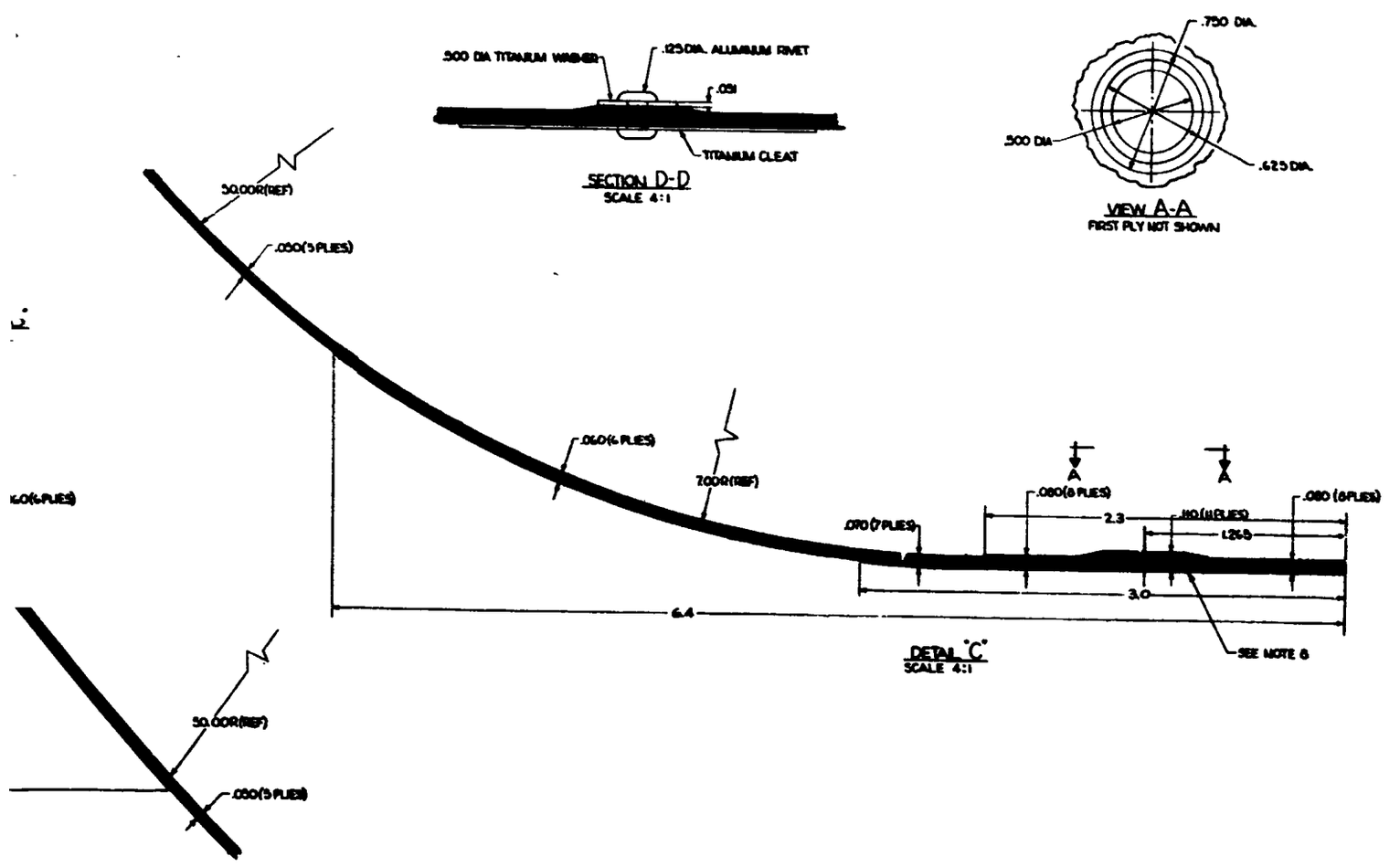

FIG. 5.2-2 DLRV WHEEL ASSEMBLY

TABLE 2-3 WHEEL DESIGN CRITERIA

	CONFIG. "A"	CONFIG. "B"
Static Design Load	55	40
Wheel Dia. with Cleats (lb)	38	38
Max. Radial Load (lb)	300	220
Max. Lateral Load (lb)	174	127
Max. Torque (lb-ft)	100	100
Effective Soil Pressure (psi)	1.0	1.0
Thermal Range (°F)	±300	±300
Life Cycles (Revs)	10^6	10^6
Cleat Type	Grouser Space Link (Typ.)	
Cleat Length (in.)	12	12

Configuration "A" - Control Module Wheels

Configuration "B" - Power and Science Module Wheels

distribution and materials is used to achieve the desired cone wheel characteristics. The conical shell is fabricated from fiberglass reinforced plastic using style 778 fiberglass and Trevarno F-161 epoxy resin. A thin surface coating of Tedlar provides protection against ultraviolet radiation and improves wear resistance. The grouser-type cleat is used to enhance the wheel's traction and obstacle negotiation capability. Titanium alloy Ti-6AL-4V has been selected for the cleat material because of its superior resistance to abrasive wear and its thermal properties. The cleat has an open right-angle cross section allowing it to penetrate the lunar soil and perform its grouser thrusting action. The cleat spacing selected is based on consideration of assembly weight, cleat reliability, and soil-bridging effects (as reported in Section 2.4.3). Tests have shown that a negligible increase in wheel rolling resistance is attributable to the cleat system. A feature of the grouser cleat system is the intercleat tensile attachment which acts to stabilize the cleat in active contact with the lunar surface and distributes the concentrated loads around the rim. This permits a lighter weight fiberglass cone to be used. A .090-inch diameter stainless steel flexible cable assembly is used for the intercleat member. The shape of the wheel is determined by load/deflection requirements and delivery vehicle stowage envelope constraints. The 38-inch diameter is the largest stowable wheel. The 17-inch depth and associated curved shape is designed to provide an initially soft spring rate to develop to develop a large static deflection and footprint, followed by gently stiffening characteristics for overload. The hub area is flat and reinforced with a lightweight core filler to provide additional strength and to accommodate the wheel drive assembly.

2.4.3 Mobility Performance

Vehicle mobility is primarily measured in terms of rolling resistance and drawbar pull capability. As part of the development program for the cone wheel concept much test data was obtained at Grumman's lunar test site and

at the Stevens Institute of Technology "Land Locomotion Laboratory" under the direction of Dr. I. R. Ehrlich. The following discussion will show how mobility performance is defined and how it is related to wheel and motor gear box requirements. Early tests with Grumman's 1 "g" LRV simulator and later tests with prototype 1/6 "g" wheels are presented. The performance data presented is the latest available and should be considered "representative" of the anticipated performance of the wheels delivered under this contract. It should be noted that some of these data require weight ratio scaling to convert 1 "g" earth simulator data to its lunar equivalent.

2.4.4 Rolling Resistance

Total wheel drag R that must be overcome by the wheel motors consists of three components:

- Rolling resistance R_z due to soil compaction and sinkage z
- Parasitic losses R_p due to wheel flexure and cleat/soil scuffing
- The gravity component R_g when climbing a slope

Hence: $R = R_z + R_p + R_g$

The latter component, R_g, is equal to $W\sin\alpha$ where W is wheel loading and α is slope angle. R_p is proportional to wheel loading and could be expressed as qW, where q is generally equal to a few percent. As to the soil compaction resistance, R_z, it can be shown that

$$R_z = \frac{bp_e^{n+1}}{(n+1)k}$$

or

$$R_z = \frac{bp_e^2}{2K} \quad \text{for } n = 1 \quad (1)$$

where b is wheel width, p_e is effective footprint pressure, k is soil sinkage modulus and n is the power of the p/z relations, with n = 1 indicating a linear relation. A one-g version of a 42" flexible cone wheel was tested at

Stevens Institute and the results are reported in Reference 1. A 1/6-g, 38"-diameter wheel was tested at Grumman's Peconic facility at various loadings and with two types of cleats. The latter wheel simulates the actual DLRV proposed wheel design. The results of the one-g wheel tests are given in Table 2-4. The 300-lb wheel loading provides a wheel deflection comparable to that of the 1/6-g wheel at 55 lbs. The tests on hard ground show a parasitic loss, R_p, of 3.8% wheel loading. The test wheel had rubber padded cleats, however, and the parasitic losses would be less for the rigid cleated DLRV wheel. The effective footprint pressures were calculated in Table 2.4 and indicate that about 37% of the measured area is effective in carrying the wheel load. The measured areas were calculated using full footprint lengths, i.e., assuming full bridging between cleats.

Two versions of the 1/6-g, 38"-diameter wheel were tested by GAC, one with 7" rectangular wood cleats and the other with 11 5/8" extruded angle cleats. The deflection characteristics and graphical footprint length of the wheel are shown in Figure 2-12. The test apparatus consisted of a single wheel canted at 15° and connected to a frictionless pivot by means of a 12-ft rigid member, as shown in Fig. 2-13. The wheel was revolved around the pivot by pulling by hand at a point near the hub. A dynamometer and a recorder capable of measuring the turning force to the nearest 1/4 lb. was used. The test was performed on asphalt and soft sand. A roto-tiller was used to loosen the sand before each pass. Cone index readings of the uncompacted sand gave a penetration gradient, G, of 1 to 2 psi/in for the top 4". It is permissible to assume that at these low values, the G parameter is nearly equal to the soil sinkage modulus k. Additional measurements of soil constants included the angle of internal friction, ϕ, by means of a "Sheargraph" and the cohesion, c, by means of a "Torvane". Values of $\phi = 35°$ and $c = 0.13$ psi were measured.

The 1/6-g wheel test results are plotted in Figure 2-14. The parasitic loss with the 7" cleats is 2.1% of wheel loading which is appreciably lower than the 3.8% measured for the one-g wheel.

TABLE 2-4

TESTS OF 1g FLEXIBLE WHEEL AT STEVENS INSTITUTE

Rubber Padded Rectangular Cleats
Wheel Loading of 330 lb
Wheel Diameter 42 inches
Cleat Length 10 inches = b

	Hard Surface	Firm Soil	Soft Soil
k, psi/in		$9 + \frac{1}{2}$	$1\frac{1}{2} \pm \frac{1}{2}$
Towing force, lb., average of 6 runs	12.4	30.3	56.2
Wheel sinkage, in, average of 6 runs	2.8	2.1	3.7
Measured footprint area, sq. in.		153	246
Footpring pressure using measured area, psi		2.16	1.34
Rolling Resistance, Rz, lb	12.4	17.9	43.8
Effective footprint pressure, $p_e = (2k\ R_z/b)^{\frac{1}{2}}$		5.68	3.62
Effective area ratio, p/p_e		.38	.37

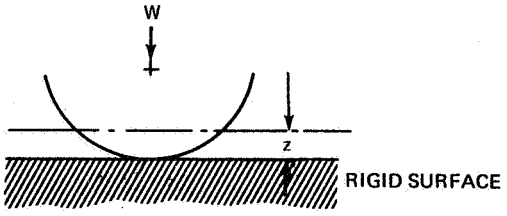

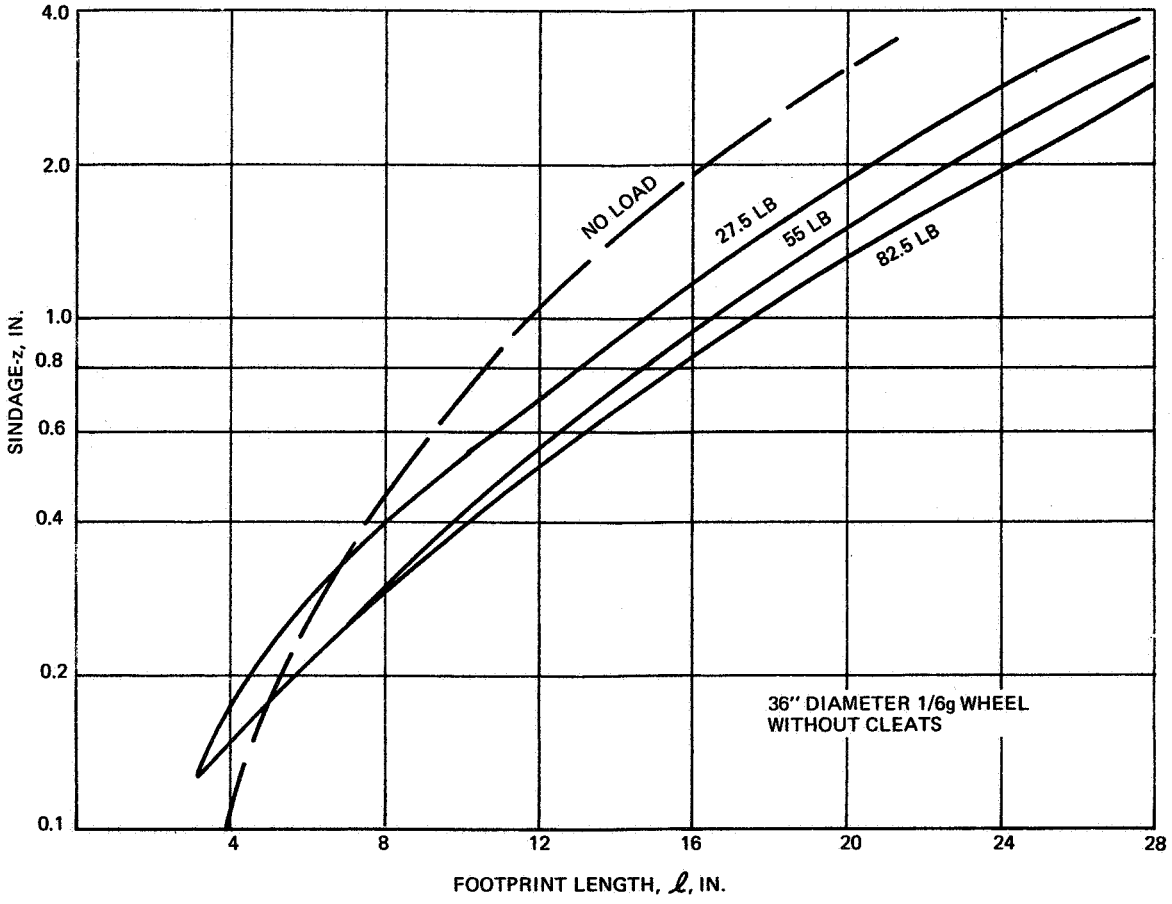

Fig. 2-12 **FOOTPRINT LENGTH VS SINKAGE**

Fig. 2-13 **TEST APPARATUS FOR ROLLING RESISTANCE**

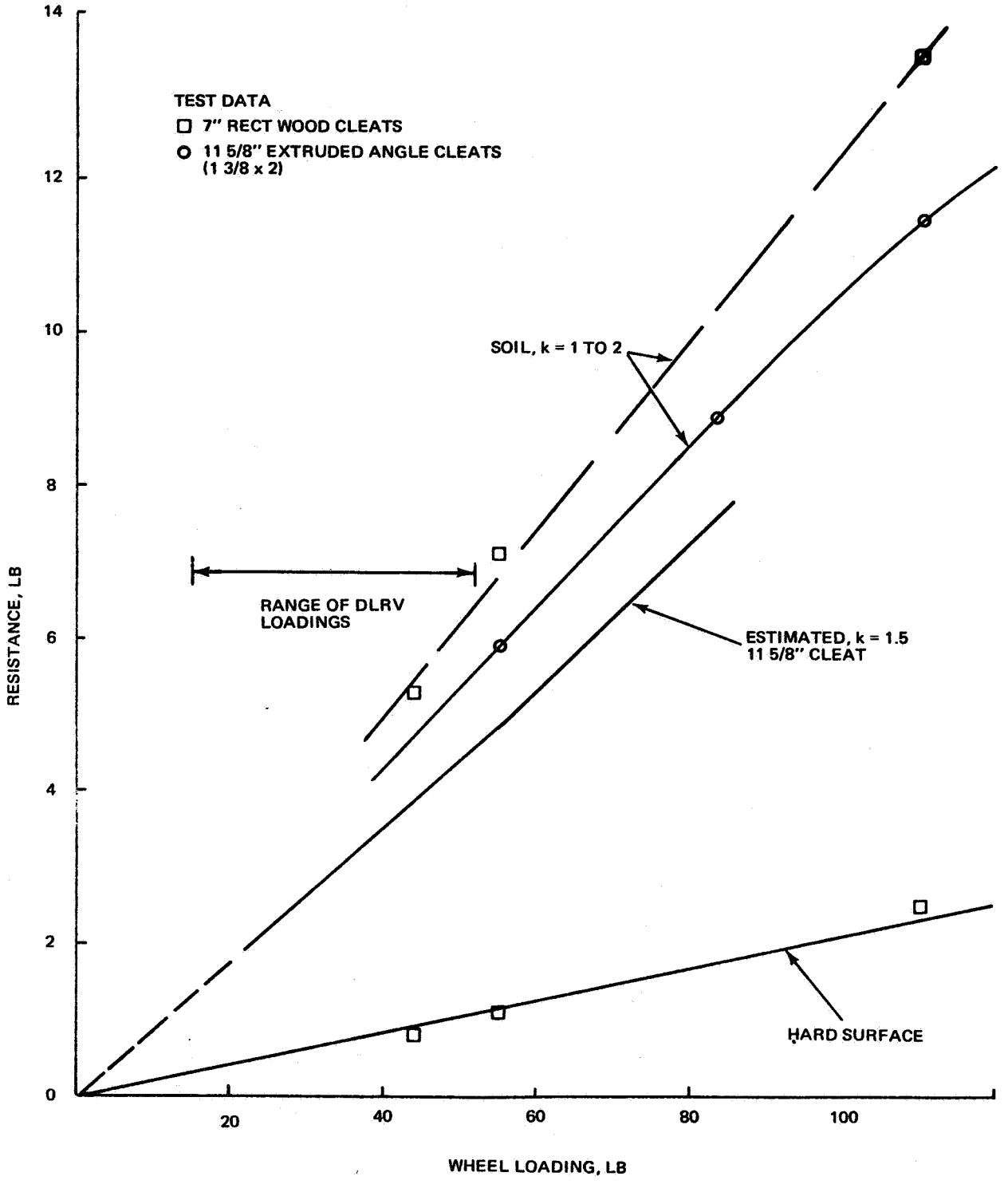

FIG. 2-14 TESTS OF 38" 1/6g WHEEL

The estimated values for the 11 5/8" cleat and k = 1.5 are also compared in Figure 2-14. These estimates were made using the following procedures:

1. The graphical footprint lengths were determined from Figure 2-12
2. The effective areas were calculated using the above lengths, the cleat length of 11 5/8, and the effective area ratio of .37 determined from the Stevens tests
3. The effective footprint pressure, p_e, and the soil pressure, $p = kz$ are plotted in Fig. 2-15. Curves intersect at the equilibrium point. Equilibrium pressures are tabulated below for k = 1.5.

W lb	Pe Psi
27.5	0.70
55.0	0.97
82.5	1.22

4. Rolling resistance was calculated from equation (1) using the equilibrium pressures. A parasitic loss of 2.1% was added.

It is seen in Figure 2-14 that the estimated resistance value is about 80% of the test value. This is attributed to non-optimum cleat spacing and cleat deflections on the test wheel. It is assumed that the estimate for k = 1.5 is representative of the rolling resistance for all lunar terrain since (1) cleat design will be refined and (2) the reduction in rolling resistance of the tracking wheels has been neglected. Grumman tests of the 38", 1/6-g wheel with the 7" cleats (k = 1-2) showed a reduction in average resistance to 92% for 2 passes and 87% for 3 passes. Wheel loading, however, was high, 110 lb. Comparable results were obtained from the Steven's tests in soft soil (k = 1 to 2) where the average resistance was reduced to 85% for 2 passes.

In order to evaluate required torque for wheel drive motors, it is necessary to determine wheel loading for both level and sloping terrain. The results of these computations are shown in Table 2-5 for representative unmanned and

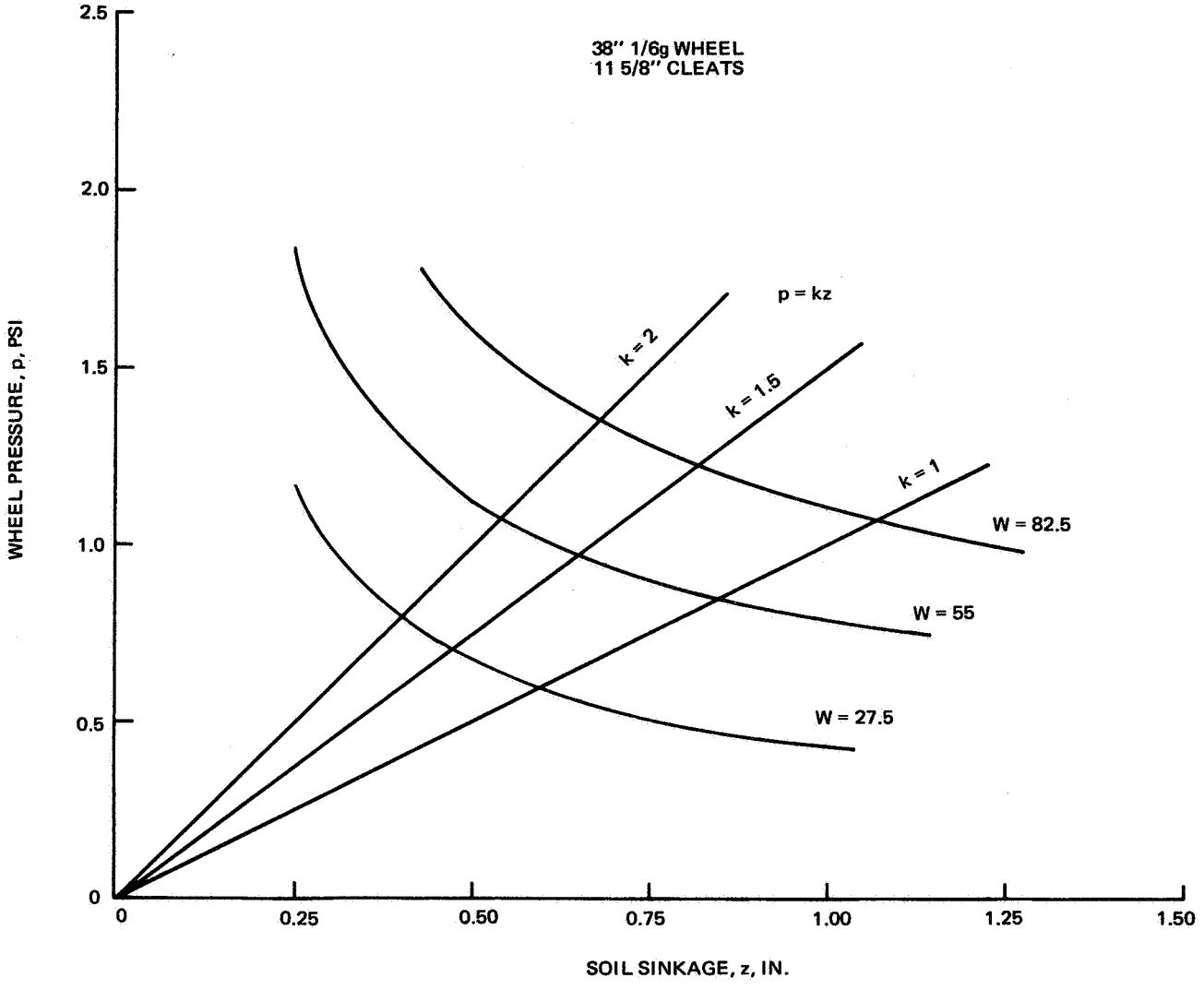

FIG. 2-15 ESTIMATED WHEEL PRESSURES VS SINKAGE

TABLE 2-5

CALCULATION OF REQUIRED WHEEL TORQUE

A. Unmanned operation with 100 lb of samples and RGM for a total vehicle weight of 972 lb

Wheel	Slope (deg)	Wheel Loading (lb)	Rolling Resistance & Parasitic Losses (lb)	Gravity Resistance (lb)	Total Resistance (lb)	Required Torque (ft-lb)
Control Module (Rear)	0	26.4	2.4	0	2.4	3.8
	20	34.0	3.0	12.4	15.4	24.4
	35	37.1	3.3	26.0	29.3	46.4
Power Module (Middle)	0	24.5	2.2	0	2.2	3.5
	20	16.7	1.5	6.1	7.6	12.0
	35	9.5	0.9	6.6	7.5	11.9
Science Module (Front	0	30.1	2.7	0	2.7	4.3
	20	25.4	2.3	9.3	11.6	18.4
	35	19.8	1.8	13.9	15.7	24.8

B. Manned operation with one astronaut and no samples for a total vehicle weight of 946 lb

Control Module (Front)	0	52.0	4.6	0	4.6	7.3
	20	39.4	3.5	14.3	17.8	26.2
	35	26.7	2.4	18.7	21.1	33.4
Power Module (Rear)	0	27.0	2.45	0	2.45	3.9
	20	34.7	3.1	12.6	15.7	24.8
	35	37.9	3.4	26.6	30.0	47.5

manned loadings. The total resistance due to the rolling resistance, R_z, and the parasitic losses, R_p, were taken from Figure 2-14 using the estimated curve for k = 1.5. Required torques vs. slope are plotted in Figure 2-16. The average level traverse torque required is 3.9 ft-lb per wheel for unmanned operation and 5.6 ft-lb per wheel for manned operation. These were rounded off conservatively to 4.0 and 6.0 ft-lb respectively for all calculations of level traverse performance.

2.4.5 Slope Climbing

The slope-climbing ability of a vehicle and its power consumption on level terrain and on slopes depend on a complex interaction of soil and wheel properties including sinkage and slip. While analytical estimates are possible, they must ultimately be verified or supplemented by full-scale field tests. The pull coefficient, or ratio of draw bar pull to wheel normal load (P/W), is essentially equal to the tangent of the slope that the vehicle can climb. The actual climbable slope will be somewhat less than this value due to such factors as redistribution of wheel loading and reductions of soil bearing strength due to the slope angle.

Two reasons contributed to the selection of wide cleats for the DLRV wheels. One reason was to take advantage of the cohesive nature of lunar soils, and the relatively large contribution of soil cohesion to the total tractive effort in a 1/6-g field. This factor argues for a large footprint, hence, for a wide cleat. The selected size, 11 5/8 inches, is the largest that can be accommodated. The other reason for selecting the wide cleat was to reduce footprint pressure and, hence, rolling resistance, as shown by test data in Figure 2-14. Soil bin tests involving a single prototype wheel are very useful as they permit a better control of the soil and wheel parameters. DLRV type wheels have been tested at Stevens Institute (Reference 1), as previously mentioned, and at Waterways Experiment Station (WES) (Reference 2). Both wheels were 42" diameter. A 1-g version was tested at Stevens, a 1/6-g

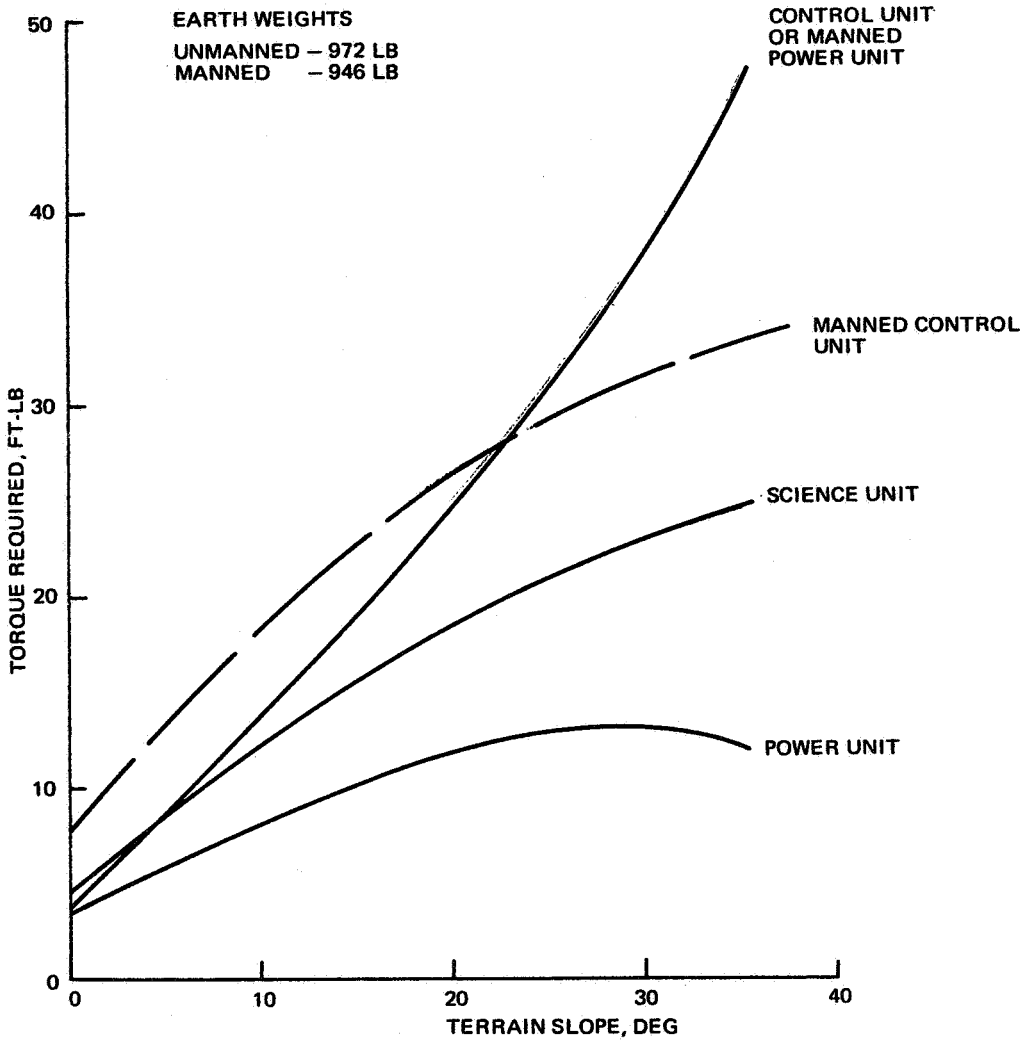

Fig. 2-16 **WHEEL TORQUE REQUIRED VS SLOPE**

version was tested at WES. The test measurements, soil conditions and cleat configurations are listed below for the Stevens tests.

SOIL BIN TEST CONDITIONS Ref. (1)

(wheel loading = 330 lbs)

Measurements	Soil Conditions	Cleat Configuration
Draw bar pull vs. slip	Cohesionless sand	10-inch flat plate
Torque vs. slip	Soft, k or G=1 to 2	12-inch, $1\frac{1}{2}$ x $1\frac{1}{2}$ in. angle cleat
Sinkage	Firm, k or G=8 to 10	
Footprint length		
Wheel and carriage speed		

The draw bar pull, torque and locomotion efficiencies vs. % slip are shown in Figs. 2-17 to 2-20 and pertinent results are summarized in Table 2-6. Locomotion efficiency is defined as

$$\eta = \frac{PR}{T}(1-s)$$

where R is nominal wheel radius, T is wheel input torque and s is slip. We may draw the following conclusions from these tests:

- In all four cases, that is regardless of soil or cleat conditions, the slip on level ground in the self-propelled mode (when DBP = 0) is 1 to 1.5 percent.
- The increase in rolling resistance due to the angle cleats is negligible on level ground or at low draw bar pull levels.
- The addition of the angle cleats increases the maximum draw bar pull by 54% in soft soil and by 50% in firm soil. However, a penalty in rolling resistance, hence, in locomotion efficiency, is paid to achieve the higher draw bar pull. This penalty is 9% in soft soil and 22% in firm soil. In conclusion, the angle cleats deliver significantly more draw bar pull in all soil conditions with less cost in efficiency in soft soil than in firm soil.

The Grumman wheel achieved a peak pull coefficient of 0.64 in the Waterways Experimental Station soil bin test, Ref. (2), as against a pull coefficient of 0.45 in the Stevens Institute soil bin test, Ref. (1). These coefficients

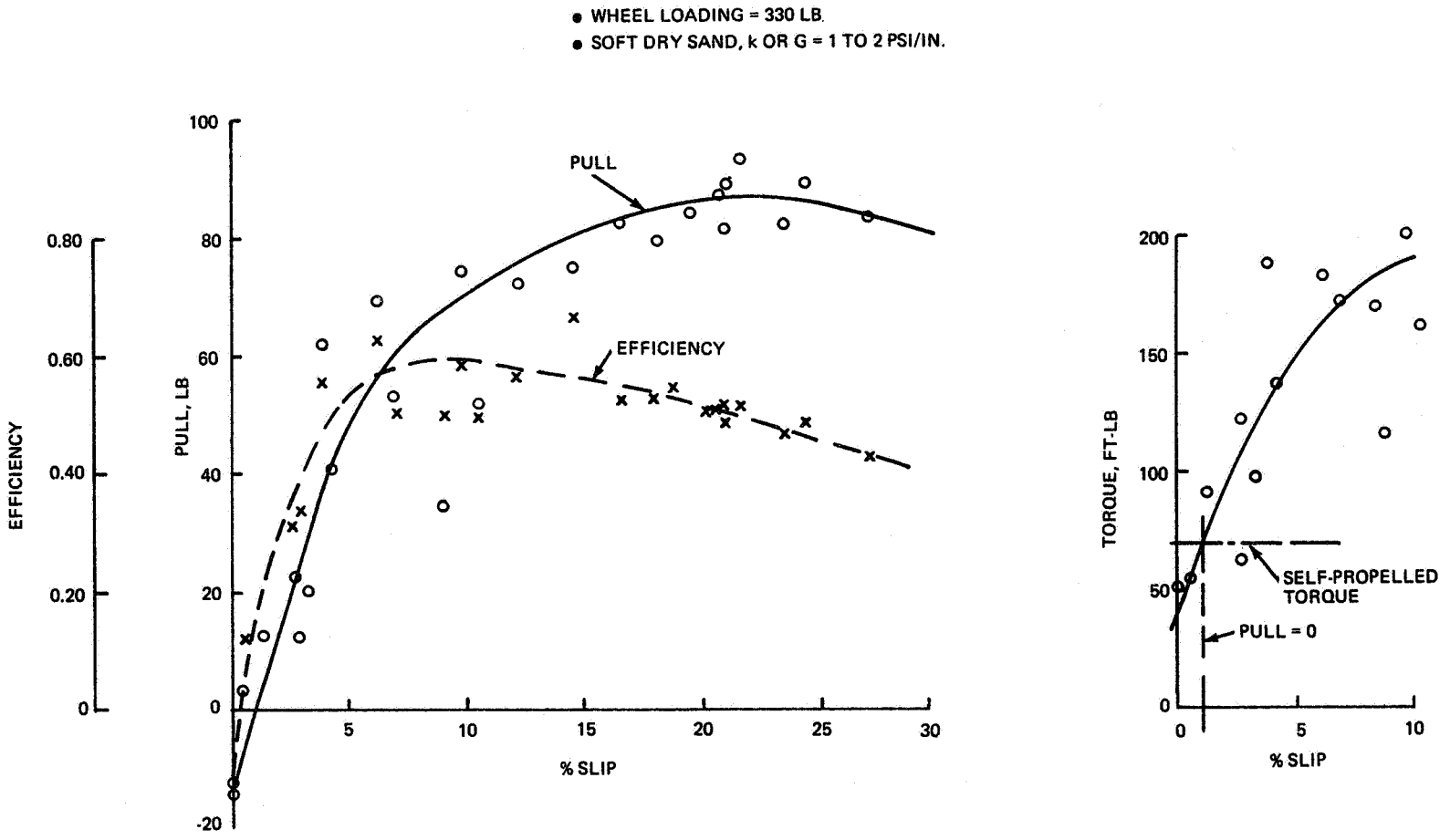

Fig. 2-17 SOFT SOIL WHEEL PERFORMANCE, 10-INCH CLEAT

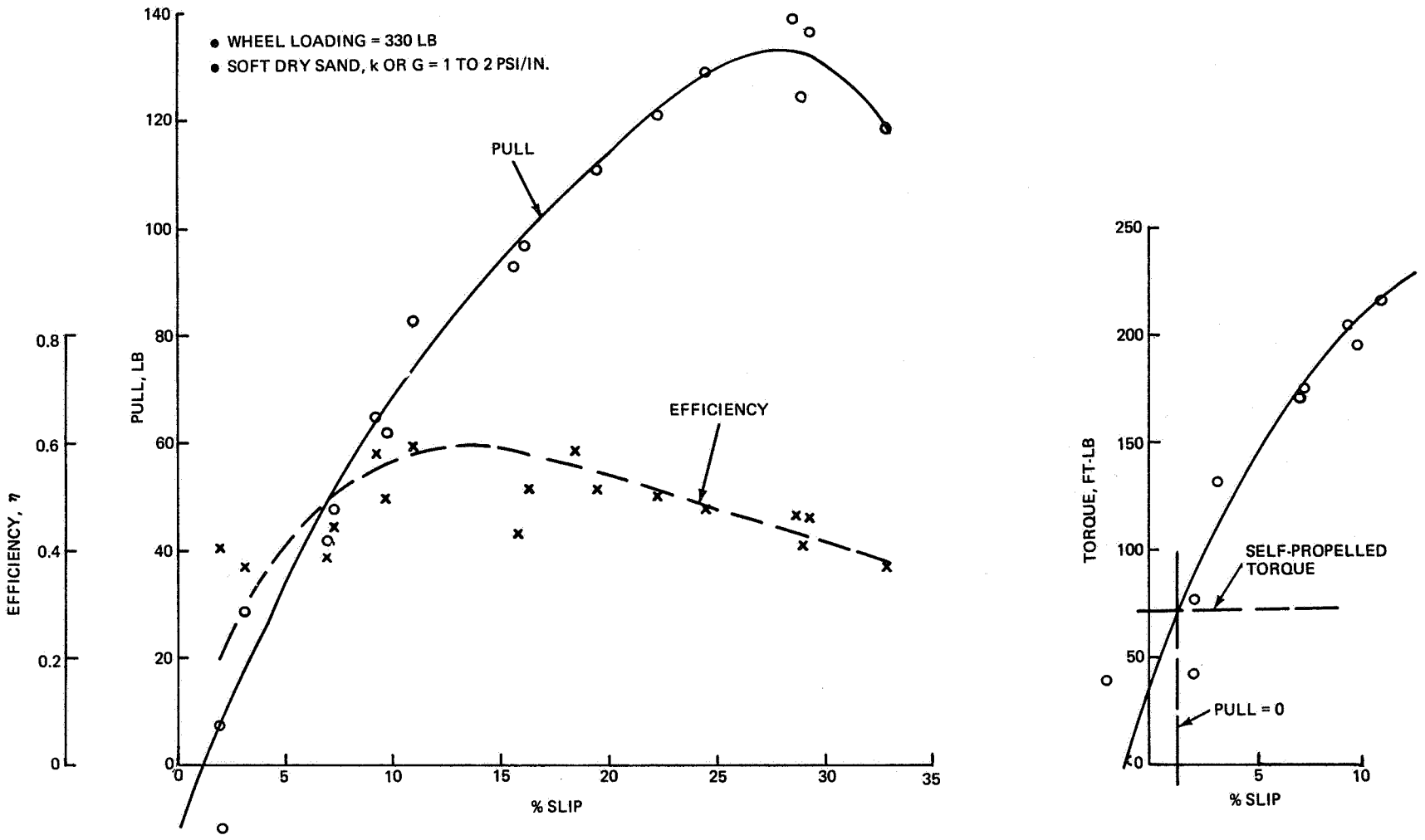

Fig. 2-18 SOFT SOIL WHEEL PERFORMANCE, ANGLE CLEATS

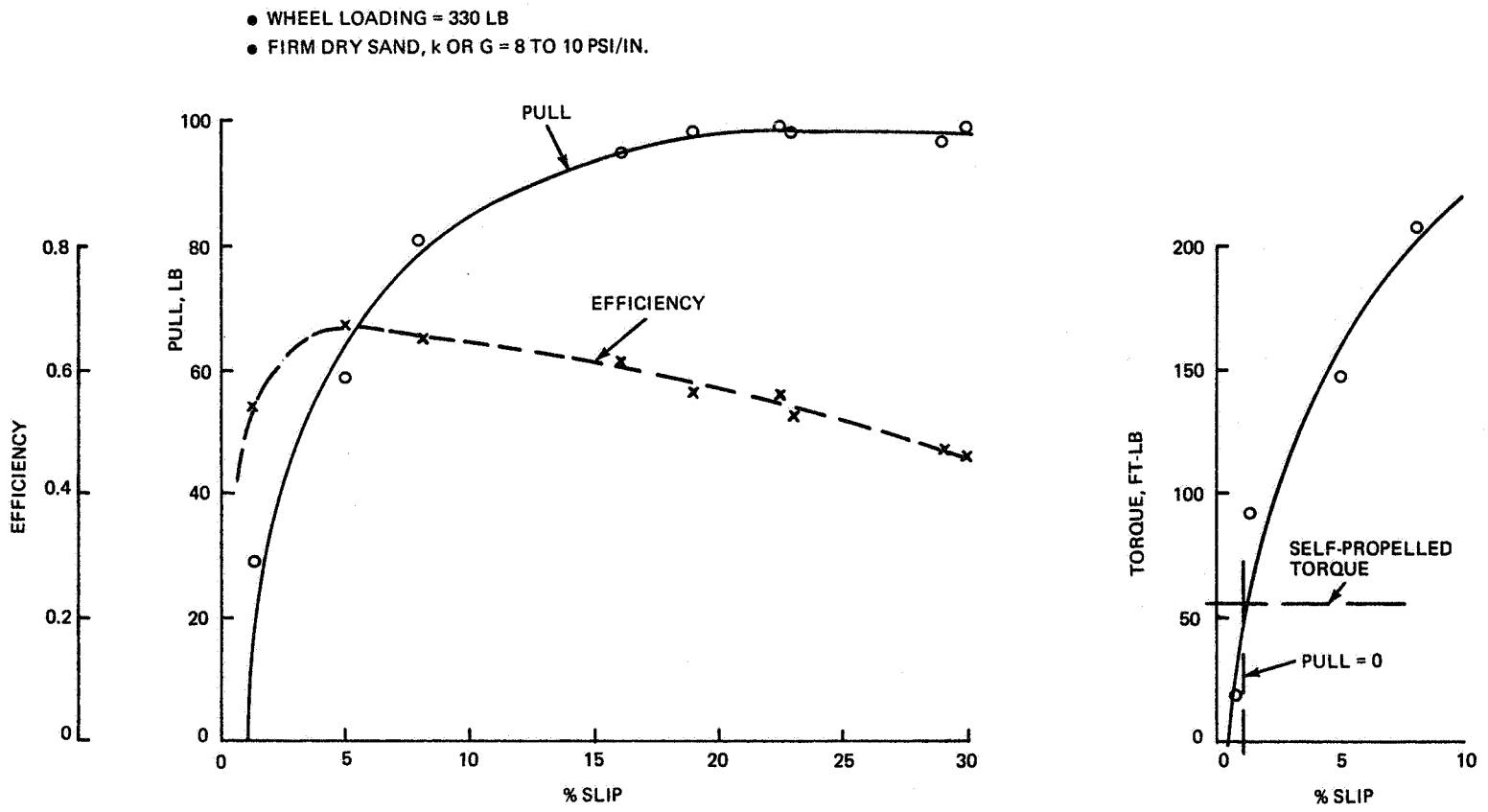

Fig. 2-19 FIRM SOIL WHEEL PERFORMANCE, 10-INCH CLEATS

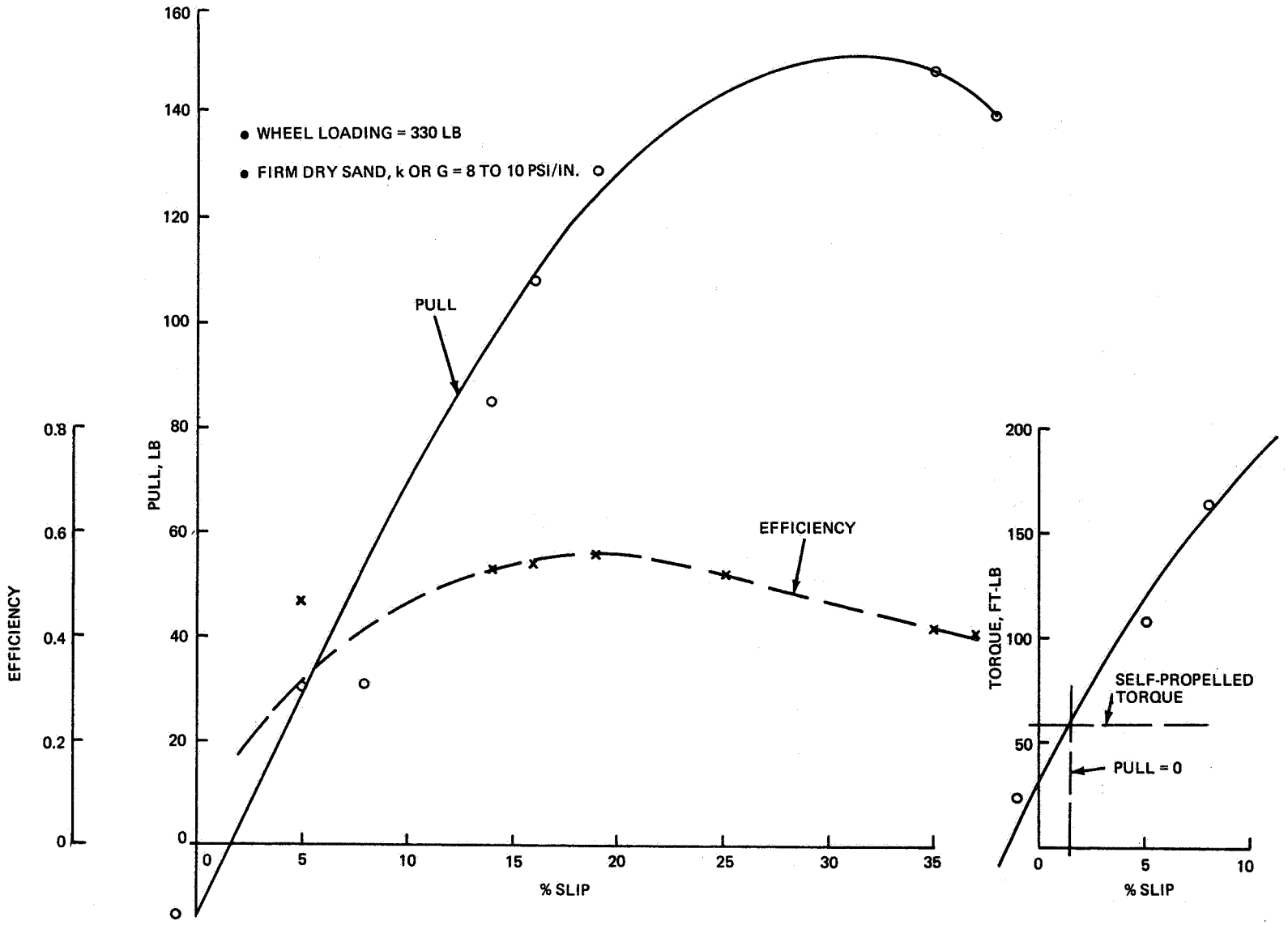

Fig. 2-20 FIRM SOIL WHEEL PERFORMANCE, ANGLE CLEATS

TABLE 2-6

STEVENS SOIL BIN TEST RESULTS

1-g Wheel, 42-inch diameter, W = 330 lb

SOIL (dry, cohesionless sand)	CLEATS	P = 0 (Level Terrain)			MAX.P/W			MAX. EFFICIENCY		
		% Slip	Torque ft-lb	Rolling Resistance lb	P/W	% Slip	% Eff.	P/W	% Slip	% Eff.
k = 1 to 2	10" flat	1	70	40	.26	22	49	.20	9	60
	12" angle	1.3	73	42	.40	28	45	.27	14	60
k = 8 to 10	10" flat	1	55	31	.30	22	55	.19	5	67
	12" angle	1.5	58	33	.45	32	45	.36	18	56

correspond to maximum climbable slopes of 33° and 24° respectively. The Cone Index gradient, G, of the soil in both tests was approximately the same; more specifically, it was 9 psi/in. (Stevens tests) and 12 psi/in. (WES tests). The discrepancy between the two test results may be adequately accounted for in terms of the following differences in the test conditions:

- o A 1-g wheel under a loading of 330 lbs was used in the Stevens tests, as against a 1/6-g wheel under a loading of 70 lbs in the WES tests
- o A dry cohesionless sand (c = 0) was used in the Stevens tests, as against a moist, relatively finer sand with a measured cohesion of 0.16 psi in the WES tests

Figure 2-21 shows the resolution of these data and the theoretical relationship between maximum climbable slope (pull coefficient) and wheel loading at various soil cohesions. Steven's P/W of .45 for c = o is considered independent of wheel loading. The effective footprint length necessary to account for the WES results at c = .16 was used on conjunction with Figure 2-12 to determine the assumed footprint length, l_e, vs. loading. P/W was then computed from

$$P/W = (P/W)_{c=o} + (P/W)$$

$$= (P/W)_{c=o} + l_e\, bc/W$$

$$= 0.45 + 12\, l_e\, c/W$$

where b = 12 in. = cleat width

Cohesion in lunar soils is necessary if the vehicle is to climb a 35° slope in the low gravity of the moon. Notice how, at a given cohesion, climbable slope increases with decreasing wheel loading

Although the wheels tested are not identical to the DLRV wheels, the results are representative of DLRV slope climbing capability. These results indicate that the DLRV wheel can climb a 35° slope under expected wheel loadings if the soil has a cohesion of the order of 0.1 to 0.2 psi. It is recommended that additional tests be performed to optimize the cleats at wheel loadings from 10 to 50 lb in soils with cohesion from 0.1 to 0.4 psi.

Although these data had been presented in the DLRV final report, insufficient time was available to incorporate the latest cleat configuration test presented herein into the overall wheel design shown for the DLRV. Section 3 of this report relates how these data were used to design the cleat for this study.

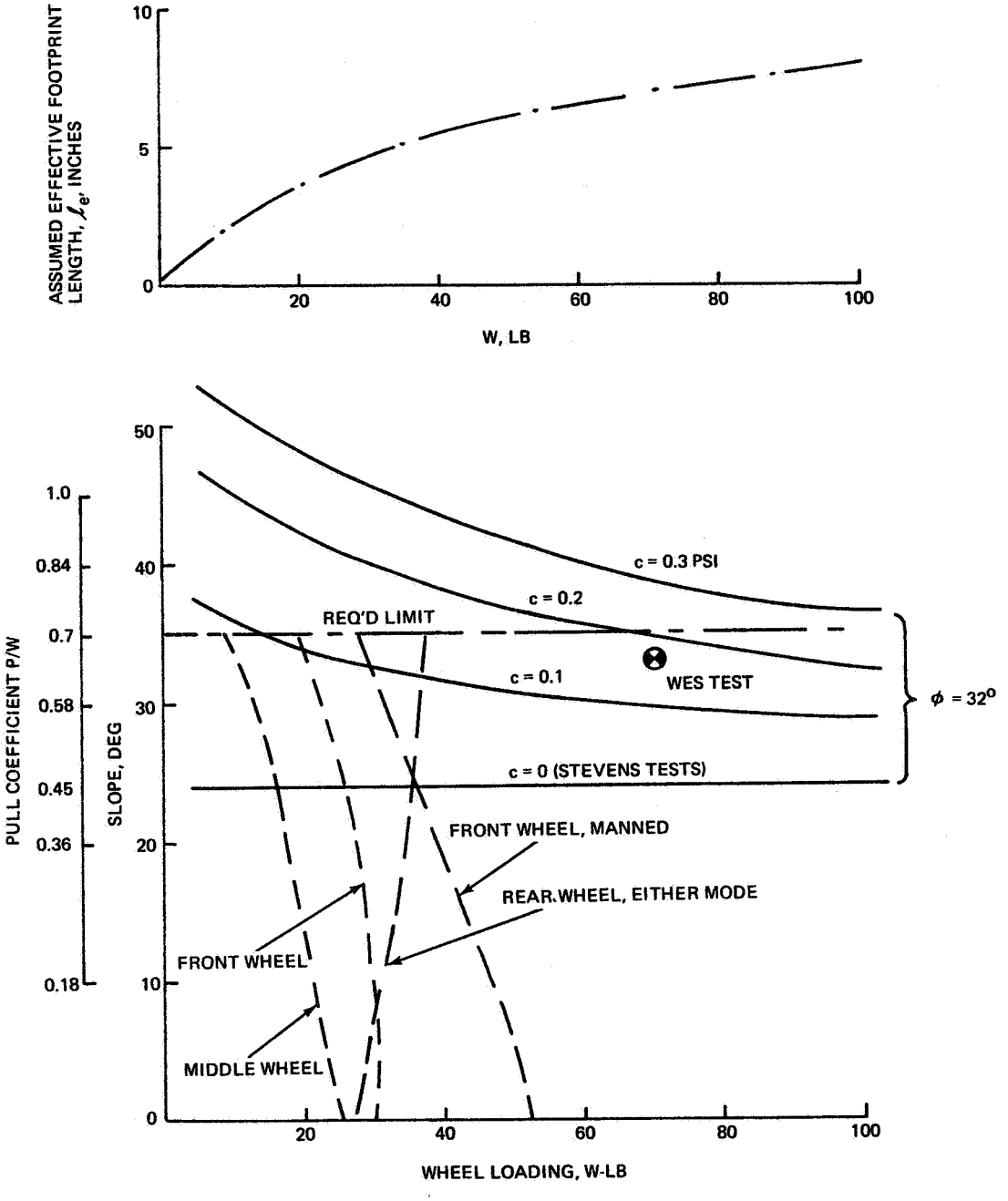

Fig. 2-21 MAXIMUM SLOPE CLIMBING ABILITY, 42" WHEEL, 12" ANGLE CLEATS

2.4.6 References for Section 2.4

1. Stevens Institute of Technology, Davidson Laboratory, "Tests of Lunar Rover Wheel", by L. I. Leviticus and I. R. Ehrlich, Report 1429, November 1969.
2. U. S. Waterways Experiment Station, "Study of Mobility Performance and Slope-Climbing/Traversing Ability of Lightly Loaded Wheeled Vehicle on Soft Soil", Fourth Monthly Progress Report, 1-30 Sept. 1969, Contract DPR H-58504A.

2.5 SUMMARY OF DYNAMIC DESIGN CRITERIA

The following data were extracted from Grummans DLRV final report specifications, updated to reflect additional testing and revision to the cleat configuration. The wheels shall be conical in shape with grouser-type cleats attached to the rim-running surface. The wheel material shall be fiberglass reinforced plastic with eight plies at the hub and rim and five plies in between. The hub section shall be reinforced and configured to accept the center line mounting of the wheel drive assembly. The wheel assemblies shall be designed to satisfy the following operational requirements:

	Control Module Wheels
Static design load (lb)	55
Max. radial load (lb)	300
Max. lateral load (lb)	174
Max. torque (lb-ft)	100
Static 1g deflection (in)	1.8
Drawbar pull per unit weight (minimum)	.6
Nominal spring rate about 1 g static (lb/in)	60
Weight (lb maximum)	15.0
Wheel diameter (in)	38

Cleats shall be formed of 0.025 inch titanium. Each wheel shall have 30 cleats equally spaced about the rim.

3 DESIGN DEVELOPMENT AND SELECTION

3.0 GENERAL

The primary study objective was to design and deliver to NASA three test wheels compatible with the DLRV mission requirements. An iterative design evaluation was followed based on Grumman's previous experience with its full scale DLRV simulator, design studies conducted for the DLRV phase B study, and additional emperical test data obtained during this study.

3.1 STRUCTURAL ANALYSIS

The cone wheel structure is a thin open shell of revolution consisting of a hub, a conic section, and a rim joined by two transition radii. The rim along with the first transition radius serves as a hoop to distribute the load to the conic section and also prevents the conic section from buckling. The conic section carries the load to the hub as a large thin-walled tapered tube and also acts as a cantilever beam for the lower segment of the conic section. In designing this type of wheel the objective is to keep the stresses in the rim area about equal to those in the hub area; this concept of having balanced stresses enhances the overall design.

Wheel deflections at the rim can be very large, making any analysis of the area quite difficult. Experimental test results have been used instead to form an emperical basis for the cone wheel design.

The area from the hub to a region near the rim is not subjected to such large deflections, and can be more readily analyzed. Grumman has a shell computer program (STARS II) that is capable of analyzing any structure that can be idealized as a combination of varying thin surfaces of revolution, including cylinder, ellipsoid, ogive, parabiloid and cone. The program obtains solutions to the equations of elasticity using assumptions of small displacement theory, and can handle symmetric and unsymmetric loadings. It has been used successfully at Grumman on a variety of shell structures including, among other, LM propulsion tanks, LM landing gear and foot pads. This program was used to size the cone wheel in the low deflection regions away from the rim.

Extensive full scale testing prior to this study on a 1/6-g FRP cone wheel, and 1 "g" earth equivalent were used to augment the analysis. Figure 3-1 shows the earlier instrumented wheel undergoing static testing. Normal loading on a flat surface, concentrated loading, and combined normal and drag loading conditions are shown. Note that the deformed shape under the concentrated load differs little from the flat surface load, indicating that there is no extreme stress build-up in the vicinity of a concentrated load with a cone wheel. The detailed results and discussion of this prior testing is included here to show continuity, and document under one cover, all relevant test data.

3.2 PRIOR GRUMMAN TESTING

3.2.1 Strain Gage Instrumented Test Wheel

Figure 3-2 shows the details of the 1/6 g cone wheel test article. The test wheel was made of 181 volan "A" fiberglass reinforced plastic (FRP). Ten strain gages were provided, covering the critical circumferential and meridional locations of interest, adjacent to the wheel rim. High elongation strain gages, identified by EP - 80 - 250 - MM - 120, were used. The hub area was not instrumented, because it was decided to concentrate the instrumentation in the rim area of the wheel.

3.2.2 Test Set-Up

A simple test fixture was erected to obtain load-deflection characteristics of the cone wheel. The test fixture, shown in Figs. 3-3 and 3-4 was designed to rigidly restrain the wheel at a 15° positive camber angle.* The test wheel was attached at the axle to a rigid hub assembly, similar to the Grumman simulator installation. Deflection at the wheel was accomplished by vertically raising the contact surface platform via two 2 calibrated hydraulic actuators. This platform was supported and guided to eliminate bending and local deformation.

* This camber angle minimizes the scuffing component of the footprint of the deflected wheel.

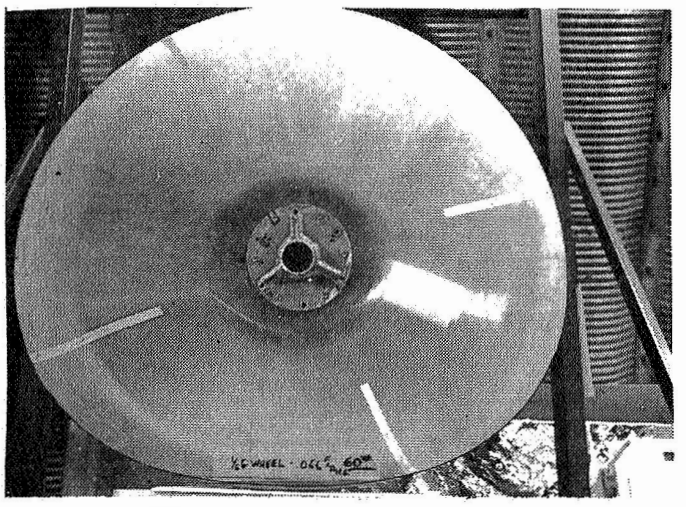

(A) TEST WHEEL AT STATIC LOAD

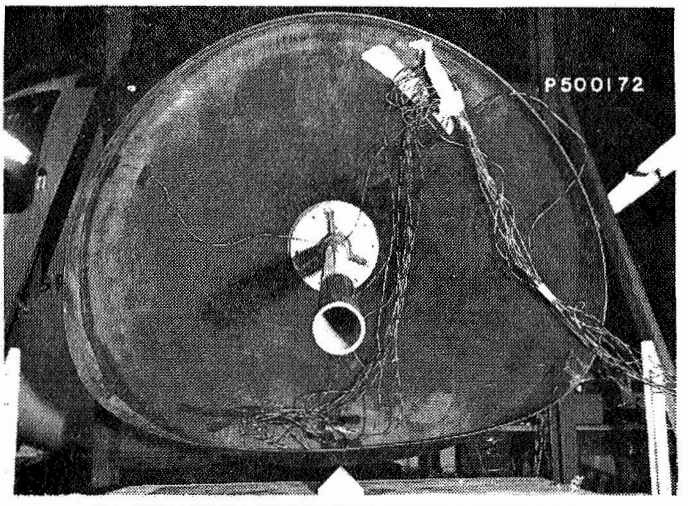

(B) STRAIN GAGED WHEEL WITH POINT LOAD

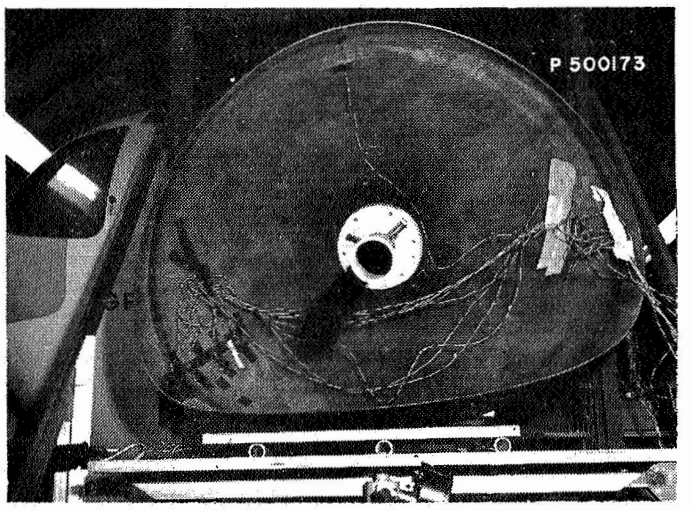

(C) STRAIN GAGED WHEEL WITH NORMAL AND DRAG LOADS APPLIED

Fig. 3-1 INSTRUMENTED DLRV WHEEL UNDERGOING TESTS

INSTRUMENTED 1/16 "g" LRV TEST WHEEL

M. KANAL

FIG. 3-2

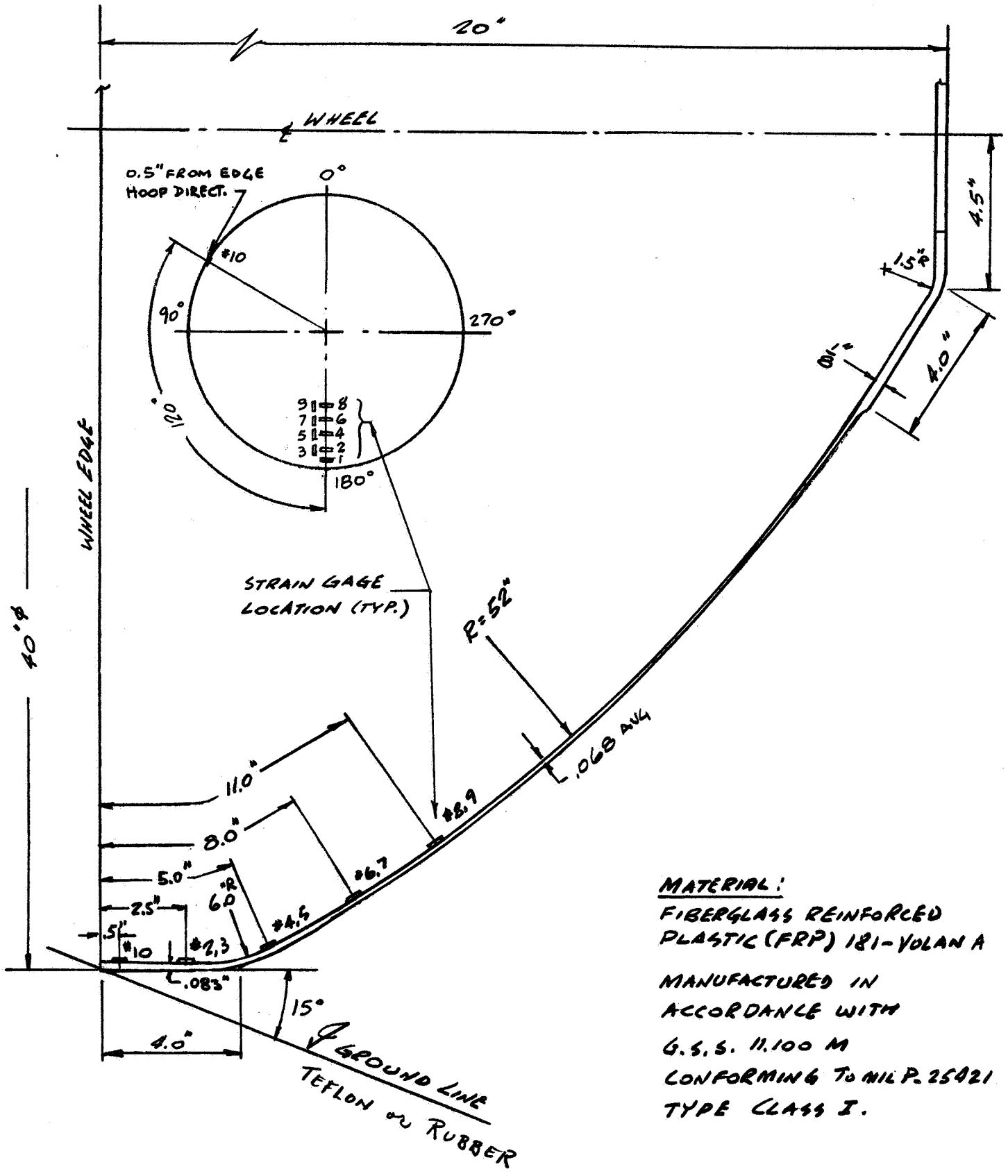

MATERIAL:
FIBERGLASS REINFORCED PLASTIC (FRP) 181-VOLAN A

MANUFACTURED IN ACCORDANCE WITH G.S.S. 11.100 M CONFORMING TO MIL P. 25421 TYPE CLASS I.

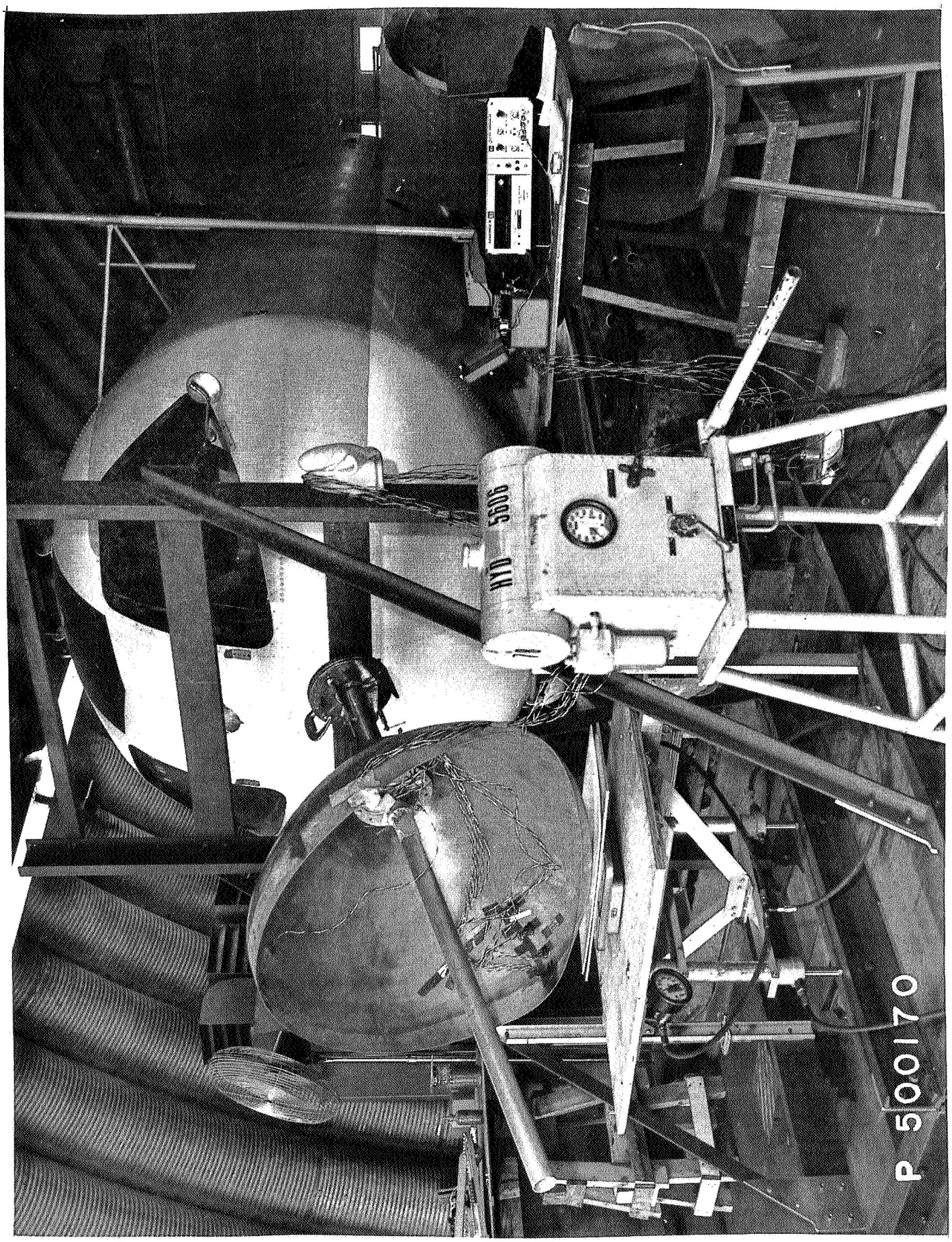

1/6 "g" Test Wheel Under Load

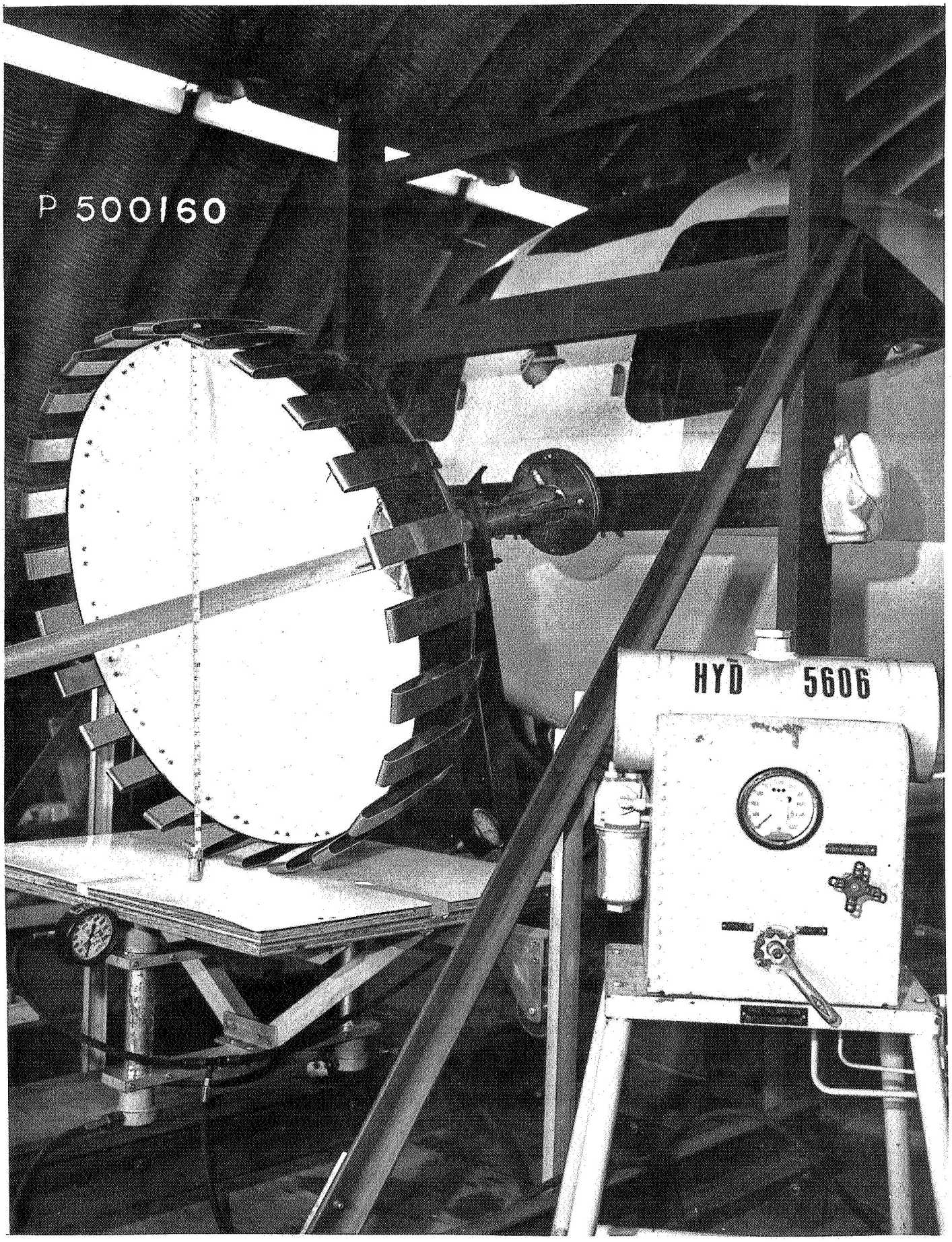

1 "g" Cleated Test Wheel Under Load

Variation of friction coefficients were tested by providing a wheel surface contact area, consisting of a) rubber $\mu = 0.8$, b) teflon $\mu = 0.1$ and c) roller supported intermediate board $\mu = 0.0$.

Provisions were made in the test fixture to allow rotation of the test wheel in $11\frac{1}{4}°$ increments in order to obtain circumferential stress variation.

The combined vertical and drag load condition was simulated by applying a drag load to the roller supported board, via a calibrated spring scale at a given vertical load as shown in Figure 3-5.

Step obstacle characteristics were evaluated with the wheel loaded against a 90° V-Block as shown in Fig. 3-6.

For purposes of comparison and reference the 1g wheel was also load-stroke tested and the change of curvature recorded. The deflected wheel is shown in Figure 3-7. This wheel was not strain gage instrumented.

3.2.3 Test Results

The main objectives were to obtain the vertical flexibility characteristics which are plotted in Fig. 3-8 for the lunar wheel and Fig. 3-9 for the earth wheel, and stress distributions which are presented in Figs. 3-10 thru 3-18.

Graphs in Figs. 3-10 thru 3-13 present the circumferential stress variation starting at 0.5 in. from the edge to 11 in. along the wheel meridian. Figs. 3-14 thru 3-18 give the meridional stress distribution at varying positions on the circumference, under different loading conditions. These graphs are otherwise self-explanatory.

A vertical load of up to 250 lb. was applied to the 1/6 g test wheel and a maximum stress of up to 24000 psi recorded. No permanent set was observed at any of the tested conditions. The 1g wheel was loaded up to 1200 lbs. also without permanent deformation.

The plotted stresses are based on a conservatively assumed Youngs modulus of elasticity $E = 3.3 \times 10^6$ psi for the 181 FRP material.

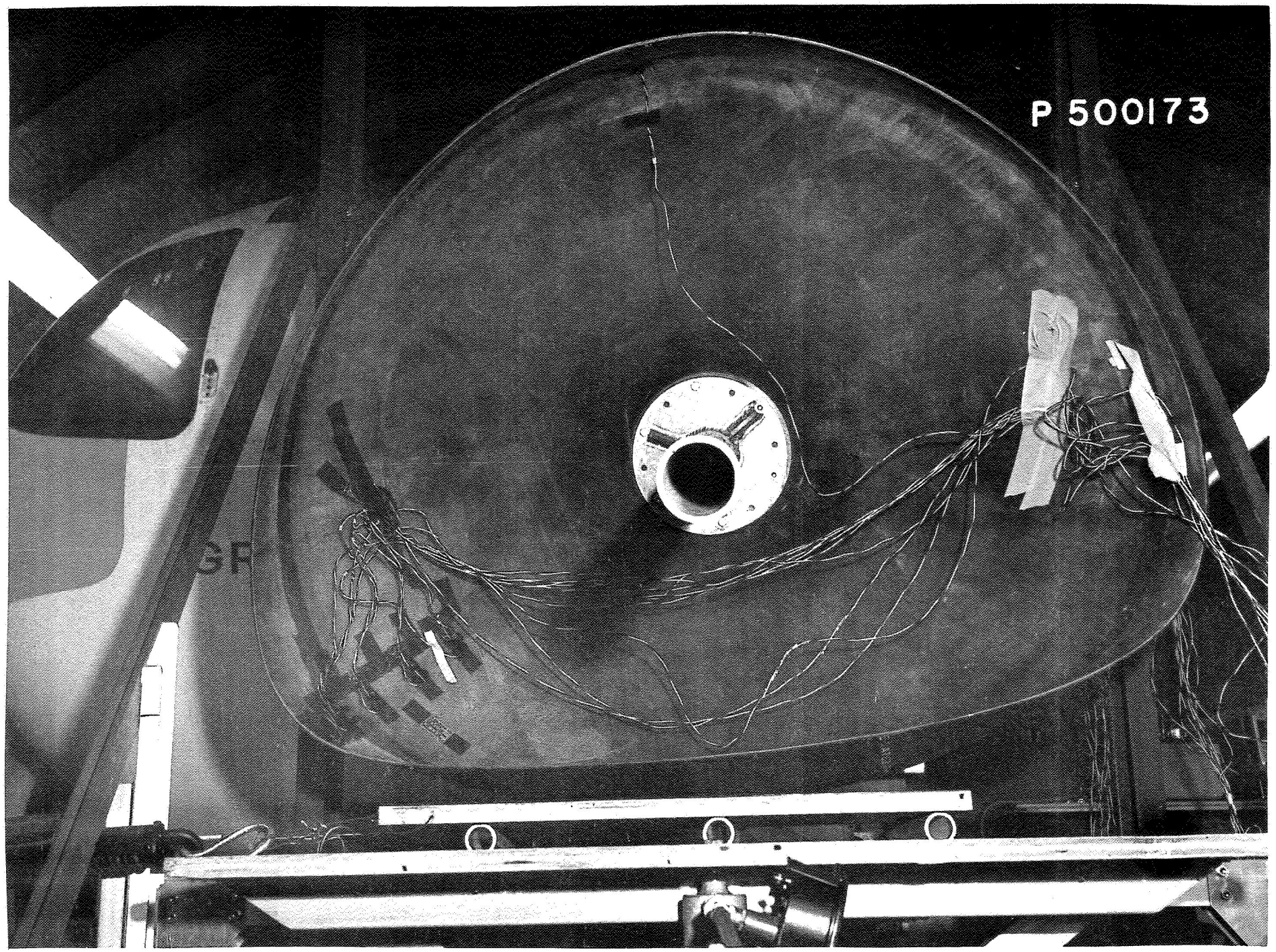

1/6 "g" Lunar Wheel Under Combined Normal and Drag Loading

FIGURE 3-5

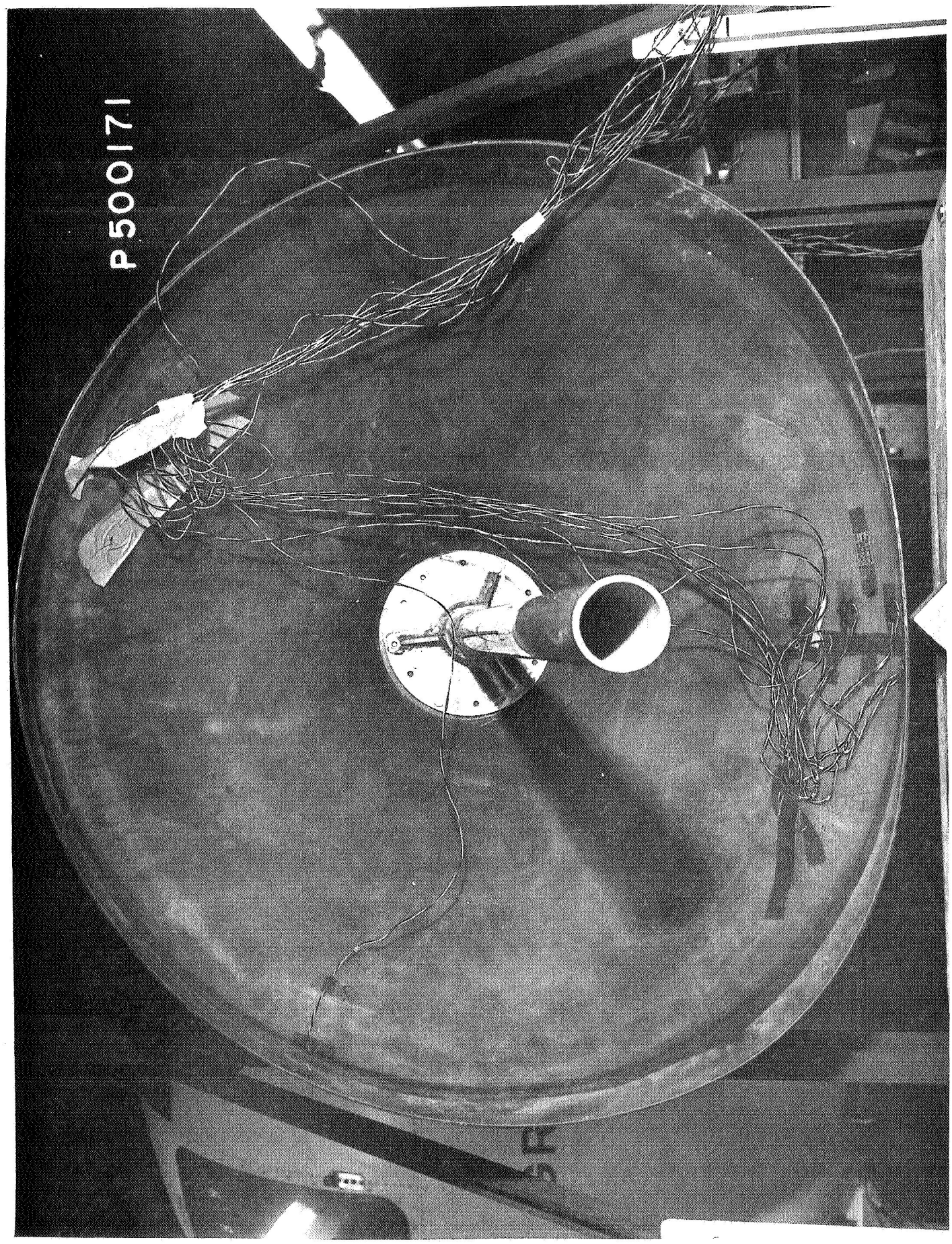

1/6 "g" Wheel Under Point Load of 1 Lunar "g"

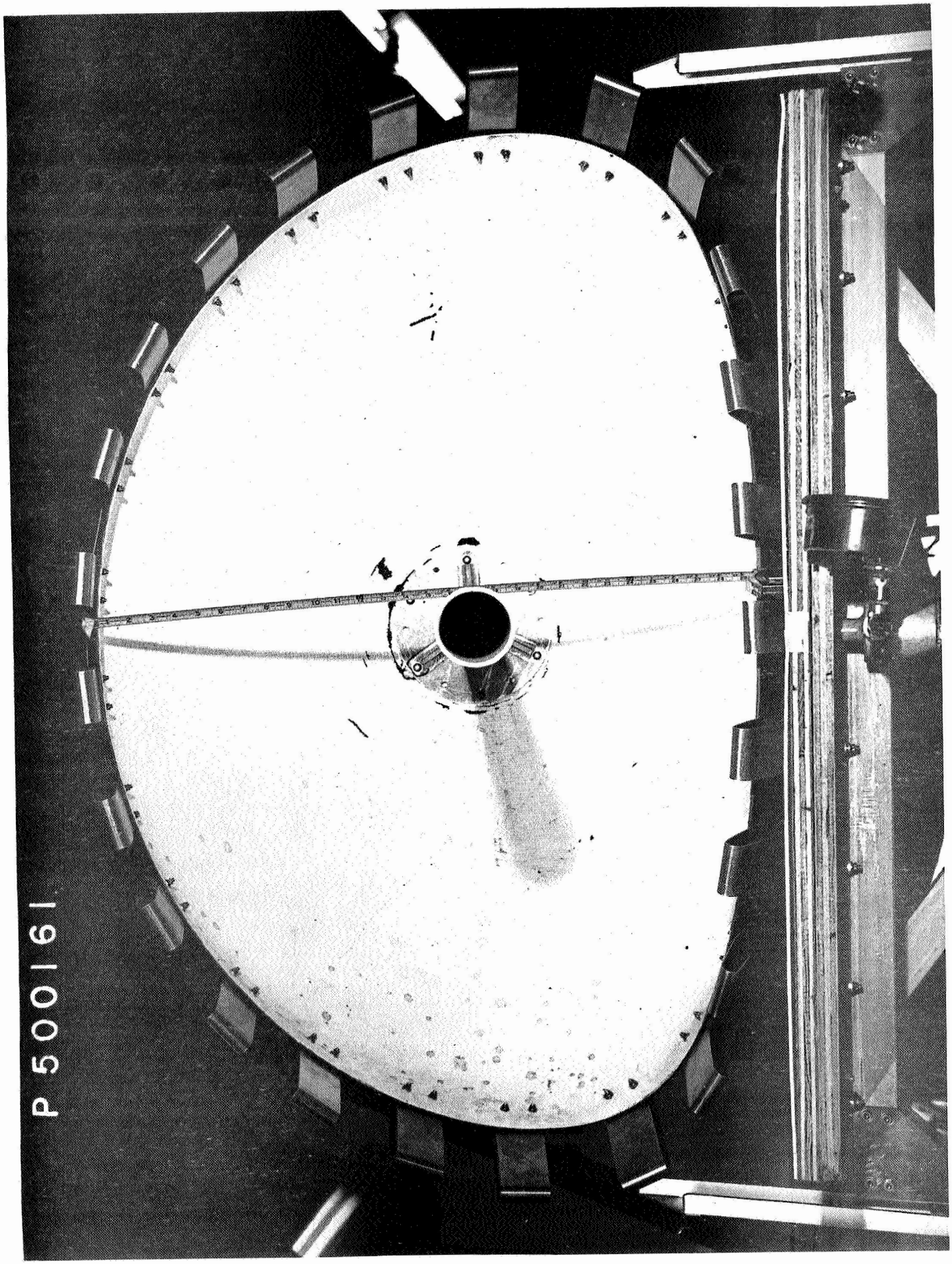

1 "g" Cleated Wheel at Overload Condition

1/6 "g" FRP CLEATLESS WHEEL
VERTICAL LOAD VS STROKE

FIGURE 3-8

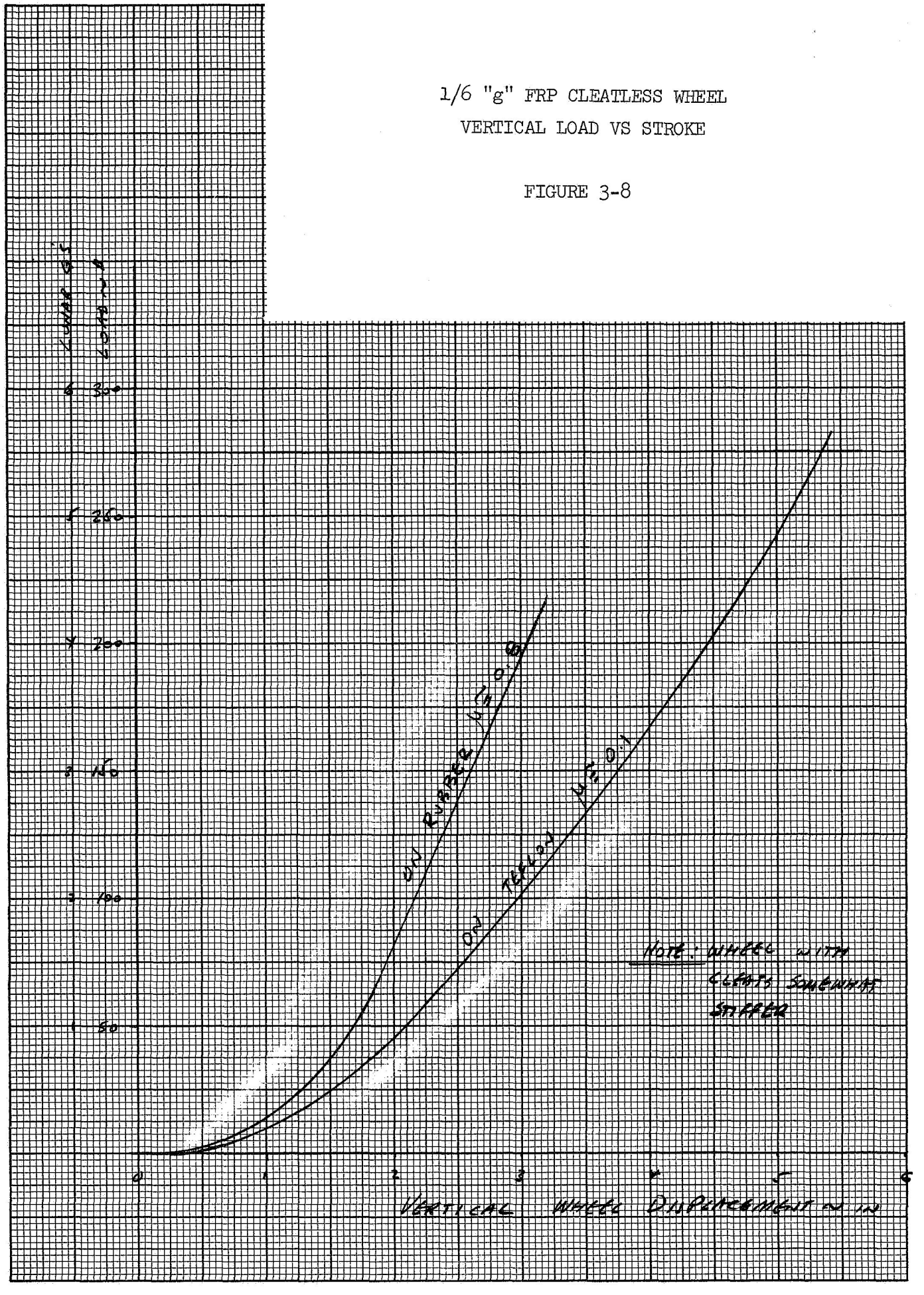

1 "g" FRP CLEATLESS WHEEL
VERTICAL LOAD VS STROKE

FIGURE 3-9

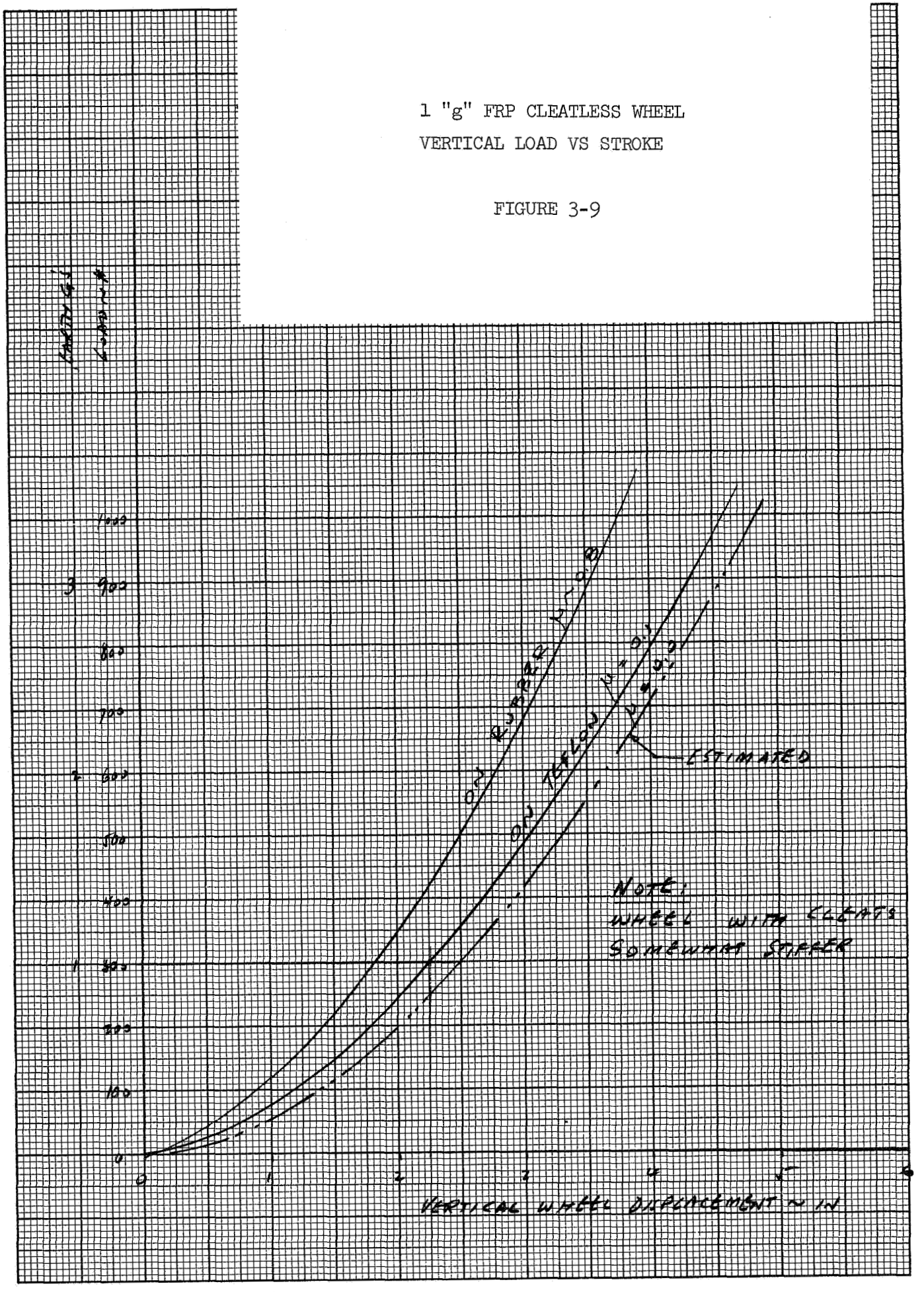

STRESS DISTRIBUTION TESTS
1/6 "g" FRP CLEATLESS WHEEL
VERTICAL LOADING ON TEFLON $\mu = .1$
GAGE 0.5 IN. FROM RIM EDGE

FIGURE 3-10

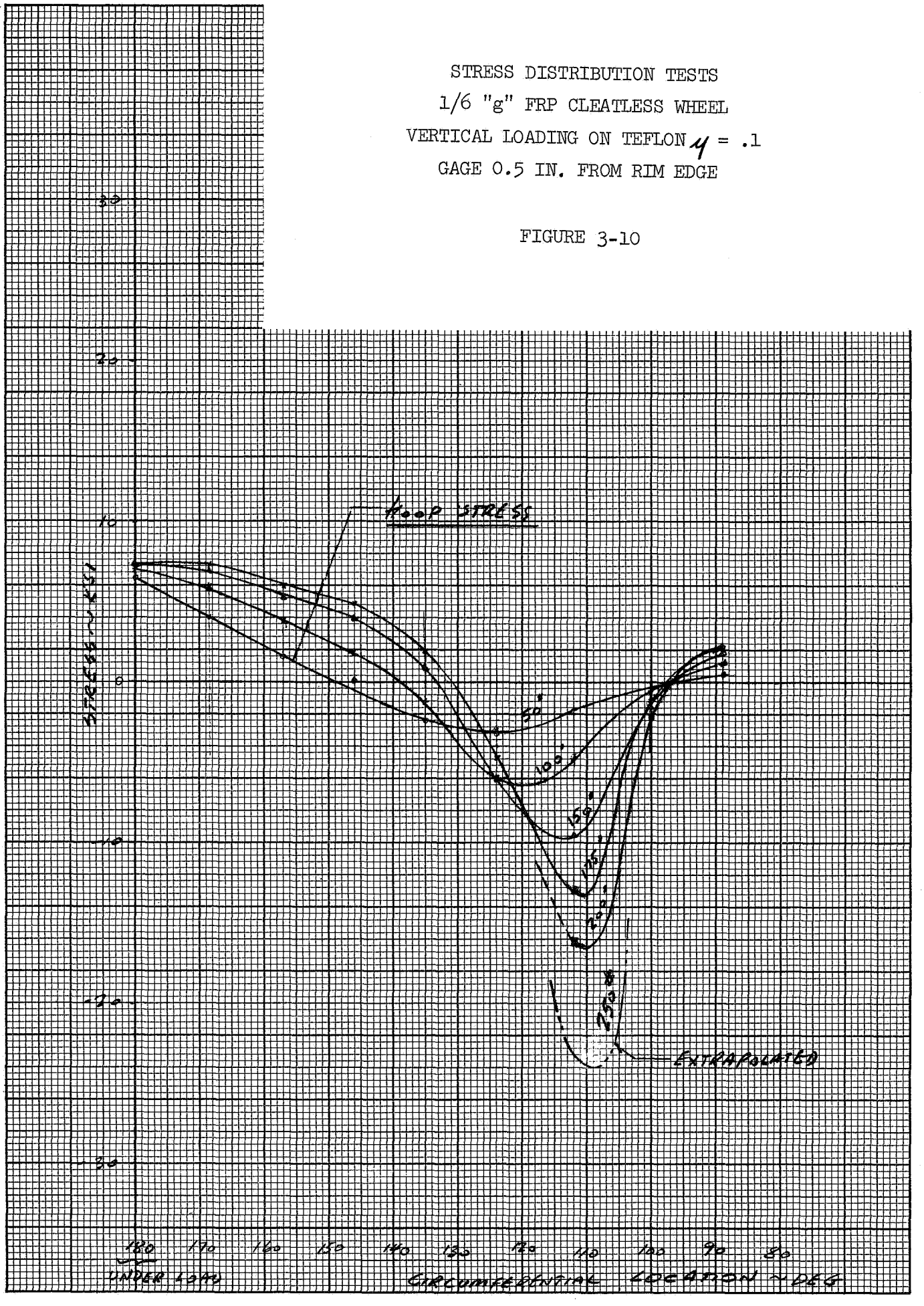

STRESS DISTRIBUTION TESTS
1/6 "g" FRP CLEATLESS WHEEL
VERTICAL LOADING ON TEFLON $\mu = .1$
GAGE 2.5 IN. FROM RIM EDGE

FIGURE 3-11

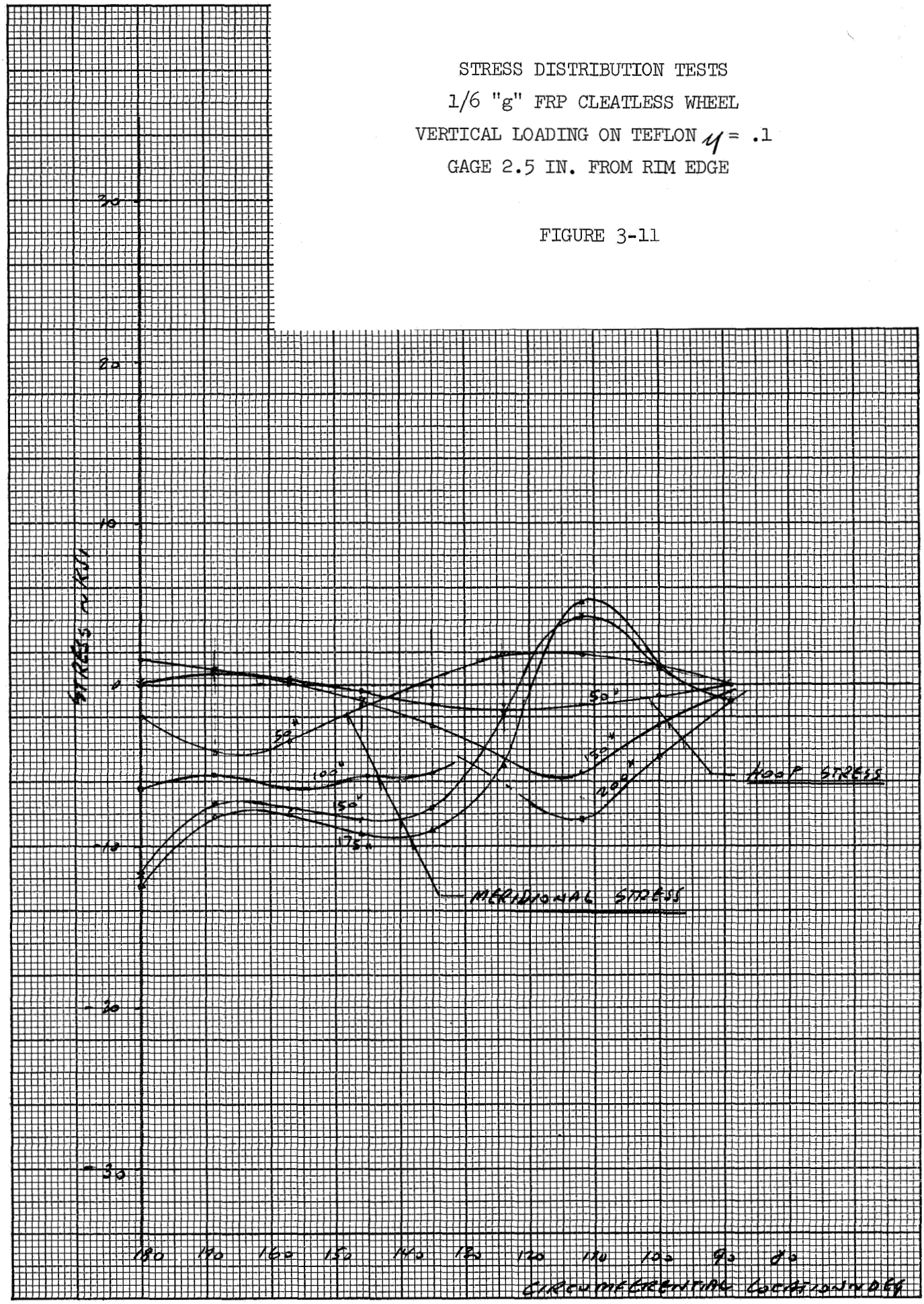

STRESS DISTRIBUTION TESTS
1/6 "g" FRP CLEATLESS WHEEL
VERTICAL LOADING ON TEFLON $\mu = .1$
GAGE 5.0 IN. FROM RIM EDGE

FIGURE 3-12

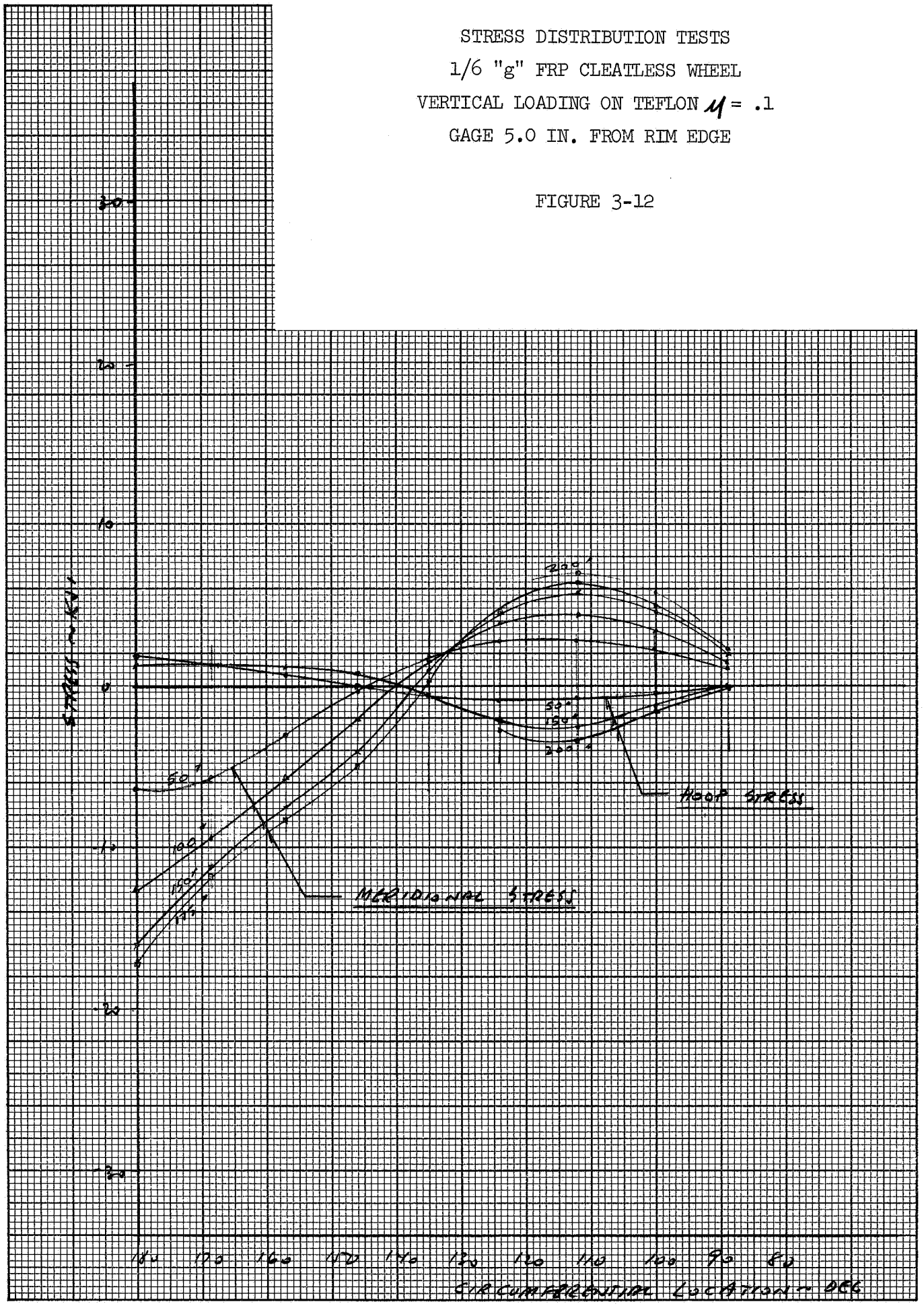

STRESS DISTRIBUTION TESTS
1/6 "g" FRP CLEATLESS WHEEL
VERTICAL LOADING ON TEFLON $\mu = .1$
GAGE 8.0 IN. FROM RIM EDGE
(11.0 IN. FROM EDGE SIMILAR)

FIGURE 3-13

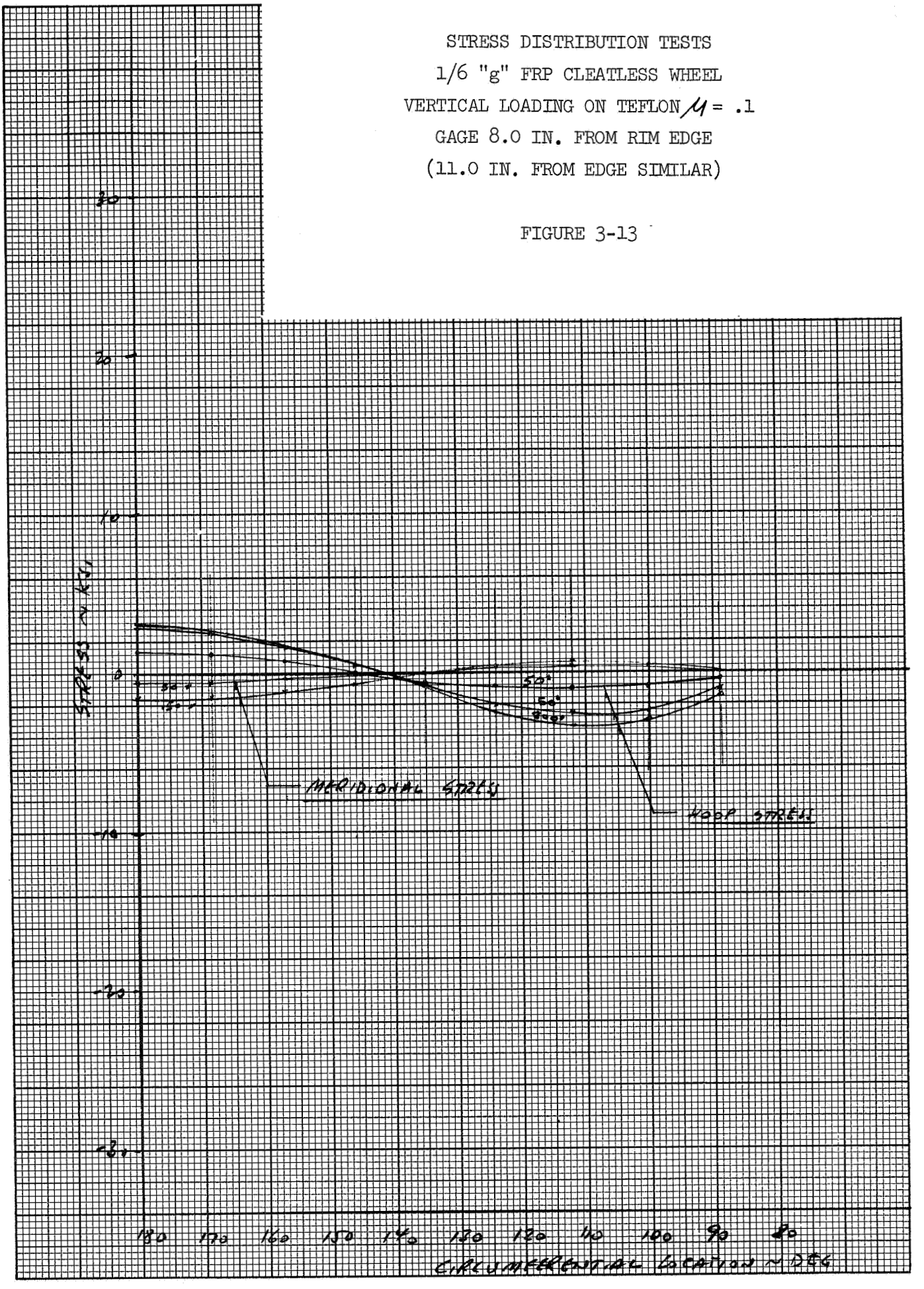

STRESS DISTRIBUTION TESTS

1/6 "g" FRP CLEATLESS WHEEL

VERTICAL LOADING ON RUBBER $\mu = .8$

$\alpha = 180°$

FIGURE 3-14

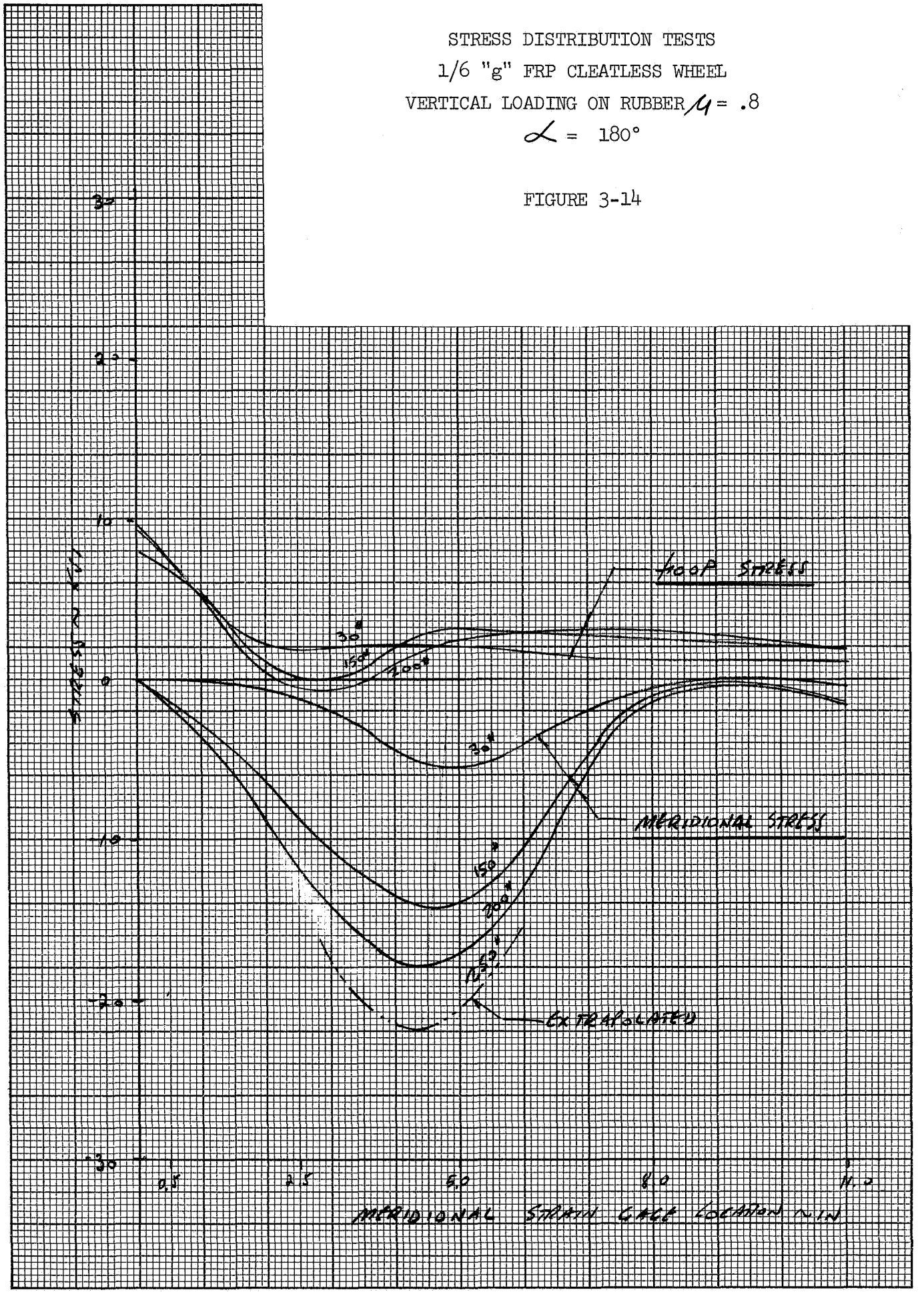

STRESS DISTRIBUTION TESTS

1/6 "g" FRP CLEATLESS WHEEL

VERTICAL LOADING ON RUBBER $\mu = .8$

$\alpha = 124°$

FIGURE 3-15

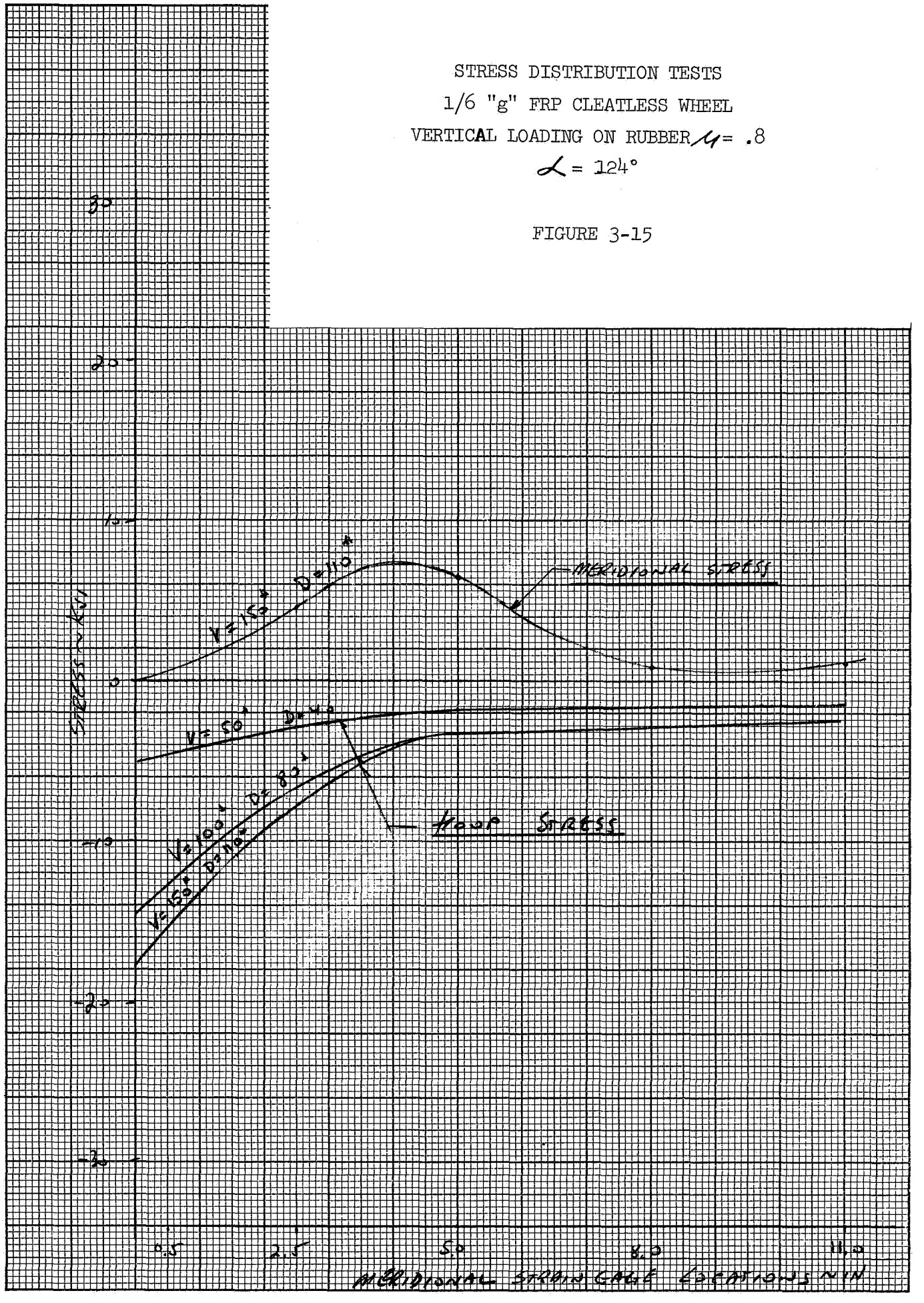

STRESS DISTRIBUTION TESTS

1/6 "g" FRP CLEATLESS WHEEL

VERTICAL LOADING ON A 90° V-BLOCK

ON TEFLON $\mu = 0.1$

$\alpha = 180°$

FIGURE 3-16

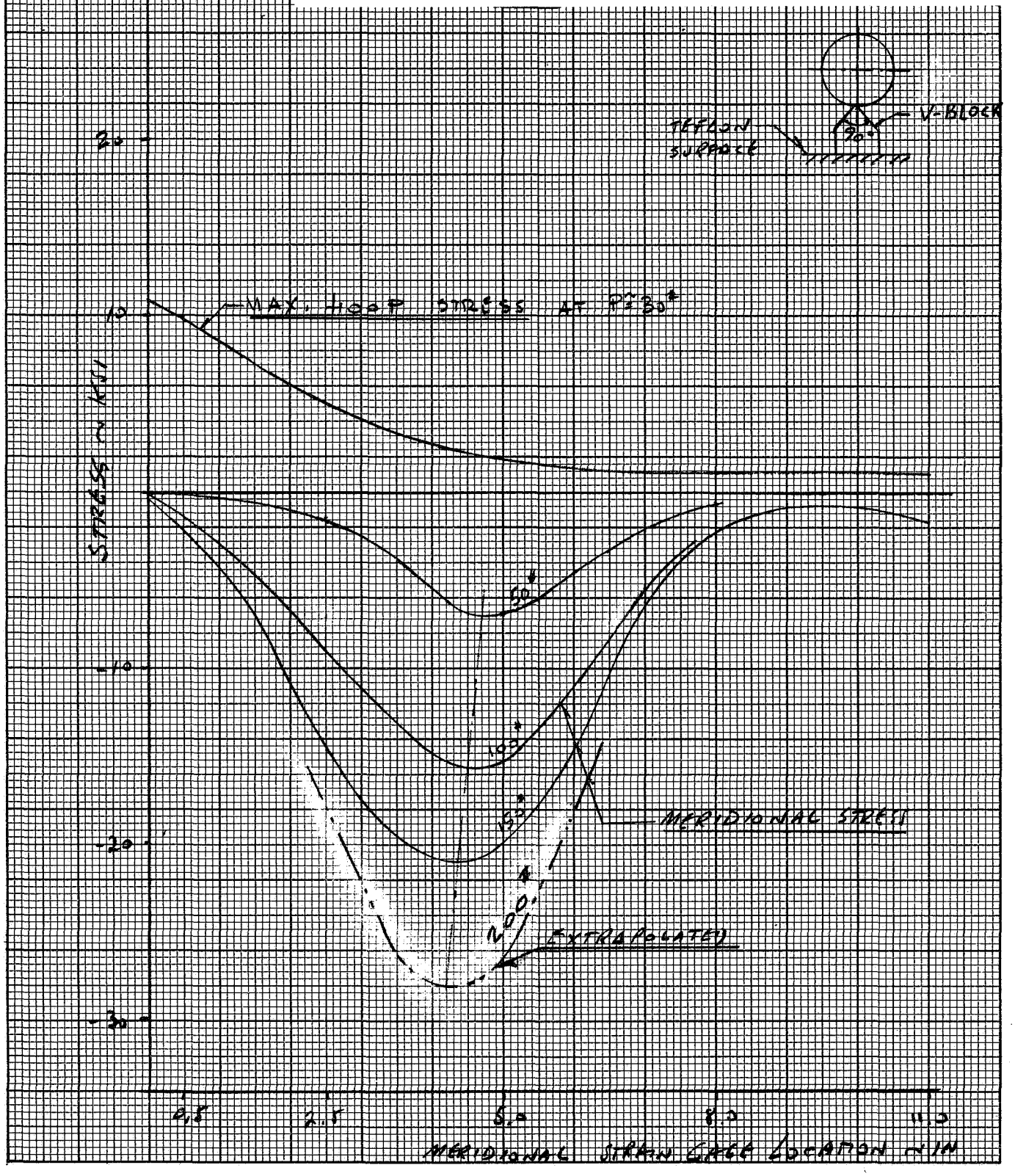

STRESS DISTRIBUTION TESTS

1/6 "g" WHEEL WITH 1 "g" CLEATS

VERTICAL LOADING ON TEFLON $\mu = 0.1$

$\alpha = 180°$

FIGURE 3-17

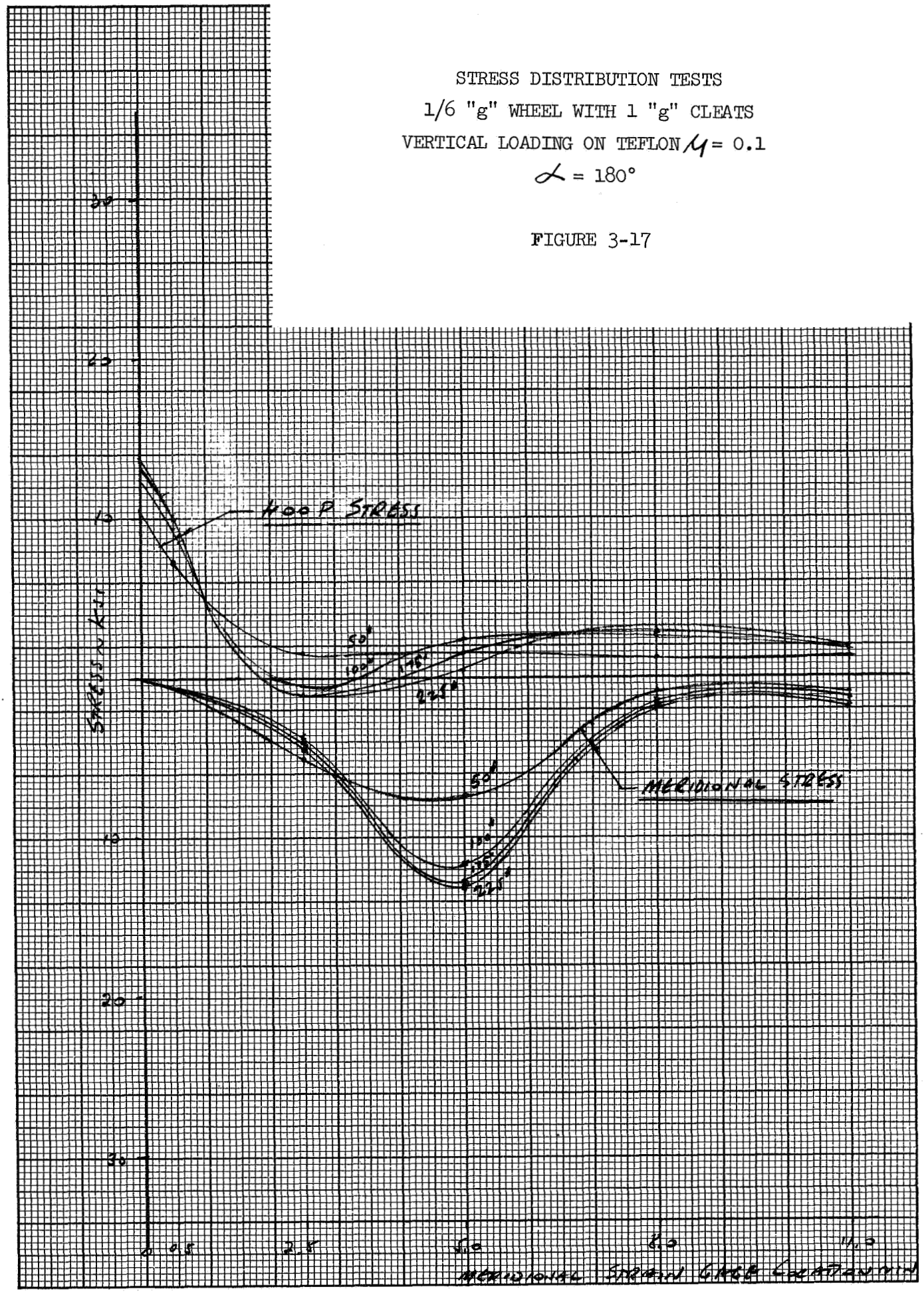

STRESS DISTRIBUTION TESTS

1/6 "g" WHEEL WITH 1 "g" CLEATS

VERTICAL LOADING ON TEFLON $\mu = 0.1$

$\alpha = 112°$

FIGURE 3-18

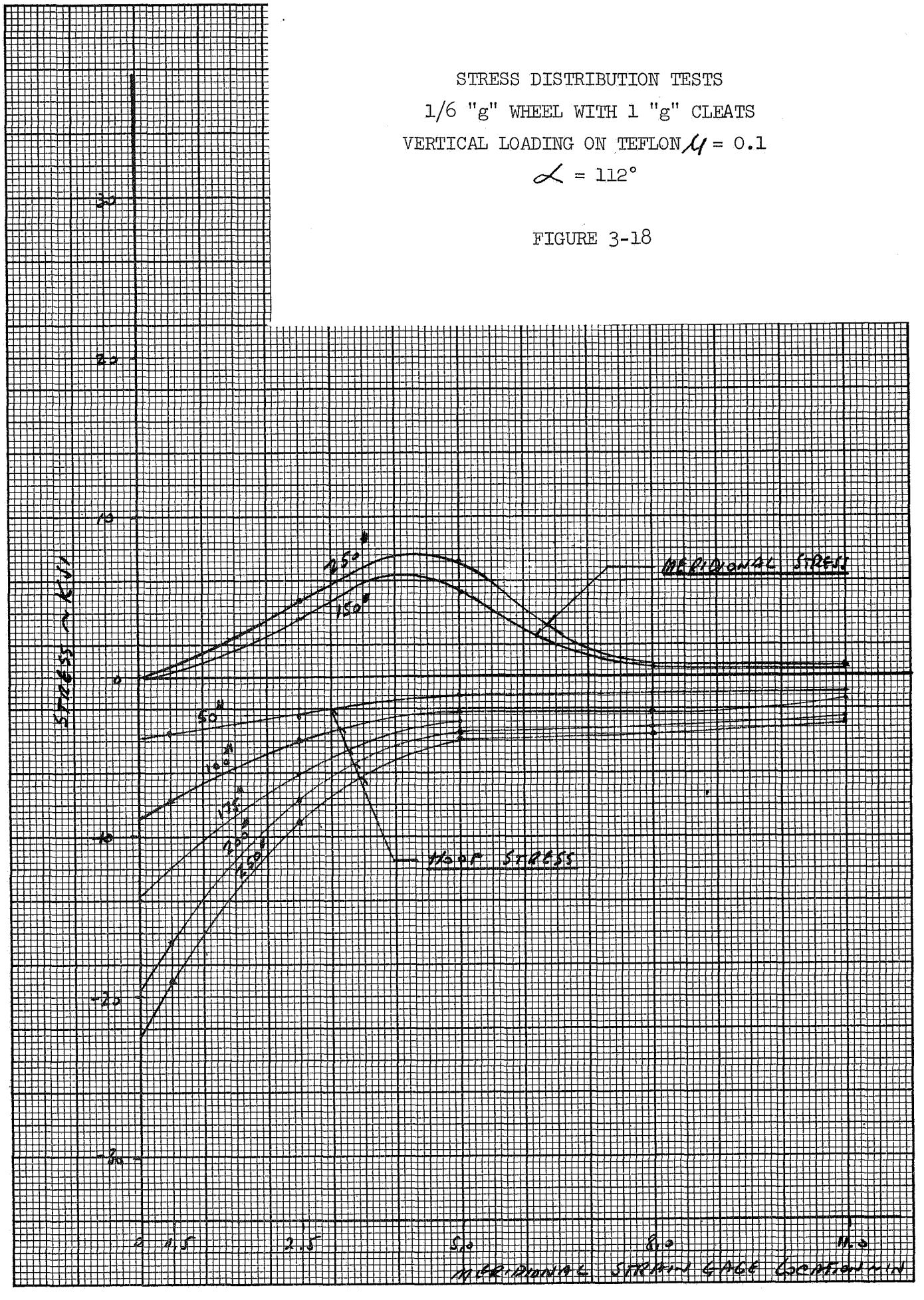

3.2.4 Evaluation of Results

- The overall relative performance of the scaled down 1/6 g test wheel is in good agreement with the 1g wheel. The static footprint of the cleated 1/6 g wheel exceeded that of the 1g wheel.
- Extrapolated strain gage data indicate better than 300 lb. radial load capability for the 1/6 g test wheel.
- The test wheel was capable of transmitting all the preliminary ground loading conditions then defined for the DLRV without permanent deformation.
- Two maximum stress areas were indicated:
  a) Hoop stresses at the rim edge, and
  b) Meridional stresses at the transition between the cylindrical and conical surface of the wheel. The provision of cleats effects an increased stress level at (a), and a stress reduction in (b). The most critically stressed area, both for ultimate and repeated loading, occurs at the rim edge of the wheel, where the following stress levels were recorded:
     (1) Nominal static loading 50 lb. — $f < 10{,}000$ psi
     (2) Vertical V = 150 lbs. with high drag load D = 110 lb. — $f \approx 18{,}000$ psi
     (3) Radial overload 250 lb. — $f \approx$ 24-25,000 psi
- Although these tests were not conducted to failure, the results indicate that the failure mode will consist of a meridional crack initiated at the rim edge. Such a failure is not envisioned to be catastrophic to the wheel, because the decreasing stress level along the conical surface, will retard crack propagation.

3.2.5 Conclusions

The relatively low 1 "g" operating stress level (less than 10,000 psi) compared to the allowable fiberglass flexural strength of about 59,000 psi indicates ample fatigue life (10^6 cycles) for the tested wheel. This is particularly so in view of the lack of stress concentrations inherent in the cone wheel design.

3.3 WHEEL DESIGN "A"

Grumman's DLRV phase "B" final report defined a cone wheel configuration based on the structural analysis and testing discussed in paragraph 3.2, and the structural and mobility design criteria discussed in section 2.0. Because of the substantial effort applied to the DLRV design, that configuration (Fig. 3-19) was selected as test wheel "A" for this study. The cleat configuration was revised (Fig. 3-20) to reflect the improved mobility performance noted in the test data presented in Section 2.4.

Twenty four-twelve (12) inch long aluminum angle extrusion cleats were provided. The cleats were mechanically fastened to the rim at two points, and were interconnected to each other by a cable restraint system.

3.3.1 Fabrication Process - Test Wheel "A"

The test wheel was manufactured of 181 fiberglass cloth and epoxy resin using a male plaster mold and structural wet layup techniques. The nuber and orientation of the plies is shown in Fig. 3-19. An average wheel gage of .060 was provided exclusive of a single-layer rim reinforcement. The low-temperature resin system permited quick, low-cost plaster mold changes for evaluating configuration changes. Differences in modulus of elasticity between the test wheels and the final wheels fabricated later with a higher temperature resin system are negligiable.

3.3.2 Test Plan

The wheel was instrumented to measure its load-stroke characteristics conincident with the stress distribution within the wheel.

Test wheel "A" had 16 high-elongation strain gages (EP-08-250-120) installed to measure hoop and axial stresses from the rim to the hub. Figure 3-21 shows the exact gage locations and measurement axis. In order to obtain radial stress distributions the test wheel was incrementally rotated and the load-stroke test repeated.

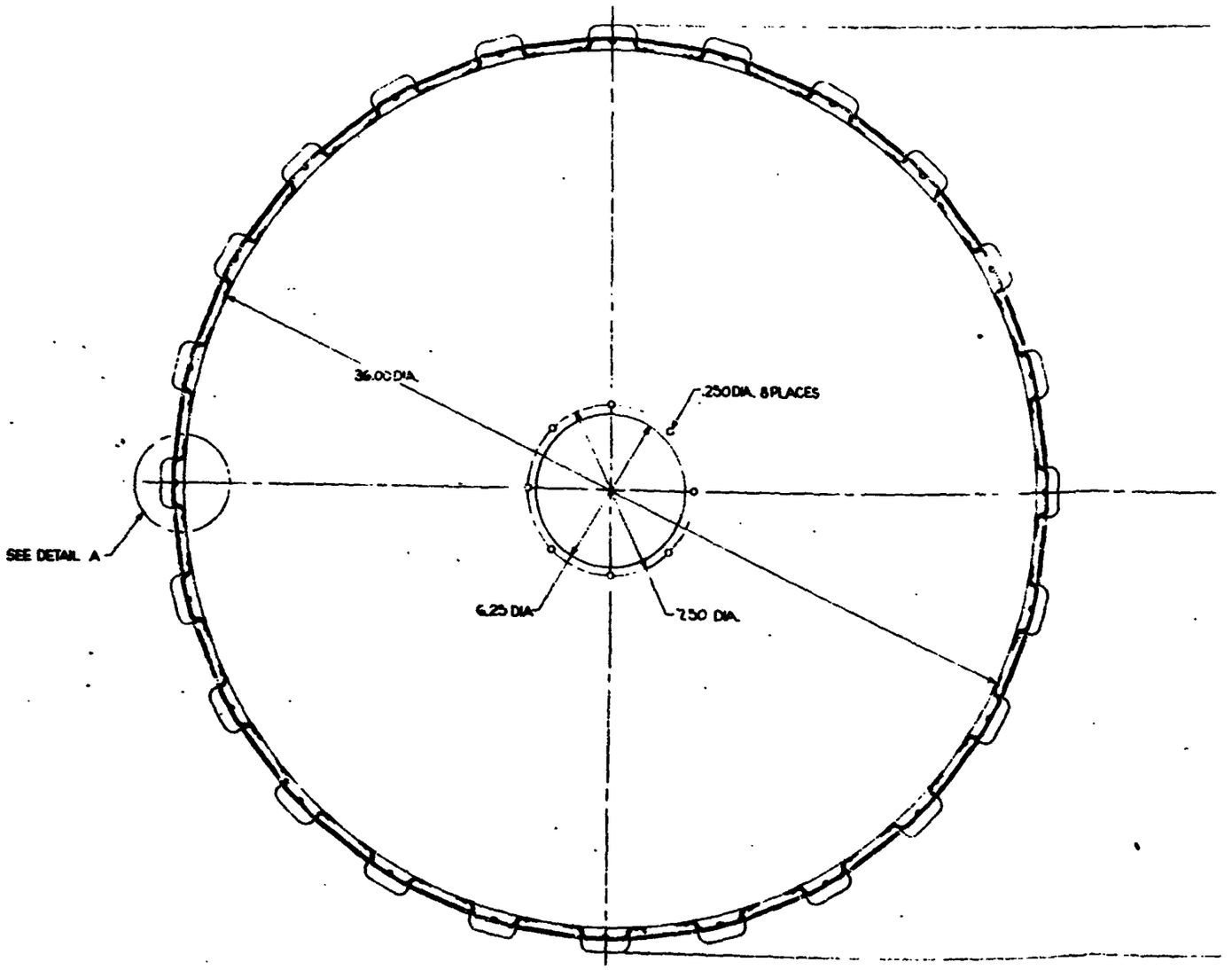

FOLDOUT FRAME 1

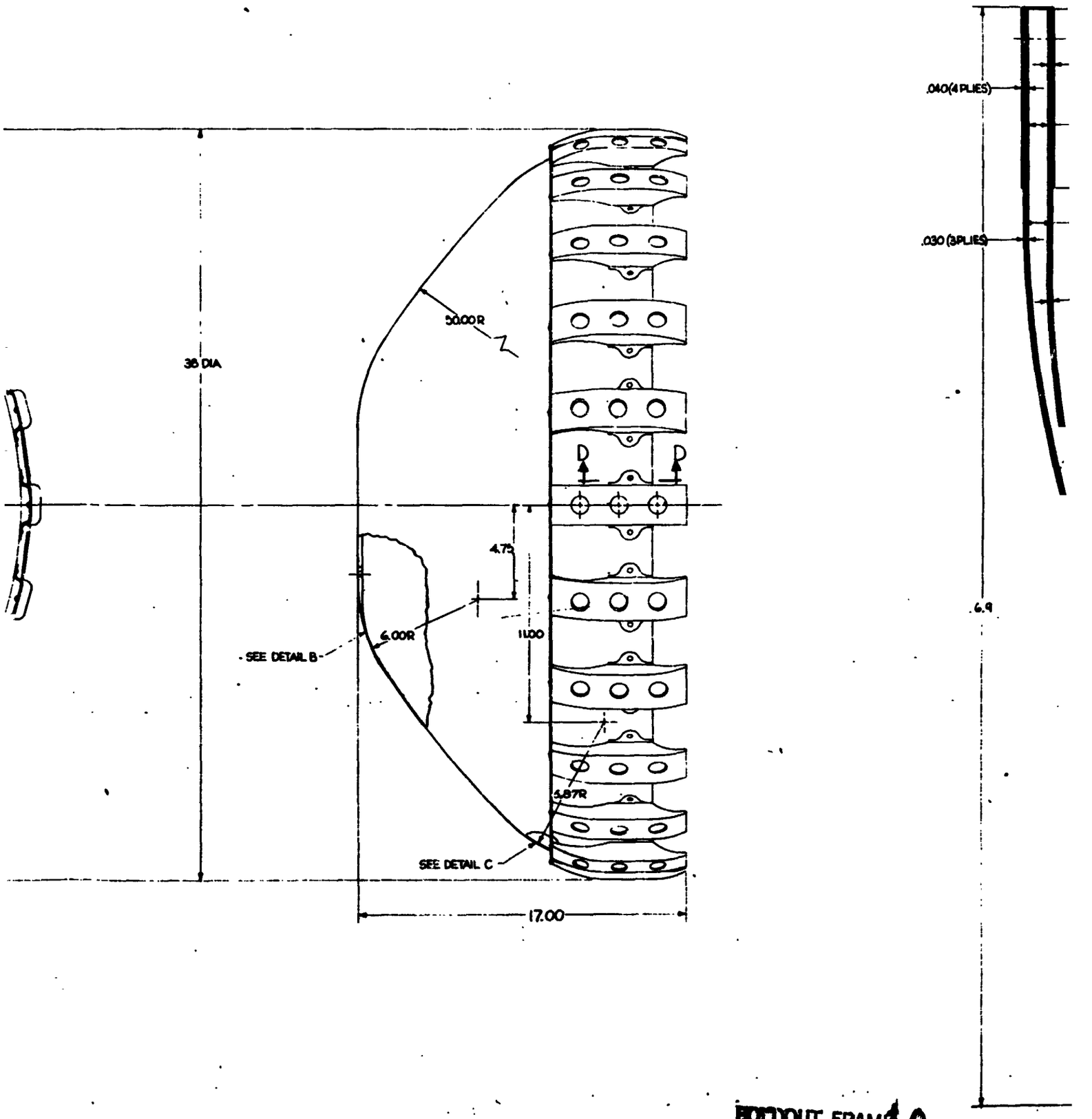

BOLDOUT FRAME 2

NOTES

1. LAYUP · FIBERGLASS C
   PLASTIC MIL-P-25421
   EPOXY RESIN 2795
   (A) DIETHYL AMINOPROPYL
   WORK TIME 2½ HOU
   OVEN CURE 100°
   200°
2. BASIC LAYUP TO BE ONE D
   SINGLE DART. SEAMS
3. TERMINATE THESE ED
4. MAKE A FLAT TEST COUPON
   WITH 72° BETWEEN S
5. NO CLEATS REQ'D
6. NO INSPECTION REQUIRED

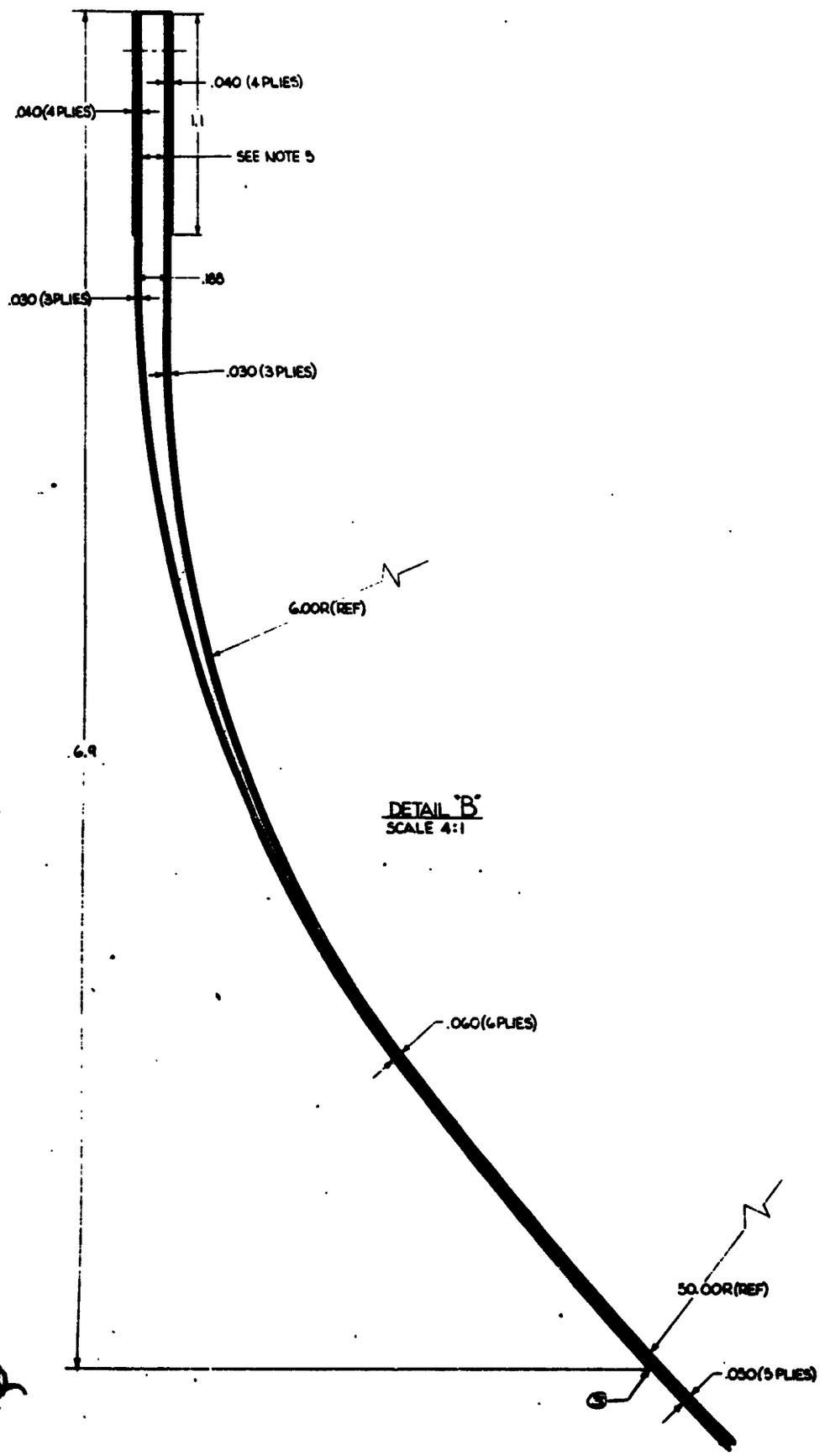

DETAIL "B"
SCALE 4:1

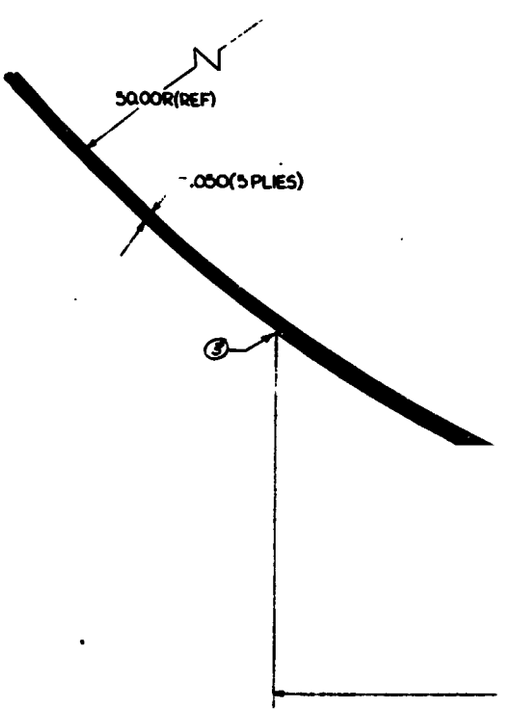

HOLDOUT FRAME 3

ES

F1

YUP · FIBERGLASS CLOTH # 181 VOLAN "A" FINISH
LASTIC MIL-P-25421 CLASS I (UNION CARBIDE) (SEE NOTE 6)
POXY RESIN 2795 HARDNER TYPE "A"
DIETHYL AMINOPROPYLAMINE 8% - TETA 5%
WORK TIME 2½ HOURS ROOM TEMP.
OVEN CURE 100° F 1HR. 150° F 1 HR. (ON MOLD)
200° F 2 HRS. (OFF MOLD)
ASK LAYUP TO BE ONE PIECE OF CLOTH WITH A
INGLE DART. SEAMS TO BE EQUALLY SPACED
ERMINATE THESE EDGES INSIDE (MARKED (3))
AKE A RAT TEST COUPON 12"x12" 5 LAYERS THICK.
" 72° BETWEEN SUCCEEDING WARPS
CLEATS REQ'D
INSPECTION REQUIRED ON RESIN SYSTEMS.

5 PLIES)

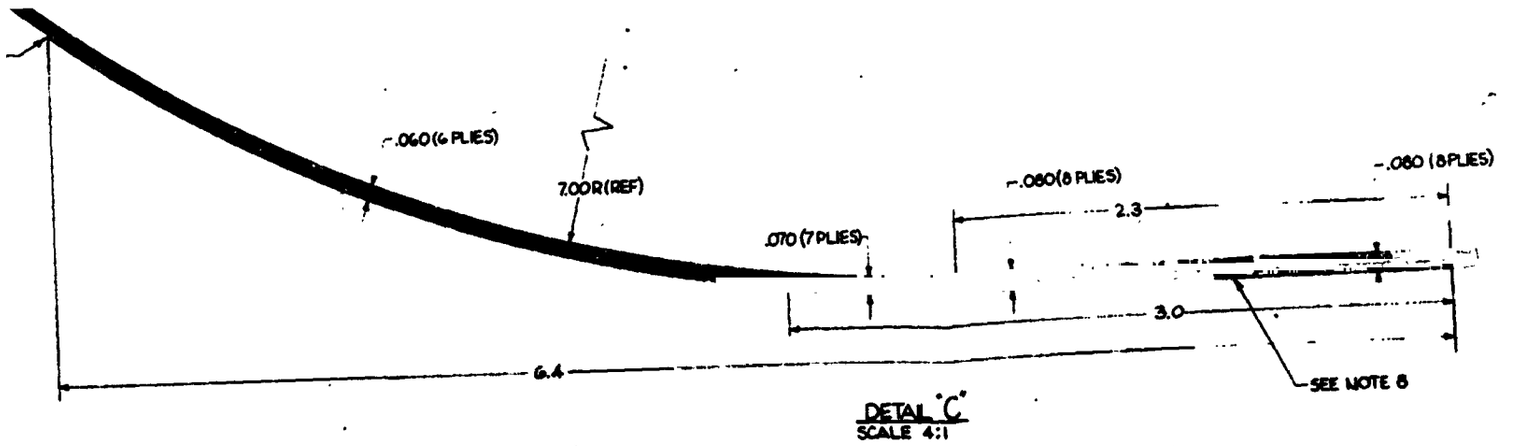

DETAIL "C"
SCALE 4:1

T FRAME 3

FOLDOUT FRAME

4

FOLDOUT FRAME

FOLDOUT FRAME

2

FIGURE 3-20

INITIAL CLEAT CONFIGURATION

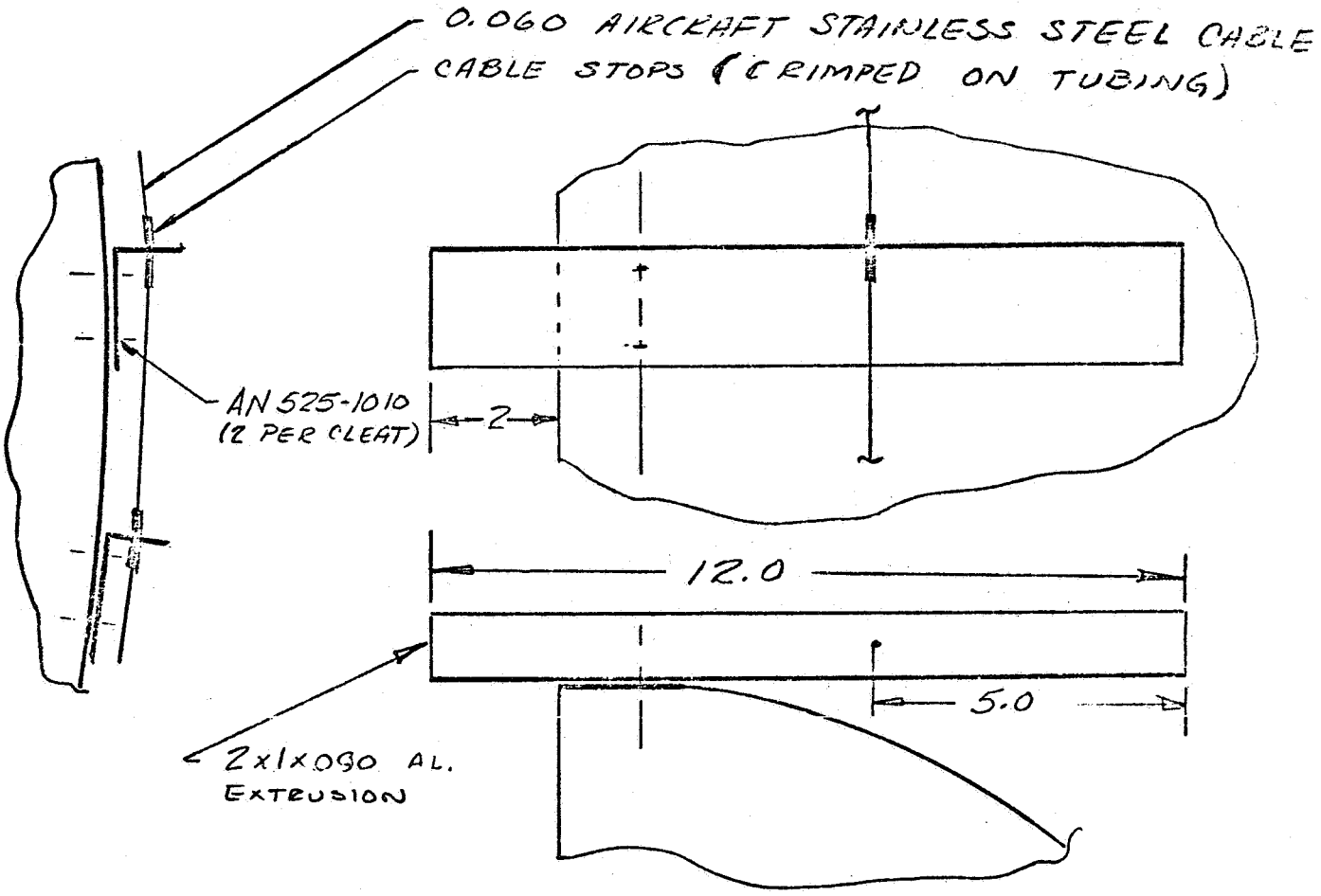

FIGURE 3-21

INSTRUMENTED TEST WHEELS

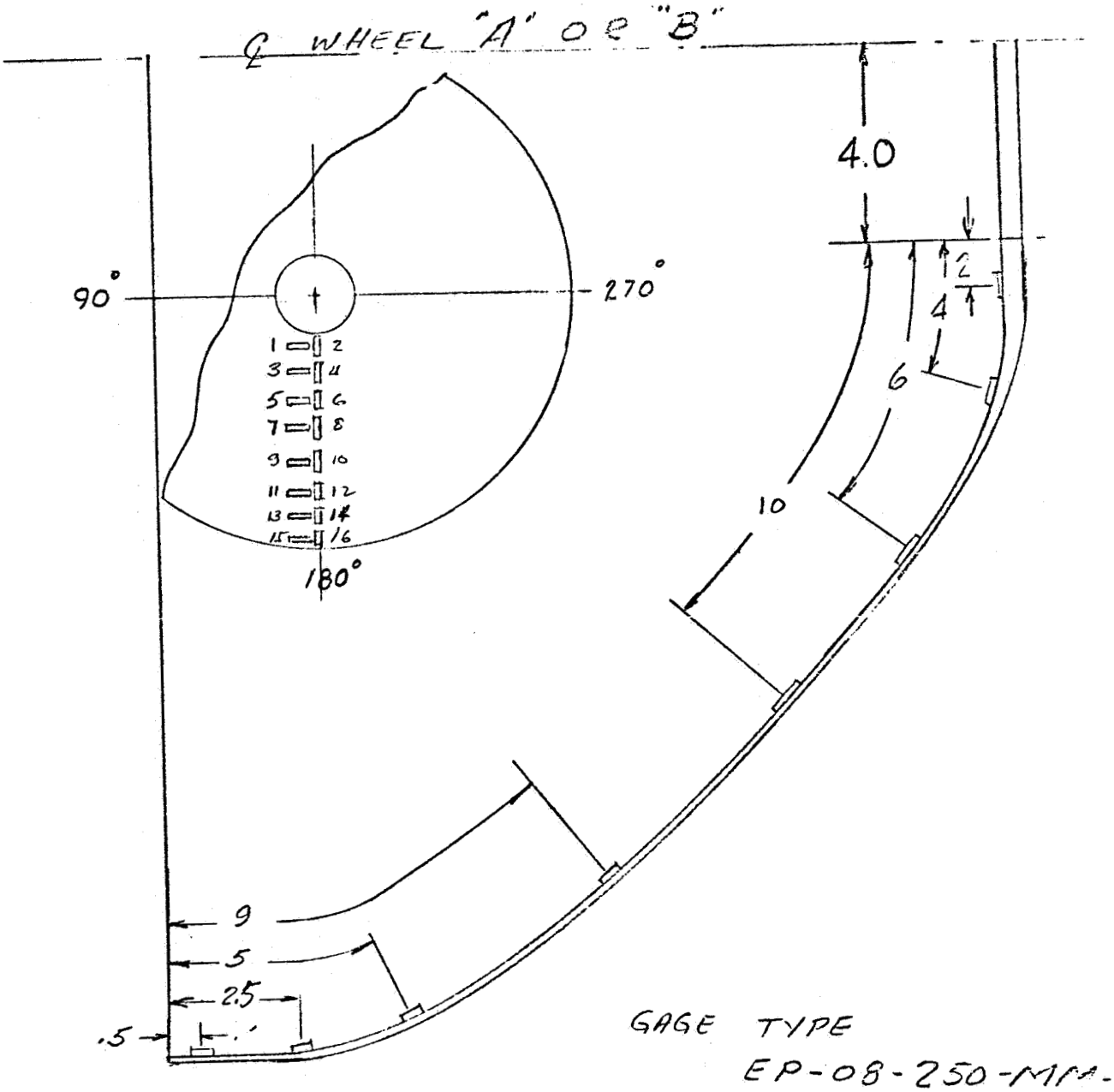

The wheel test fixture was designed to rigidly restrain the wheel at a 15° positive camber angle to the contacting surface. Wheel deflection was accomplished by vertically raising the contact surface. The contact surface was teflon coated and free to scuff laterally providing a minimum friction coefficient interface. The test fixture and procedures were identical to those noted in the previous tests (para. 3.2).

3.3.3 Test Results

Analysis of the wheel test data with no cleats attached indicated good footprint characteristics at the nominal 1-g lunar load (55 lb), and a projected capacity to easily support a 300 lb load with the cleated wheel. A maximum stress of 25,000 psi at 250 lbs load and 10,000 psi at 110 lbs were measured at the wheel hub. This stress level would confidently assure no fatigue failures for DLRV mission.

The addition of cleats stiffened the wheel spring rate and as anticipated increased its load carrying capacity over the basic wheel. Figure 3-22 shows both load-deflection curves. However, rim distortion, attributable to the cleats, was noted at the higher loadings, and the test was terminated prior to obtaining the stress distribution data. During the test, the cleats were noted to be in full ground contact from 55 to 300 lbs.

Figure 3-23 a and b shows how the load applied to the leg of the angle is reacted on the relatively soft rim outside of the base of the bolt pattern. This causes a moment to be applied to the rim, resulting in a local deflection with sinsoidal characteristics. Figure 3-23c shows a revised configuration "T" cleat with the applied load passing inside the bolt pattern, resulting in no moment applied to the rim.

The "T" section cleats were incorporated on wheel "A" and the tests were satisfactorily completed. Measured stress distributions with "T" section cleats are tabulated in Table 3-1. Figures 3-24 and 3-25 summarize in plotted form typical meridional and hoop stress distribution. Maximum stress values are shown in Figures 3-26 and 3-27. These stress levels confidently indicate

Wheel Load Vs Deflection

Fig. 3-22

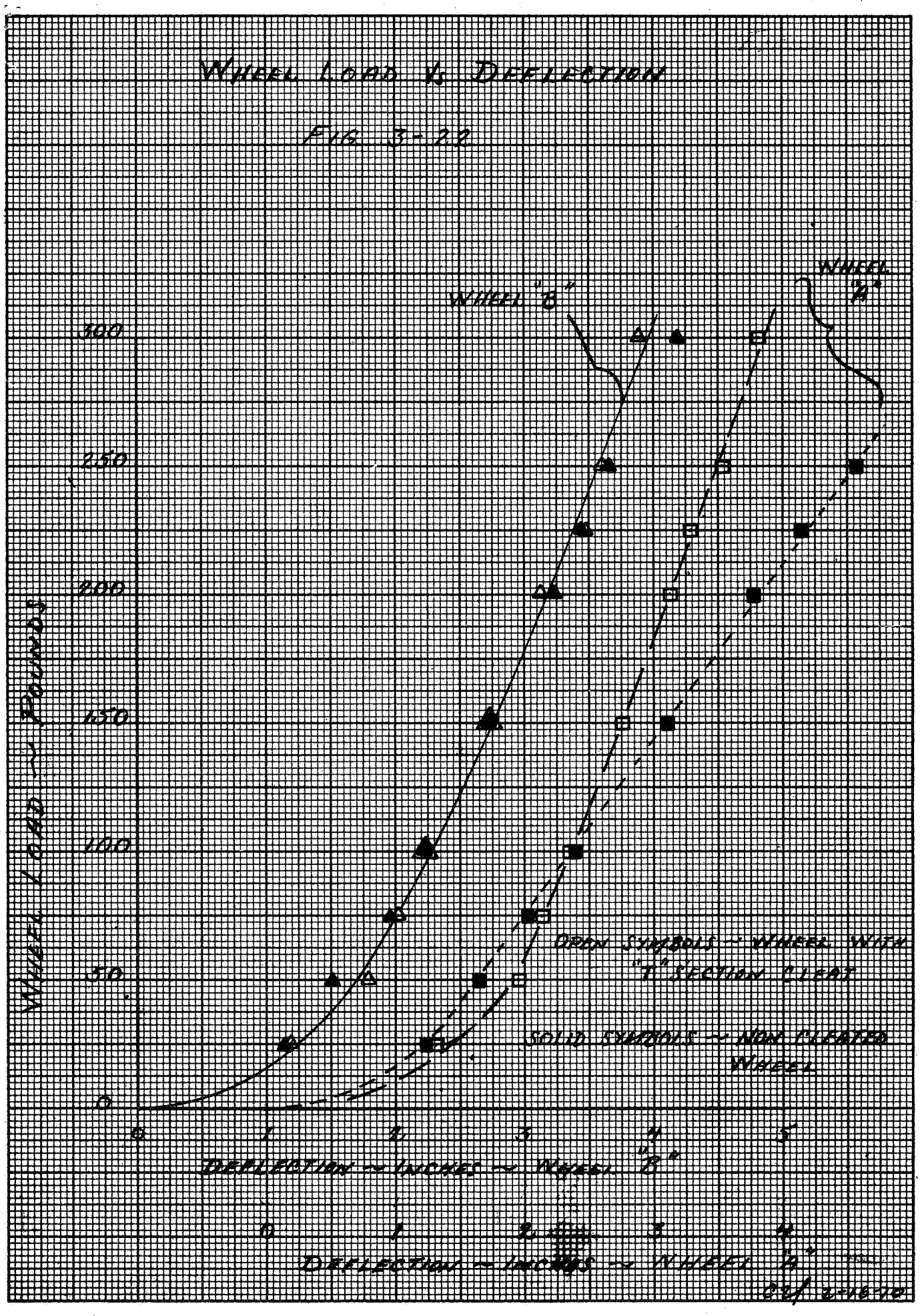

FIGURE 3-23

(a) Sketch showing sinsoidal rim deflection at 300 lb. load.

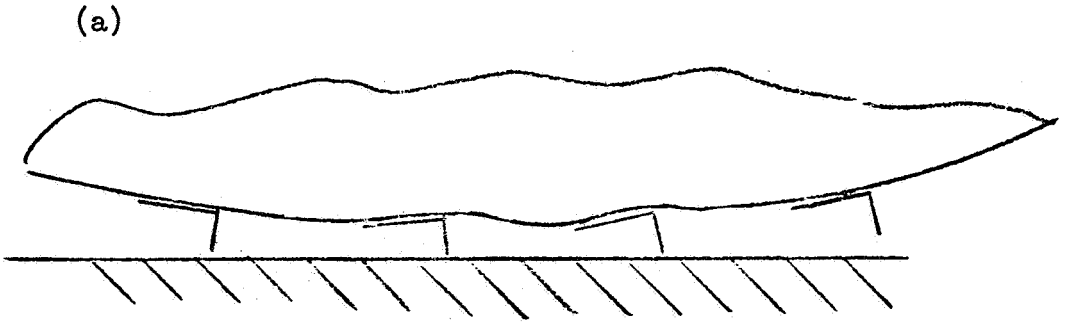

(b) Moment applied to rim is approximately equal to P x e

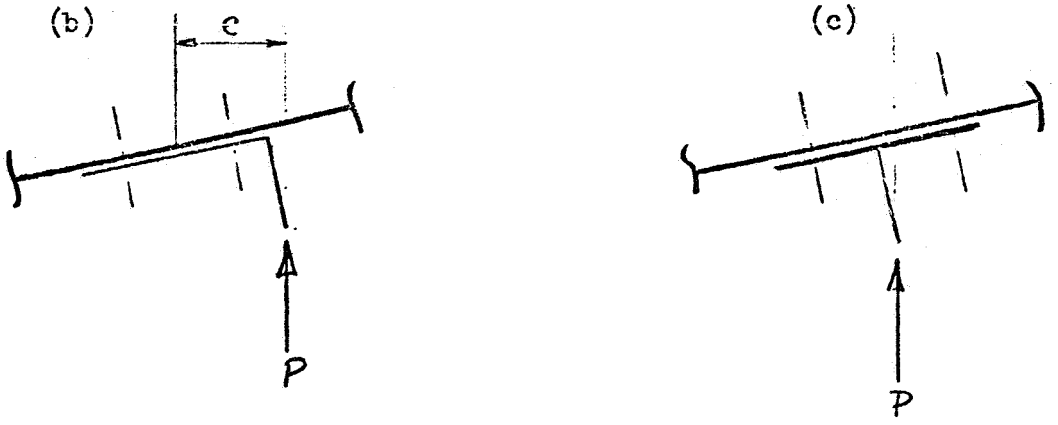

(c) Since p is inside the bolt pattern there is no momemnt applied to rim.

TABLE 3-1

"A" TEST WHEEL - WITH "T" EXTRUSION CLEATS

+ = TENSION, - = COMPRESSION

GRUMMAN AIRCRAFT ENGINEERING CORPORATION
ENGINEERING DEPARTMENT

LOAD		STRAIN GAGE POSITION →																LOAD APPLI-CATION
		1	2	3	4	5	6	7	8	9	10	11	12	13	14	15	16	
LBS.		STRESS ~PSI →																
0		0	0	0	0	0	0	0	0	0	0	0	0	0	0	0	0	180°
25		595	-4940	030	003	270	027	419	-095	552	-81	703	-2495	837	-3600	3340	-661	
50		735	-5040	-040	127	345	022	543	-143	735	-143	1012	-3500	489	-3710	4410	-756	
75		813	-5810	-089	227	370	013	611	-173	809	-173	1210	-3960	-54	-2820	4880	-756	
100		889	-6610	-135	316	416	013	678	-189	905	-203	1427	-4500	-792	-1461	5340	-819	
150		1067	-8450	-200	446	530	000	843	-244	1120	-284	1980	-6140	-3040	+2420	6110	-1123	
200		1222	-9910	-232	527	610	-27	961	-311	1240	-356	2510	-8050	-6050	+5980	6100	-1204	
225		1335	-10760	-246	573	645	-59	1008	-352	1273	-373	2545	-9200	-6770	+7110	7380	-1082	
250		1478	-11690	-219	595	700	-54	1074	-397	1306	-324	2140	-10,900	-8110	+8260	7100	-675	
300		1654	-12830	-176	595	773	-76	1160	-454	1368	-162	1059	-11,600	-9460	+9300	6850	-427	
0		0	0	0	0	0	0	0	0	0	0	0	0	0	0	0	0	202°
25		260	-1902	-162	289	073	-014	111	-003	141	-030	065	-513	-413	-405	514	-302	
50		419	-3040	-268	457	116	-032	190	-014	246	-062	162	-1027	-683	-960	1410	-651	
75		459	-3530	-297	503	160	-038	249	-011	332	-081	244	-1353	-586	-1430	1930	-722	
100		500	-4020	-324	530	214	-046	316	-019	421	-108	311	-1130	-556	-1892	2510	-819	
150		640	-5180	-419	675	260	-070	403	-049	538	-149	373	-2380	-589	-2420	3470	-972	
200		784	-6150	-475	770	305	-103	460	-070	627	-179	386	-2915	-792	-2580	4320	-1118	
225		862	-6770	-510	824	324	-125	500	-092	670	-203	381	-3230	-900	-2610	4740	-1190	
250		945	-7310	-532	851	340	-146	524	-111	710	-219	357	-3500	-995	-2600	5100	-1248	
300		1055	-8030	-565	902	364	-168	560	-168	765	-219	214	-3780	-1210	-2350	5430	-1302	
0		0	0	0	0	0	0	0	0	0	0	0	0	0	0	0	0	
25		000	443	-068	152	-089	-027	-160	043	-246	024	-314	875	-927	1292	-681	062	225°
50		000	546	-116	227	-116	-046	-233	059	-332	032	-429	1097	-1260	1545	-809	016	
75		030	525	-135	266	-141	-054	-257	065	-360	038	-465	1138	-1306	1490	-811	003	
100		019	625	-157	417	-160	-065	-289	073	-400	043	-514	1217	-1409	1498	-805	041	
150		-038	754	-249	430	-203	-095	-357	106	-478	051	-622	1332	-1850	1509	-508	-260	
200		-068	814	-292	487	-216	-116	-386	130	-505	057	-662	1312	-1995	1219	-114	-408	
225		-059	768	-302	502	-216	-125	-394	149	-505	062	-667	1272	-2050	1023	+146	-487	
250		-114	920	-284	435	-189	-135	-384	165	-487	062	-678	1249	-2275	892	+546	-638	
300		-168	1010	-292	386	-165	-146	-381	184	-476	059	-695	1148	-2545	746	+1093	-849	

ENG-47

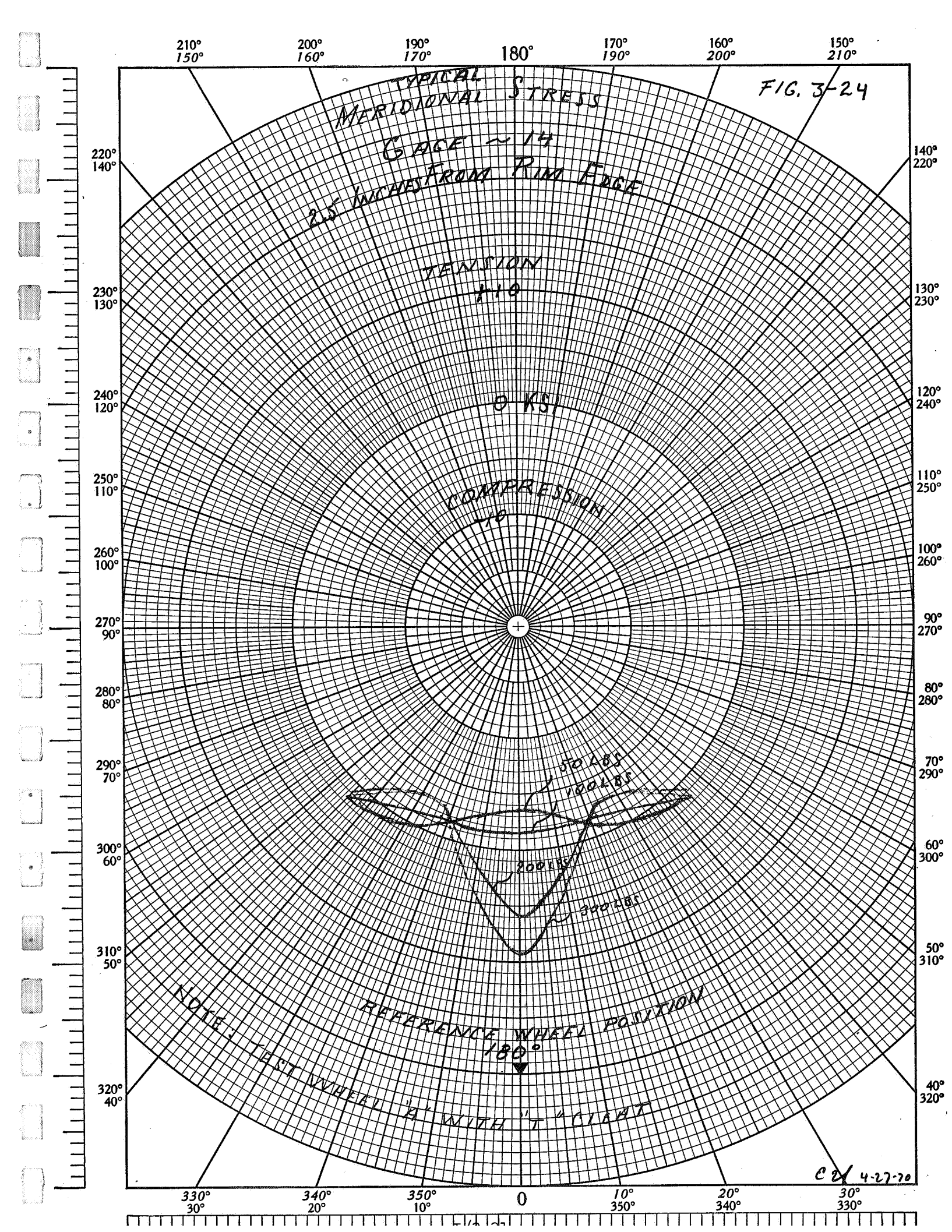
FIG. 3-24
TYPICAL MERIDIONAL STRESS
GAGE ~ 14
2.5 INCHES FROM RIM EDGE
TENSION
+10
0 KSI
COMPRESSION
-10
150 LBS
100 LBS
200 LBS
300 LBS
REFERENCE WHEEL POSITION
180°
NOTE: TEST WHEEL 14" WITH 1" CLEAT
C2 4-27-70
210° 150°
200° 160°
190° 170°
180°
170° 190°
160° 200°
150° 210°
220° 140°
230° 130°
240° 120°
250° 110°
260° 100°
270° 90°
280° 80°
290° 70°
300° 60°
310° 50°
320° 40°
330° 30°
340° 20°
350° 10°
0
10° 350°
20° 340°
30° 330°
140° 220°
130° 230°
120° 240°
110° 250°
100° 260°
90° 270°
80° 280°
70° 290°
60° 300°
50° 310°
40° 320°

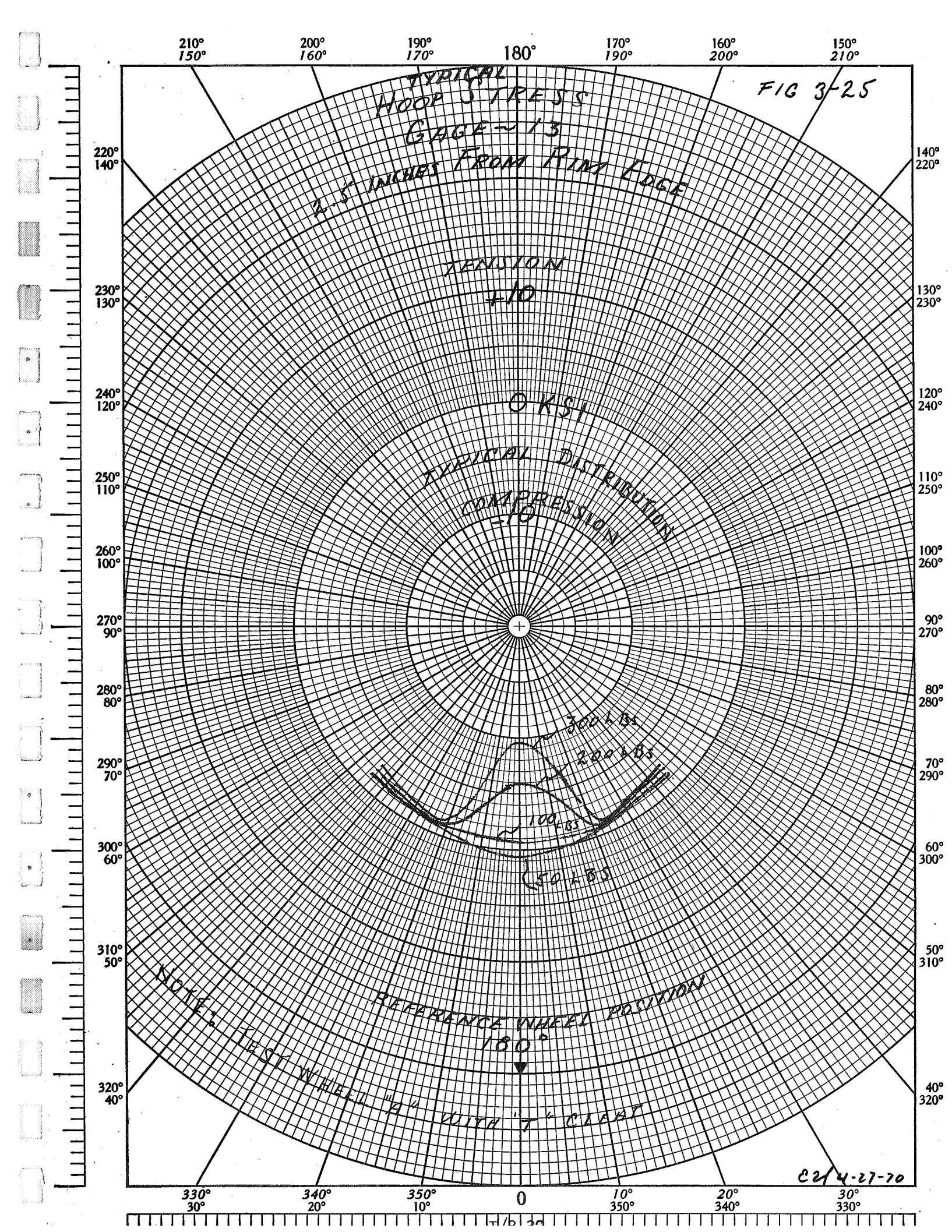
FIG 3-25
TYPICAL HOOP STRESS GAGE ~ 13
2.5 INCHES FROM RIM EDGE
TENSION +10
0 KSI
TYPICAL DISTRIBUTION
COMPRESSION -10
300 LBS
200 LBS
100 LBS
50 LBS
REFERENCE WHEEL POSITION 180°
NOTE: TEST WHEEL 14" WITH 1" CLEAT
C2 4-27-70
210° 150°
200° 160°
190° 170°
180°
170° 190°
160° 200°
150° 210°
220° 140°
230° 130°
240° 120°
250° 110°
260° 100°
270° 90°
280° 80°
290° 70°
300° 60°
310° 50°
320° 40°
330° 30°
340° 20°
350° 10°
0
10° 350°
20° 340°
30° 330°
140° 220°
130° 230°
120° 240°
110° 250°
100° 260°
90° 270°
80° 280°
70° 290°
60° 300°
50° 310°
40° 320°

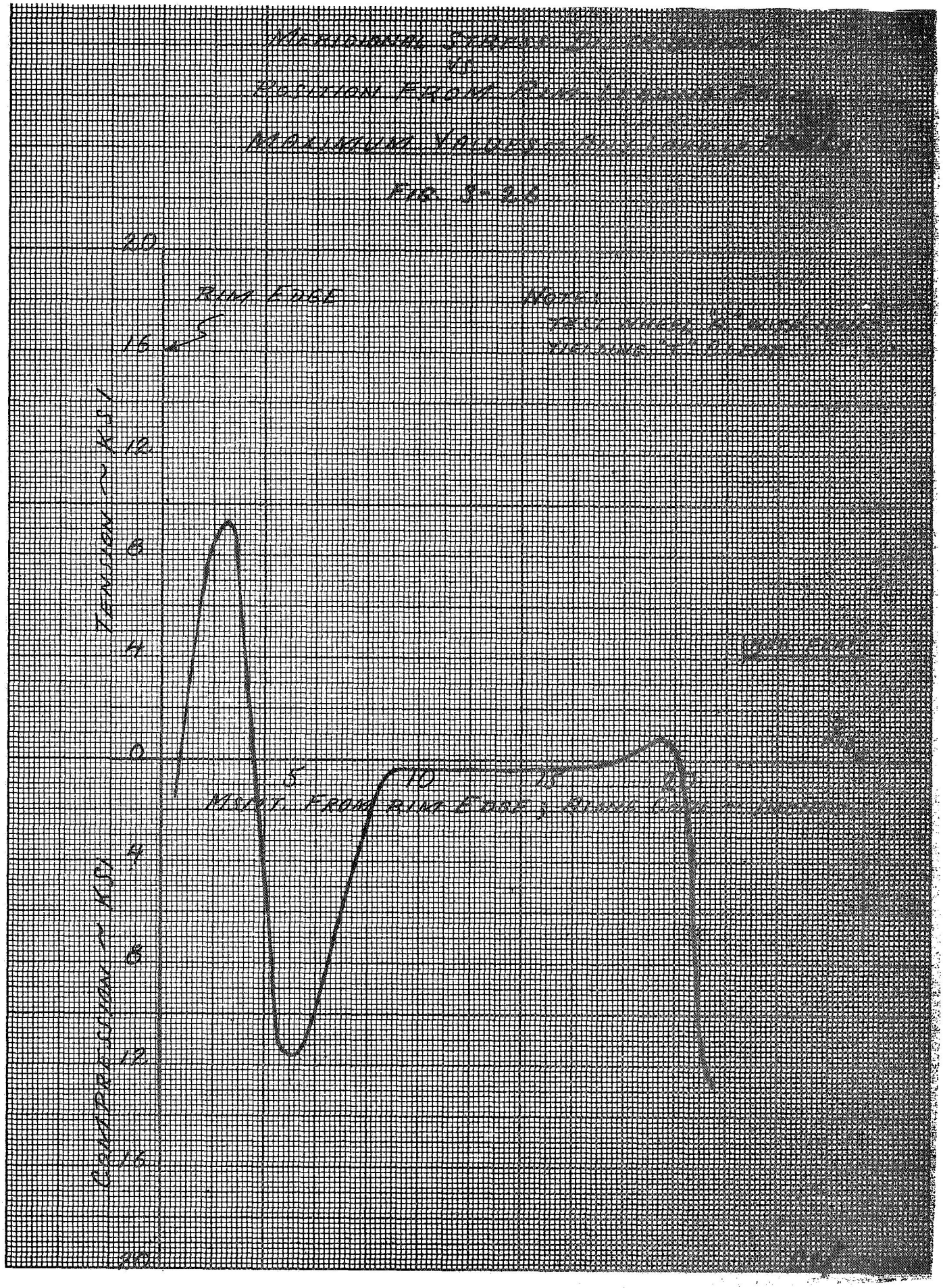
Rim Edge
20
16
12
8
4
0
4
8
12
16
20
5
10
15
20
Meas. From Rim Edge, Inches

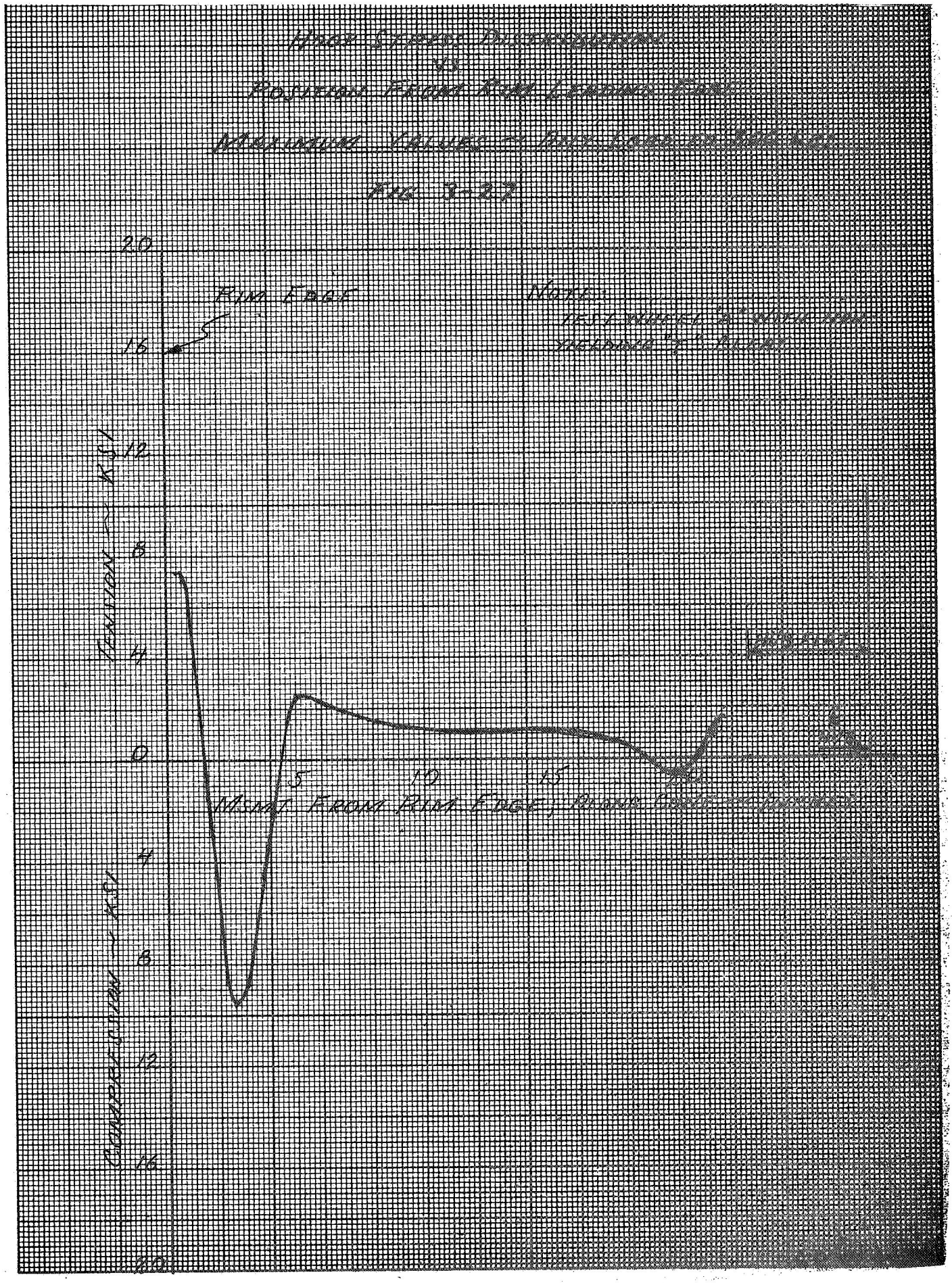
20
16
12
8
4
0
4
8
12
16
20
5
10
15

adequate fatigue life for the DLRV missions, coincident with a wheel that provides the required spring rate and footprint characteristics necessary for operating on real lunar soils.

3.4 DESIGN ITERATION

The design of a second test wheel (wheel "B") was initiated to further improve the weak soil mobility while maintaining the 300 pound load capacity. Figure 3-28 shows the revised wheel configuration. The diameter was reduced from 36 to 34 inches while the wheel depth was increased from 15 to 16 inches. The reduction in diameter was done in order to allow a larger transition radius (9.7" radius) between the conic section and the rim. The larger radius was intended to provide a lower initial spring rate, which would give a larger static footprint. Both modifications are in the direction of increasing the static ground contact area for improved traction.

Based on the problem noted with the 90° extrusion cleat, the "T"-section cleat of the same dimensions was used for this wheel.

No changes were made in the manufacturing materials techniques, or instrumentation. Wheel gage was also maintained, except in the rim to conic section transition area where the gage was reduced from 0.070 to 0.060.

3.4.1 Test Results

Wheel "B" was tested using the same loading fixture and test procedures. Analysis of the data indicated the anticipated general softening of the spring-rate on wheel "B" was not realized (Fig. 3-22), indicating that the deflection is more strongly influenced by wheel diameter than the increased (7" - 10") rim to conic section transition radius, the increased wheel depth (15" - 16"), or the reduction in gage (.070" - .060") at the rim transition area. The rim/transition area acts as a hoop which must deform in order to have any wheel deflection. The reduced diameter hoop (36" - 34") increased the wheels stiffness, negating the expected effects of the other changes.

Additionally noted was a local deflection on the "B" wheel caused by the cleats bearing on the lower, transition radius between the rim and cone causing the initiation of a secondary buckle at loads above 150 pounds. A combination of factors including a decrease in the rim-cone transition gage, the increased rim - conic section transition radius, and the unyielding "T" section cleat contributed to the problem. Normally, when the wheel is stroked without cleats the lip curls upward from the ground at highloads, enhancing the local strength. When the rigid cleats are installed, this curling is completely inhibited on a rigid surface. This restraint of the rim by the cleat causes a local buckling condition. The larger transistion radius of wheel "B" is less stiff and therefore buckles more readily.

Close examination of wheel "A" showed a similar problem, however, only slight local deflections occur at about 250 pounds and at the 300 pound design point a much less sever condition exists than that noted on wheel "B". Neither wheel exhibited any problems in the uncleated configuration, and both used the "T" cleats for all other tests. The stress distributions shown in Table 3-2 do not reflect this condition because of it's localized nature. Figures 3-29 and 30 and 3-31 and 32 show graphically a typical and maximum stress profile.

3.5 FINAL DESIGN SELECTION

Based on these data wheel "A" with a revised cleat configuration, was selected as the final design. The revised cleat is designed to deflect under eccentric loads in excess of two lunar "g's", thus minimizing the adverse load transfer to the wheel, while still providing the aggressive soil-wheel interface necessary for tractive mobility. A prototype titanium deflecting cleat was tested on wheel "A" in the load-deflection fixture prior to final fabrication. Figures 3-33 and 3-34 show the nominal cleat footprint, and the cleat reaction to an eccentrically applied load inboard of the rim edge. No local deflections were noted in the wheel, and the cleat returned to its original configuration when the load was removed. Since previous instrumented tests had not detected high stress concentrations no additional quantitative data was obtained with

TABLE 3-2

"B" TEST WHEEL - WITH "T" EXTRUSION CLEATS

+ = TENSION, - = COMPRESSION

GRUMMAN AIRCRAFT ENGINEERING CORPORATION
ENGINEERING DEPARTMENT

LOAD		STRAIN GAGE POSITION →																LOAD APPLI-CATION
		1	2	3	4	5	6	7	8	9	10	11	12	13	14	15	16	
LBS.		STRESS ~PSI →																
0		0	0	0	0	0	0	0	0	0	0	0	0	0	0	-2975	-338	180°
25		-166	-832	157	181	589	-198	419	-011	332	-608	751	-1662	778	-2600	+1315	-905	
50		-214	-1568	306	335	956	-276	665	000	495	-908	1092	-2605	497	-2825	+2980	-1085	
75		-076	-1960	400	424	1089	-289	740	-016	551	-1030	1249	-3120	-184	-2170	4040	-1272	
100		+054	-2515	443	457	1178	-368	773	-076	582	-1210	1446	-4010	-1458	-729	5320	-1520	
150		+338	-3850	624	532	1501	-514	991	-147	745	-1572	1942	-6490	-5050	+2925	7200	-1842	
200		+625	-4790	878	692	1905	-557	1285	-138	989	-1694	1858	-7950	-9140	+6440	8190	-1835	
225		+754	-5340	983	702	2085	-641	1405	-189	1074	-1682	0481	-7080	-12700	+8100	8380	-1788	
250		+916	-5710	1110	788	2250	-651	1509	-192	1152	-1680	-530	-5770	-14510	+8760	8460	-1798	
300		+1163	-6510	1298	851	2505	-727	1650	-254	1298	-1658	-2300	-2930	-17980	+9820	8350	-1660	
0		0	0	0	0	0	0	0	0	0	0	0	0	0	0	*-2915	* -216	202°
25		-051	-286	-111	359	035	038	000	103	-049	032	-095	238	-816	122	-3690	-038	
50		-078	-530	-157	560	100	008	027	135	-054	-051	-040	000	-1217	-502	-2490	-268	
75		-097	-726	-179	627	133	-043	041	108	-054	-176	-008	-249	-1178	-1005	-1829	-441	
100		-154	-826	-208	654	162	-089	073	103	-027	-257	+062	-473	-1263	-1453	-943	-605	
150		-157	-1130	-219	802	292	-141	192	119	+243	-394	+181	-919	-1500	-1815	+567	-838	
200		-054	-1628	-222	960	421	-195	265	135	+100	-519	+230	-1359	-1812	-1909	+1819	-1012	
225		+057	-1829	-203	1089	473	-173	343	171	+108	-505	+152	-1440	-2020	-1723	+1921	-1012	
250		+146	-2045	-198	1172	490	-171	348	176	+92	-540	+011	-1545	-2260	-1490	+1995	-1031	
300		+208	-2395	-181	1231	570	-227	408	157	+173	-711	-062	-2030	-3500	+244	+2700	-1158	
0		0	0	0	0	0	0	0	0	0	0	0	0	0	0	*-3115	* -179	225°
25		+019	454	-348	+244	-532	+089	-432	+003	-346	389	-370	956	-1112	1335	-4680	+195	
50		-114	732	-678	+351	-937	108	-724	000	-613	562	-638	1490	-2050	2015	-5560	+368	
75		-157	781	-758	400	-1000	119	-743	016	-675	570	-632	1609	-2115	2085	-5740	+427	
100		-184	900	-816	419	-1067	127	-772	035	-705	624	-686	1705	-2260	2110	-5960	+408	
150		-127	1489	-716	810	-991	432	-618	381	-551	1058	-678	2185	-2625	2325	-6075	+446	
200		-130	1448	-1000	748	-1302	605	-599	562	-554	1278	-670	2380	-3045	2120	-5760	+203	
225		-068	1570	-1018	826	-1323	351	-908	322	-878	1050	-1012	2125	-3015	1559	-5540	+125	
250		-014	1579	-821	875	-1400	354	-956	338	-894	1110	-1012	2160	-3740	1409	-5230	-016	
300		NOT COMPLETED																

* Caused by minor local deformation when cleat was installed.

ENG-67

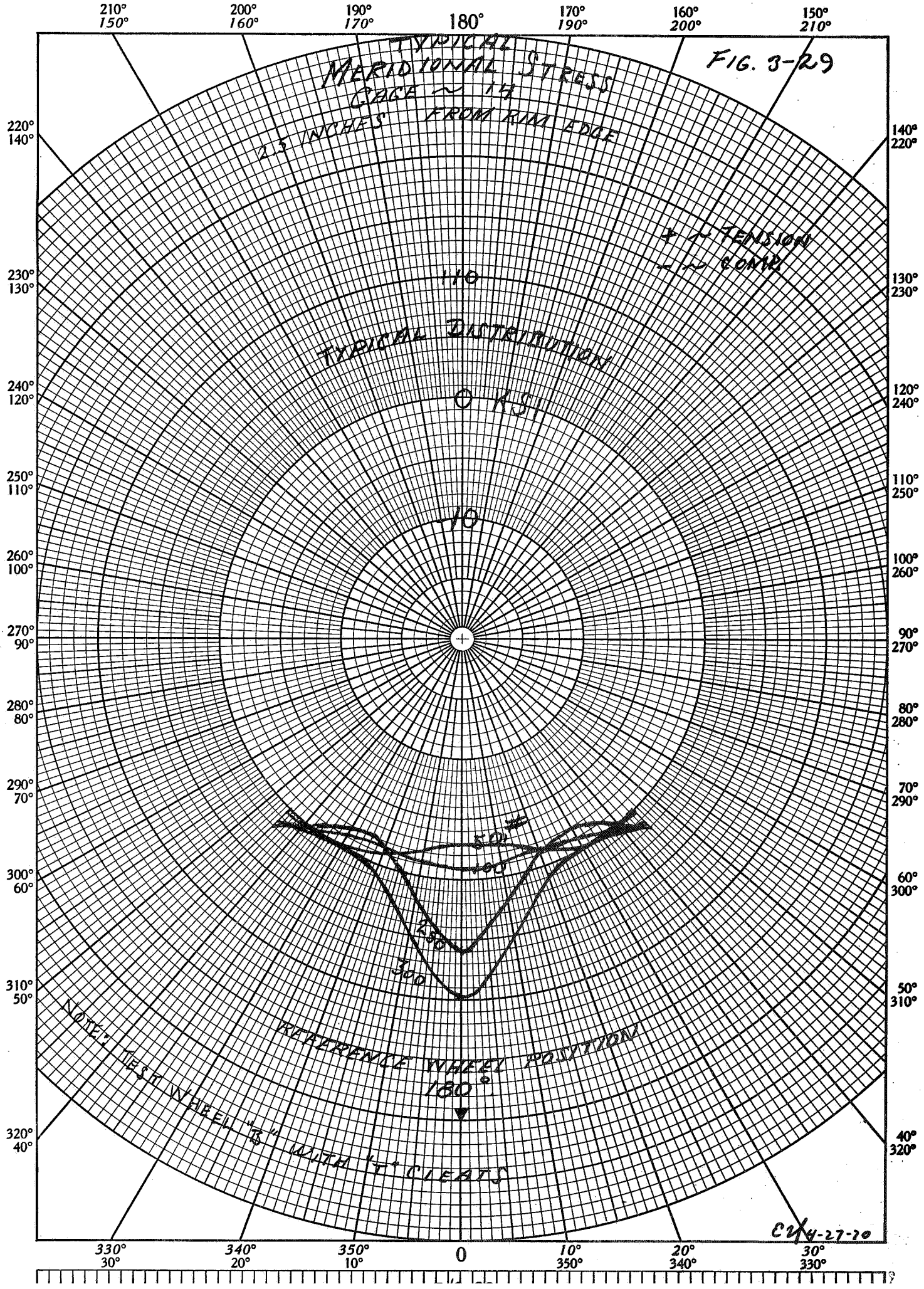
FIG. 3-29
TYPICAL MERIDIONAL STRESS GAGE ~ 14 1/2 INCHES FROM RIM EDGE
+ ~ TENSION
- ~ COMP.
110
TYPICAL DISTRIBUTION
0 KSI
10
50
100
200
300
REFERENCE WHEEL POSITION
180°
NOTE: TEST WHEEL "B" WITH 1" CLEATS
C.Y. 4-27-70
210° 150°
200° 160°
190° 170°
180°
170° 190°
160° 200°
150° 210°
220° 140°
230° 130°
240° 120°
250° 110°
260° 100°
270° 90°
280° 80°
290° 70°
300° 60°
310° 50°
320° 40°
330° 30°
340° 20°
350° 10°
0
10° 350°
20° 340°
30° 330°
140° 220°
130° 230°
120° 240°
110° 250°
100° 260°
90° 270°
80° 280°
70° 290°
60° 300°
50° 310°
40° 320°

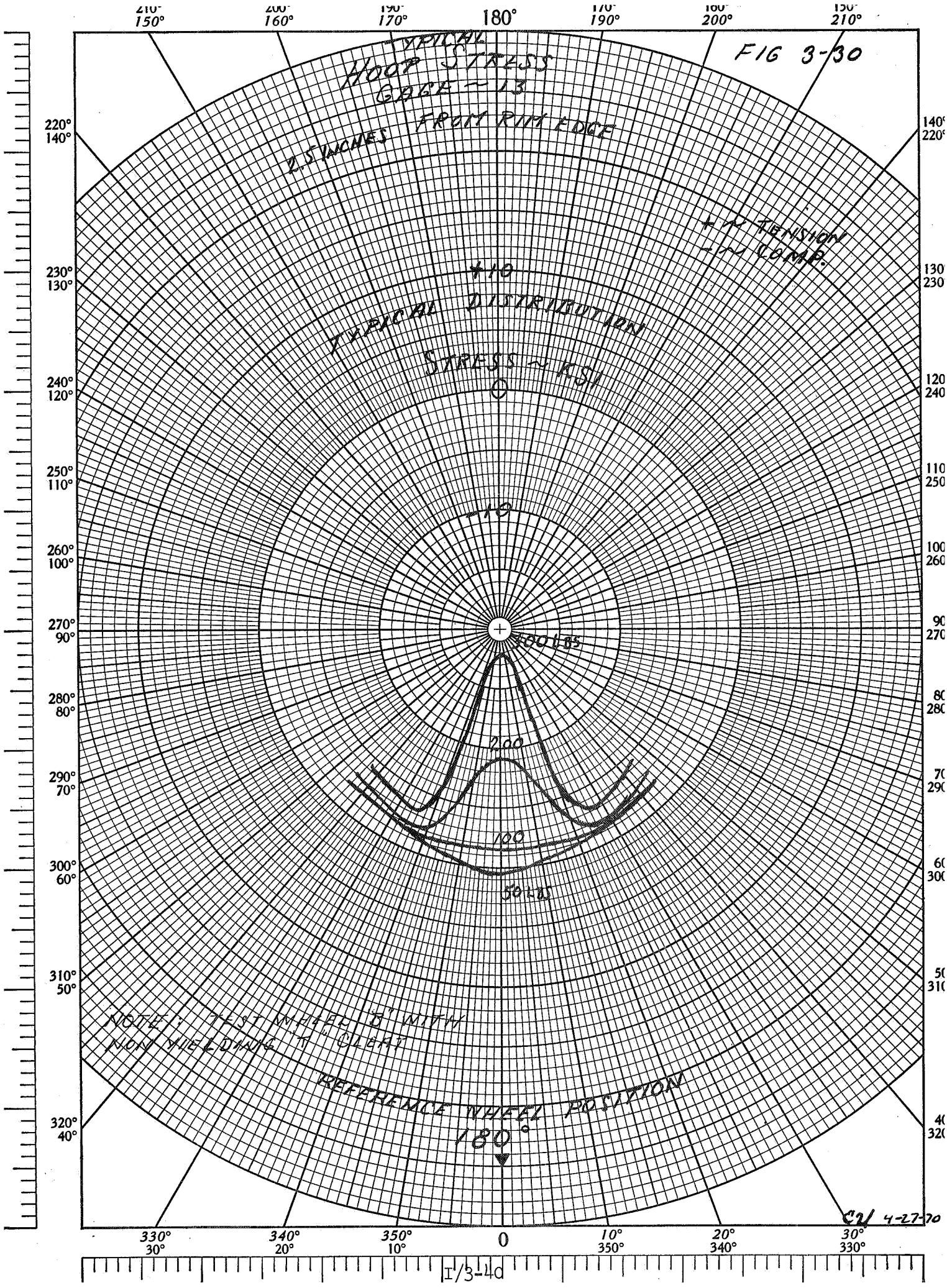
FIG 3-30
TYPICAL HOOP STRESS GAGE = 13
2.5 INCHES FROM RIM EDGE
+ TENSION
- COMP.
+10
TYPICAL DISTRIBUTION
STRESS - KSI
0
-10
300 LBS
200
100
50 LBS
NOTE: TEST WHEEL SLIGHTLY NON YIELDING IN CLAY
REFERENCE WHEEL POSITION
180°
0
180°
4-27-70

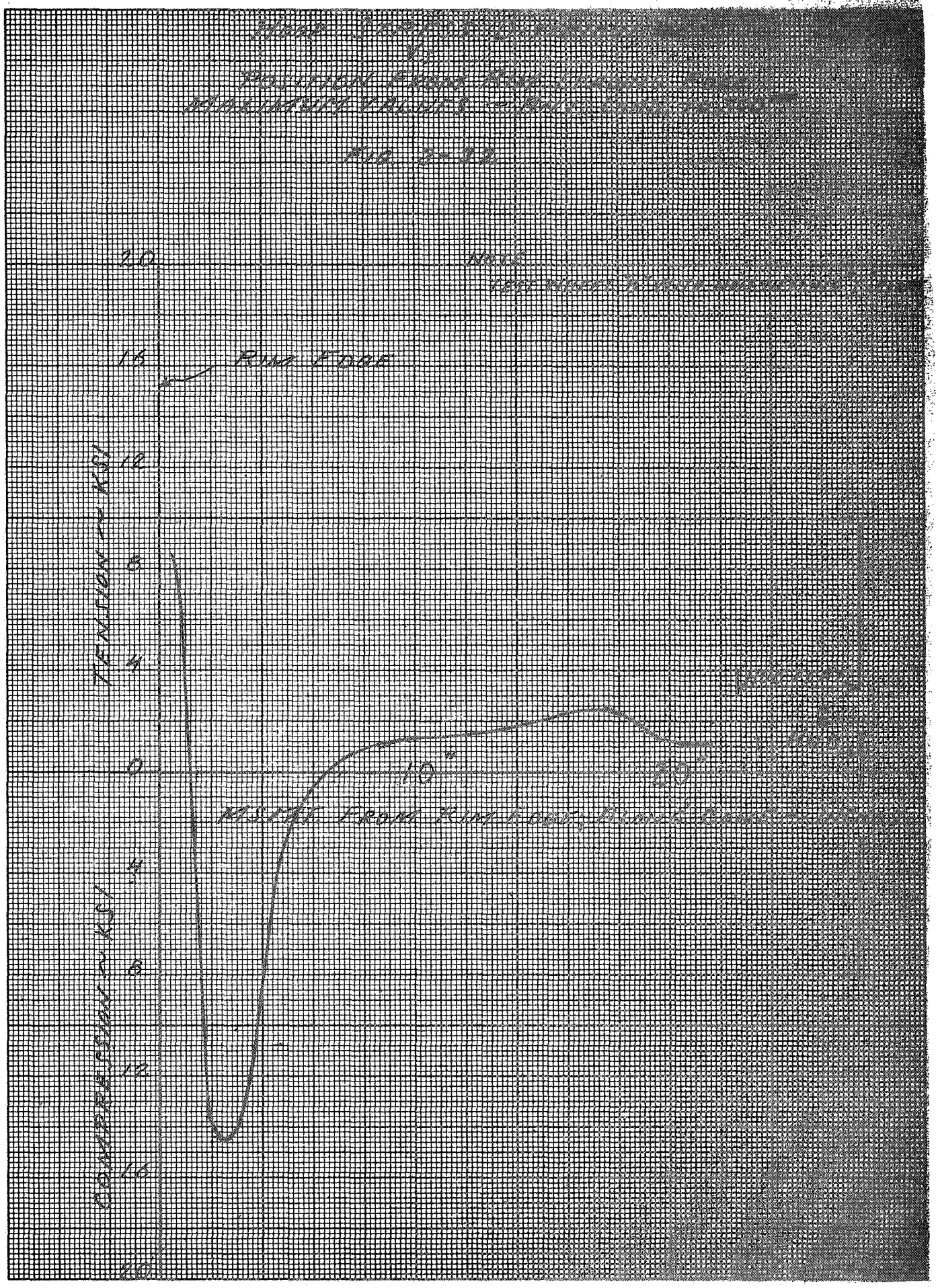
20
16
12
8
4
0
4
8
12
16
20
10°
20°
Ring Force

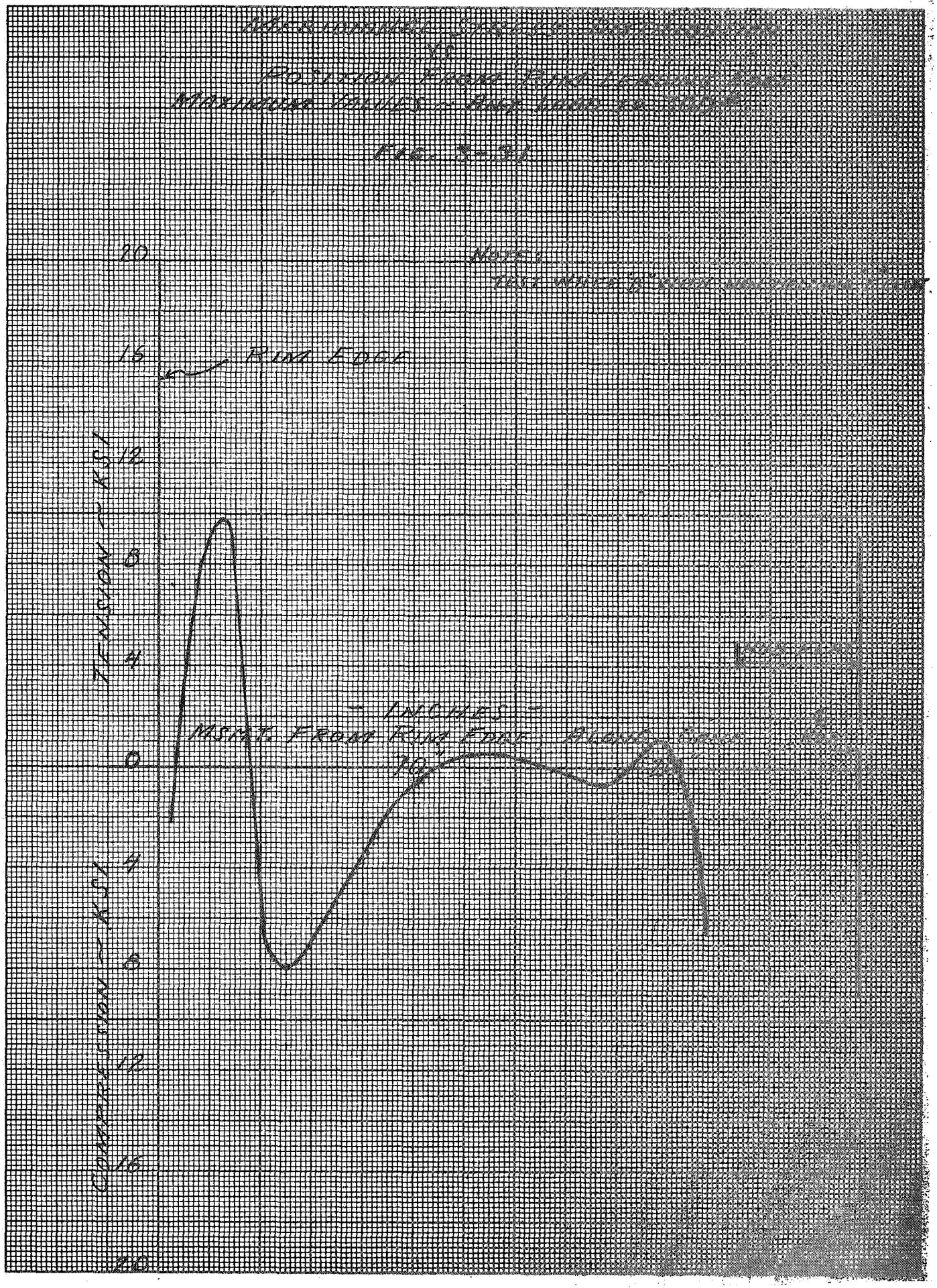
20
16
12
8
4
0
4
8
12
16
20

ELASTIC TITANIUM CLEAT SHOWING UNIFORM SINKAGE AT NOMINAL LOADING

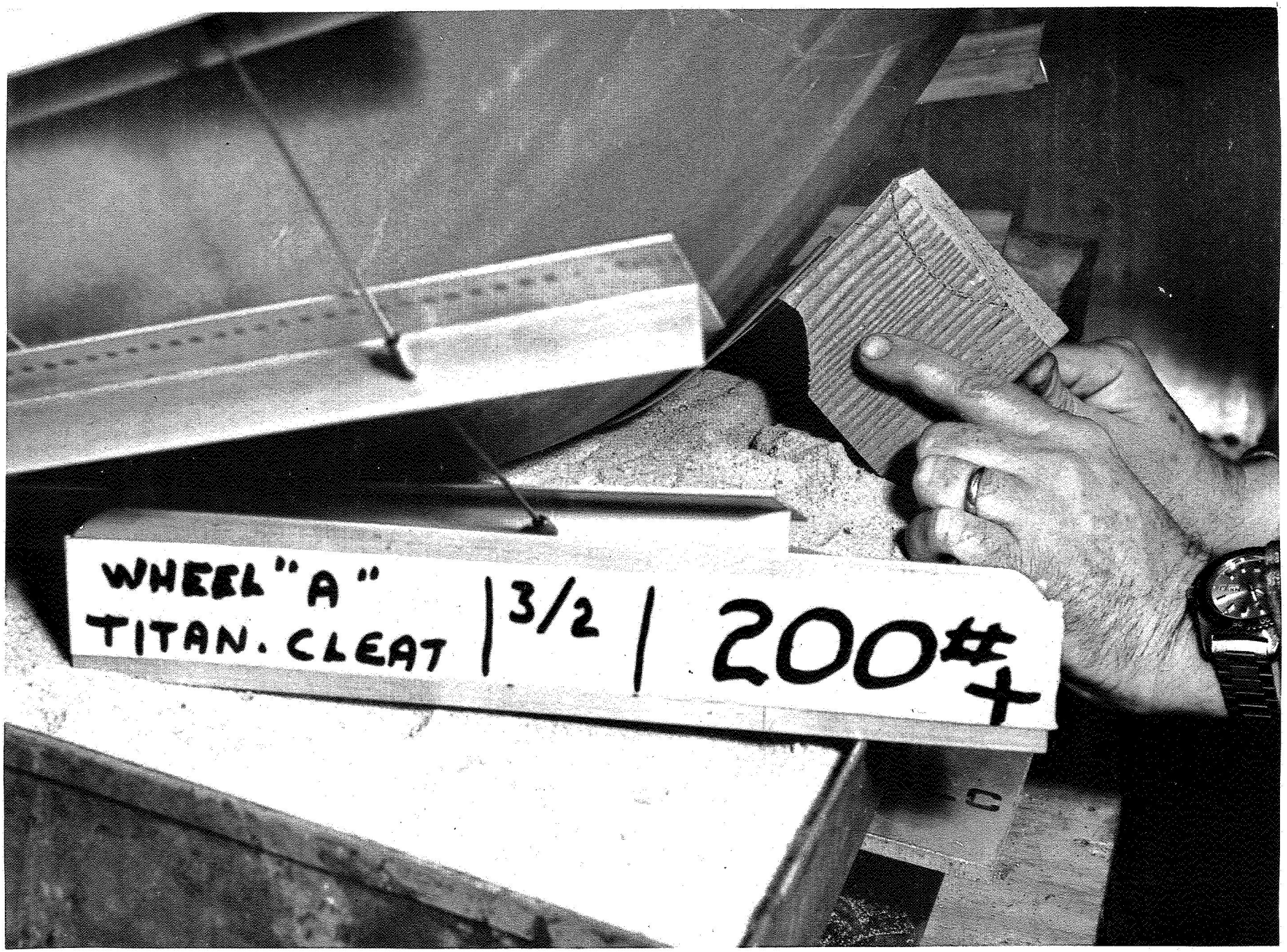

ELASTIC BEHAVIOR OF CLEAT FOR ECCENTRIC POINT LOADS

FIGURE 3-34

the deflecting cleat. Tests of wheels "A" and "B" used a 24 cleat configuration. A 30 cleat configuration was selected for the final design. This increase will enhance the tractive performance of the wheel by reducing ground pressures, plus providing an increased area of rim coverage minimizing the possibility of impact damage to the wheel. Figures 3-35 and 3-36 show the selected wheel-cleat configuration and assembly.

3.5.1 Final Design Characteristics

This study did not require testing of the final design, however, based on wheels "A" and "B" the following characteristics are anticipated.

3.5.1.1 Spring Rate

The spring rate of the uncleated wheel should closely approximate that of wheel "A", being affected only by a small difference in the modulas of elasticity ("E") between the wet layup and the "prepreg" Trevarno 161 fiberglass systems, however, the cleated wheel may exhibit a slightly lower spring rate due to a less restrictive cable system with the deflecting cleat.

3.5.1.2 Stress Distribution

The measured stress distributions of wheel "A" should not be significantly different than that of the delivered wheels. Slight changes could be anticipated primarily in the rim area, again due to the revised load transfer behavior of the deflecting cleat.

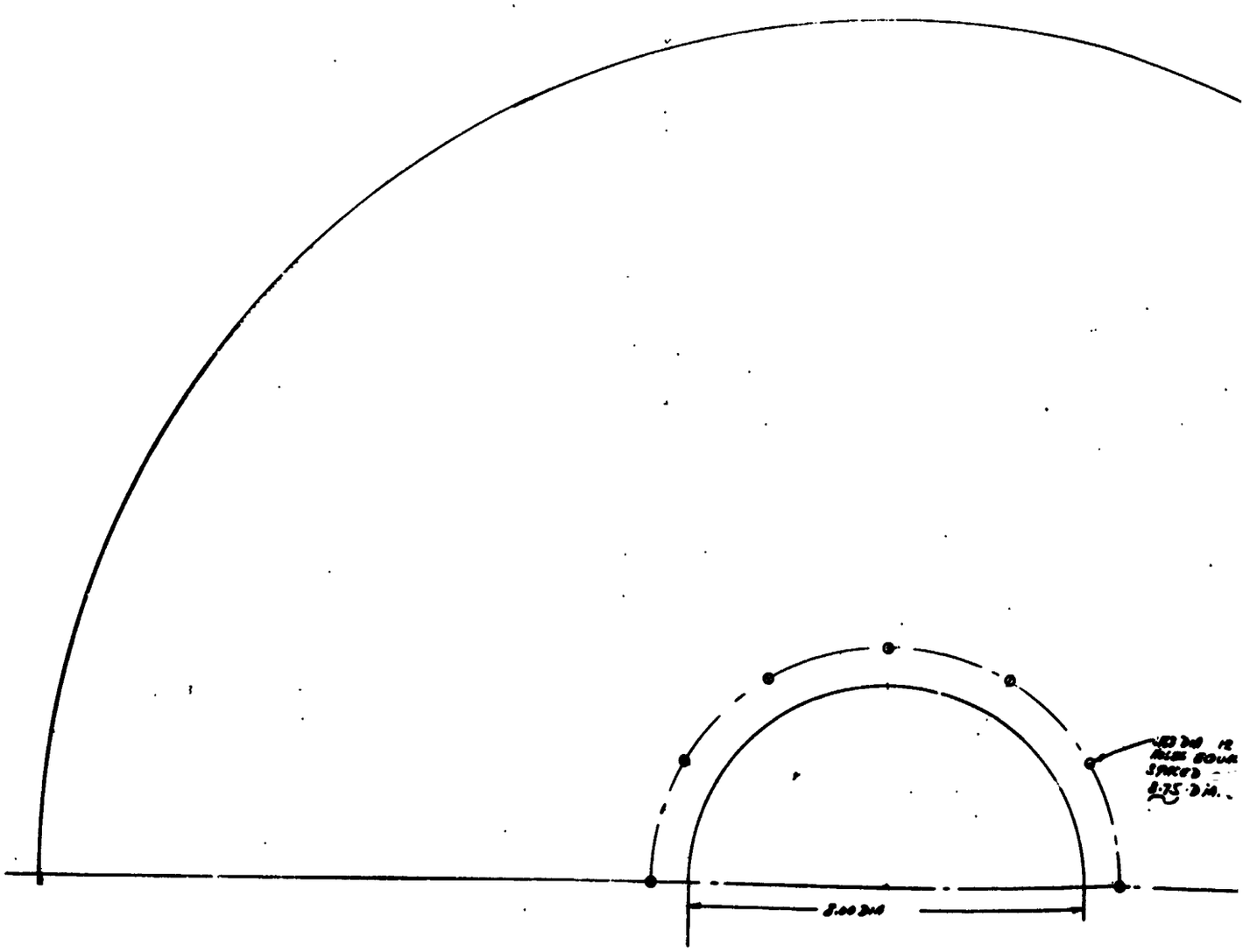

FOLDOUT FRAME 1

NOTES:

1. LAYUP - FIBERGLASS CLOTH @ 181 VOLAN "A"
FINISH - PLASTIC MIL-P-25421 CLASS I (CARBON & SEE NOTE 5
~~CARBIDE) EPOXY RESIN TYPE HARDNER TYPE "B"~~
~~@ [illegible]~~
~~(to [illegible] Resin and Resin)~~
~~OVEN CURE [illegible]~~
~~[illegible]~~

2. Basic LAYUP TO BE DONE IN 6 SEGMENTS WITH 1 ± 1/4 INCH OVERLAP WARP TO GO FROM HUB TO RIM - SEAMS TO BE EVENLY STAGGERED AROUND CIRCUMFERENCE
3. RIM WRAP (4 DIMENSIONS) WARP DIRECTION TO BE CIRCUMFERENTIAL
4. MAKE A FLAT TEST SPECIMEN .050 THICK 12"x12" ALL WARP IN SAME DIRECTION.
5. Epoxy Resin SHELL EPON 828 - CURE SYSTEM MNA / BDMA
OVEN CURE 2 HRS @ 250°F
POST CURE (OUT SIDE) 2 HRS @ 400°F

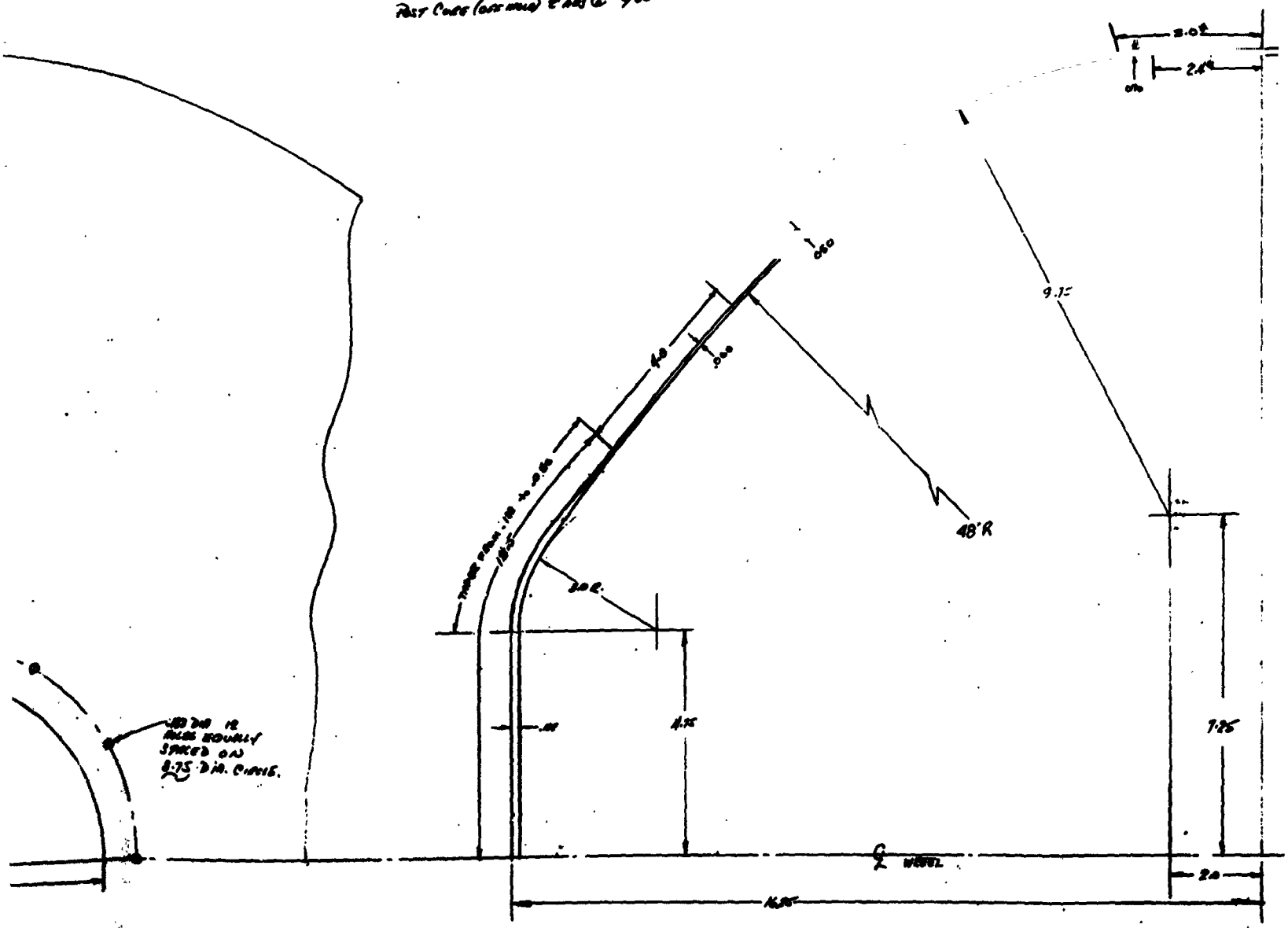

FOLDOUT FRAME 2

"A" CHANGE - ADDED NOTE 5 - 12/6/64 MJB

FIG 3-28

"A"
* SEE NOTE 5

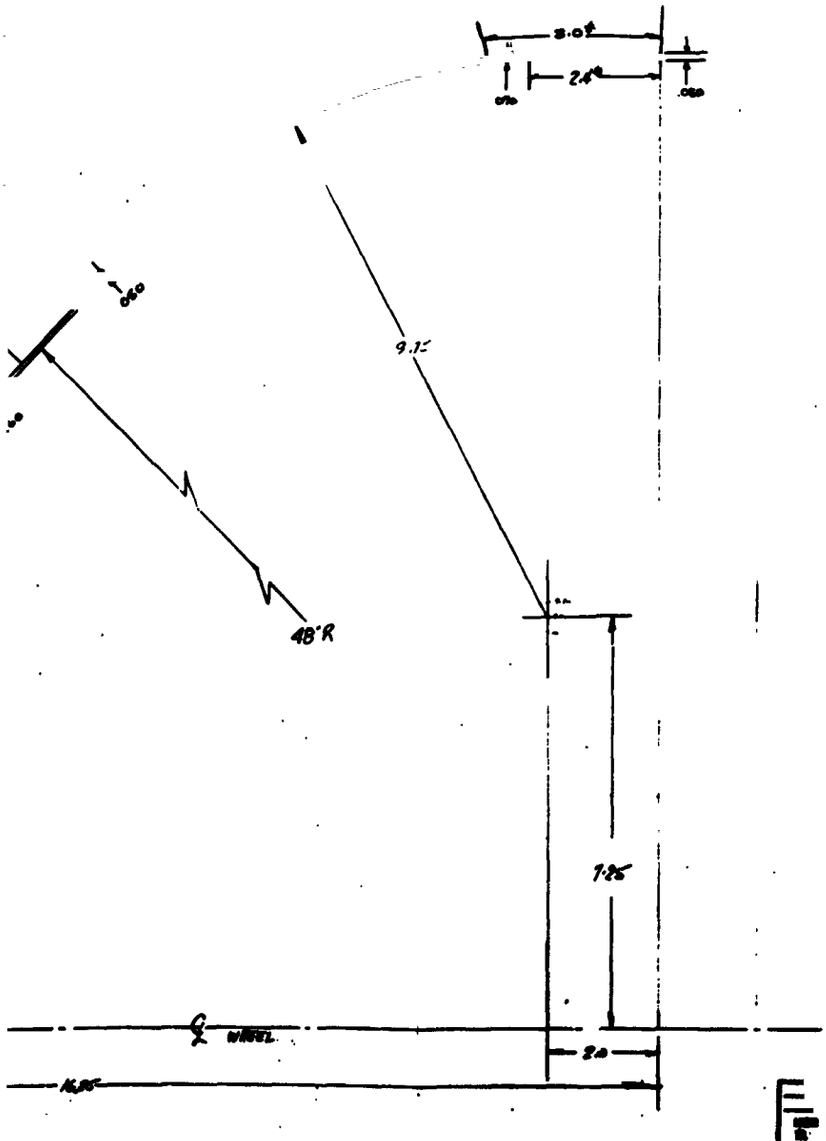

FOLDOUT FRAME 3

FOLDOUT FRAME 2

PJ I/3-36

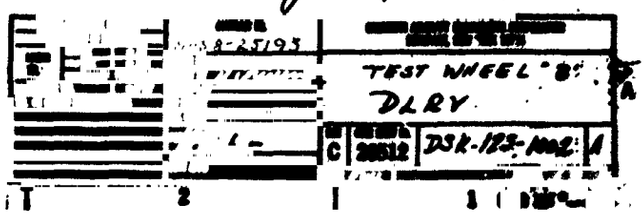

4 FABRICATION PROCESS

4.0 FABRICATION REQUIREMENTS

A Total of five wheels, two for configuration development testing, and three for delivery to NASA for DLRV qualification testing were provided. Both the test wheels and the deliverable wheels will have grouser cleats as developed during this study.

4.1 TEST WHEELS

The major difference between the development test, and delivery wheels is in the tooling and laminating processes used to fabricate the fiberglass shell. The test wheels used inexpensive short lead time, easily modified plaster tooling and structural wet layup techniques. The basic wheel was made of 181 Volan "A" fiberglass reinforced plastic (FRP) with Epon 828 resin and Shell curing agent A. During layup the plies were checked for fiber orientation and seam location on the mold. After completion of the layups a vacuum was drawn around the tool removing any entrapped air or excess resin. The wheel was then oven cured at 200°F for 2 hours.

4.2 DELIVERABLE WHEELS

The final three wheels which were delivered to NASA were made from a pre-impregnated fiberglass (style 7781) cloth containing Trevarno F161 epoxy resin. The individual plies were laid up as noted on the drawings, and a vacuum bag applied as before to remove any entrapped air or resin. The wheel was then autoclave cured at 50 psi for one hour at 350°F. A steel male mold was fabricated to withstand the required cure cycle without degrading. The Trevarno was selected because of its ability to withstand the extreme temperature range associated with lunar day and night operations.

The bare wheel was coated inside and outside with a TFE filled polyurethane paint to eliminate any ultra violet (UV) induced degradation, and to protect the wheel from light scuffing.

4.3 CLEAT FABRICATION

Cleats for the test wheels were fabricated from standard aluminum extrusions. The deliverable wheels were fitted with cleats to satisfy the wear and loading requirements associated with the DLRV mission. The cleats were made of 0.025 gage 6AL-4V titanium, with standard AN3C-4 hardware used for attaching them to the wheel. RTV88 potting compound was used between the faying surfaces, and also as a fillet seat to minimize the possibility of debris ingestion between the wheel and cleat. A total of 30 cleats per wheel are provided with an interconnecting 1/16 inch stainless cable. The cable system stabilizes the cleat at the wheel soil interface, and helps to more evenly distribute both torque loads and any higher than nominal vertical loadings.

4.4 WHEEL WEIGHT

The total weight of the completed wheel assembly is approximately 14 lb. 9 oz. The basic shell with the polyurethane coating weighs 9 pounds, with the cleats, cable assembly, AN hardware and potting compound accounting for the remaining 5 lbs. 9 oz. Individual wheel weights are listed below.

Wheel #	Weight
1	14 lbs 11 oz
2	14 lbs 8 oz
3	14 lbs 9 oz

Weight reductions on the order of 0.5 lbs per wheel can be achieved with the use of lightening holes in non structural areas of the cleat, and by replacing the AN3C-4 hardware with lighter weight fasteners with a shorter shank.